Projected changes in the atmospheric system over the Northern Hemisphere and in the North Atlantic, Arctic and North Pacific Oceans from 22 CMIP6 ESMs

Zeliang Wang, Brendan DeTracey, Blair Greenan, David Brickman, Frederic Cyr, Peter S. Galbraith, Nadja Steiner and James Christian

Fisheries and Oceans Canada
Bedford Institute of Oceanography
1 Challenger Drive
Dartmouth, Nova Scotia, B2Y 4A2

2026

Canadian Technical Report of
Hydrography and Ocean Sciences 419

Fisheries and Oceans Canada | Pêches et Océans Canada

Canada

Canadian Technical Report of Hydrography and Ocean Sciences

Technical reports contain scientific and technical information of a type that represents a contribution to existing knowledge but which is not normally found in the primary literature. The subject matter is generally related to programs and interests of the Oceans and Science sectors of Fisheries and Oceans Canada.

Technical reports may be cited as full publications. The correct citation appears above the abstract of each report. Each report is abstracted in the data base *Aquatic Sciences and Fisheries Abstracts.*

Technical reports are produced regionally but are numbered nationally. Requests for individual reports will be filled by the issuing establishment listed on the front cover and title page.

Regional and headquarters establishments of Ocean Science and Surveys ceased publication of their various report series as of December 1981. A complete listing of these publications and the last number issued under each title are published in the *Canadian Journal of Fisheries and Aquatic Sciences*, Volume 38: Index to Publications 1981. The current series began with Report Number 1 in January 1982.

Rapport technique canadien sur l'hydrographie et les sciences océaniques

Les rapports techniques contiennent des renseignements scientifiques et techniques qui constituent une contribution aux connaissances actuelles mais que l'on ne trouve pas normalement dans les revues scientifiques. Le sujet est généralement rattaché aux programmes et intérêts des secteurs des Océans et des Sciences de Pêches et Océans Canada.

Les rapports techniques peuvent être cités comme des publications à part entière. Le titre exact figure au-dessus du résumé de chaque rapport. Les rapports techniques sont résumés dans la base de données *Résumés des sciences aquatiques et halieutiques*.

Les rapports techniques sont produits à l'échelon régional, mais numérotés à l'échelon national. Les demandes de rapports seront satisfaites par l'établissement auteur dont le nom figure sur la couverture et la page de titre.

Les établissements de l’ancien secteur des Sciences et Levés océaniques dans les régions et à l'administration centrale ont cessé de publier leurs diverses séries de rapports en décembre 1981. Vous trouverez dans l'index des publications du volume 38 du *Journal canadien des sciences halieutiques et aquatiques*, la liste de ces publications ainsi que le dernier numéro paru dans chaque catégorie. La nouvelle série a commencé avec la publication du rapport numéro 1 en janvier 1982.

Canadian Technical Report of
Hydrography and Ocean Sciences 419

2026

PROJECTED CHANGES IN THE ATMOSPHERIC SYSTEM OVER THE NORTHERN HEMISPHERE AND IN THE NORTH ATLANTIC, ARCTIC AND NORTH PACIFIC OCEANS FROM 22 CMIP6 ESMS

By

Zeliang Wang[1], Brendan DeTracey[1], Blair Greenan[1], David Brickman[1], Frederic Cyr[2], Peter S. Galbraith[3], Nadja Steiner[4], and James Christian[4]

[1]Fisheries and Oceans Canada
Bedford Institute of Oceanography
1 Challenger Drive
Dartmouth, Nova Scotia, B2Y 4A2

[2]Fisheries and Oceans Canada
Northwest Atlantic Fisheries Centre
80 East White Hills Road
St. John's, Newfoundland and Labrador, A1C 5X1

[3]Fisheries and Oceans Canada
Maurice Lamontagne Institute
Mont-Joli, Québec, G5H 3Z4

[4]Fisheries and Oceans Canada
Institute of Ocean Sciences
9860 West Saanich Road
Sidney, British Columbia, V8L 4B2

Cat. No. Fs 97-18/419E-PDF ISBN 978-0-660-99729-2 ISSN 1488-5417

Correct citation for this publication:

Wang, Z., DeTracey, B., Greenan, B., Brickman, D., Cyr, F., Galbraith, P., Steiner, N., and Christian, J. 2026. Projected changes in the atmospheric system over the Northern Hemisphere and in the North Atlantic, Arctic and North Pacific Oceans from 22 CMIP6 ESMs. Can. Tech. Rep. Hydrogr. Ocean Sci. 419: v + 123 p.

TABLE OF CONTENTS

ABSTRACT

Wang, Z., DeTracey, B., Greenan, B., Brickman, D., Cyr, F., Galbraith, P., Steiner, N., and Christian, J. 2026. Projected changes in the atmospheric system over the Northern Hemisphere and in the North Atlantic, Arctic and North Pacific Oceans from 22 CMIP6 ESMs. Can. Tech. Rep. Hydrogr. Ocean Sci. 419: v + 123 p.

Four climate scenarios (Shared Socioeconomic Pathways [SSPs]) for the 2015-2059 period, SSP126, SSP245, SSP370 and SSP585, were analyzed to investigate changes in the atmospheric system over the northern hemisphere, and changes in the North Atlantic, Arctic, and North Pacific Oceans. Ensemble analysis of the sea level pressure over the northern hemisphere suggested that the NPO (North Pacific Oscillation) increased its variability from SSP126 to SSP585. No clear pattern can be drawn for the NAO/AO (North Atlantic Oscillation/Arctic Oscillation), although they showed stronger variability in the four scenarios than in the historical period (1955-2014). Near-surface air temperature over the northern hemisphere had dominant warming trends, except for the subpolar North Atlantic Ocean, and its variability increased from SSP126 to SSP585 with increasing warming trends. The North Atlantic Ocean from the low to mid-latitudes had dominant warming trends in Sea Surface Temperature (SST) in all the four scenarios, and the warming trends increase from SSP126 to SSP585. The subpolar region had a cooling trend which decreased from SSP126 to SSP585. The whole North Pacific Ocean had warming trends in SST, and the warming trends increased from SSP126 to SSP585. Ensemble analysis of the declining summer sea ice trends suggested the earliest year of the summer ice-free Arctic Ocean was 2046 under scenario SSP585.

RÉSUMÉ

Wang, Z., DeTracey, B., Greenan, B., Brickman, D., Cyr, F., Galbraith, P., Steiner, N., and Christian, J. 2026. Projected changes in the atmospheric system over the Northern Hemisphere and in the North Atlantic, Arctic and North Pacific Oceans from 22 CMIP6 ESMs. Can. Tech. Rep. Hydrogr. Ocean Sci. 419: v + 123 p.

Quatre scénarios climatiques (Shared Socioeconomic Pathways [SSP]) pour la période 2015-2059 (SSP126, SSP245, SSP370 et SSP585) ont été analysés afin d'étudier les changements du système atmosphérique dans l'hémisphère Nord, ainsi que les évolutions dans les océans Atlantique Nord, Arctique et Pacifique Nord. L'analyse d'ensemble de la pression au niveau de la mer dans l'hémisphère Nord suggère que l'Oscillation du Pacifique Nord (NPO) voit sa variabilité augmenter du scénario SSP126 au SSP585. Aucun schéma clair n'a pu être établi pour l'Oscillation Nord-Atlantique (NAO) ou l'Oscillation Arctique (AO), bien qu'elles présentent une variabilité plus forte dans les quatre scénarios que durant la période historique (1955-2014). La température de l'air proche de la surface dans l'hémisphère Nord présente des tendances au réchauffement dominantes, à l'exception de la zone subpolaire de l'océan Atlantique Nord ; sa variabilité s'accentue de SSP126 à SSP585 parallèlement à l'intensification du réchauffement. Dans l'océan Atlantique Nord, des basses aux moyennes latitudes, les températures de surface de la mer (SST) affichent des tendances au réchauffement marquées dans les quatre scénarios, lesquelles s'accentuent de SSP126 à SSP585. La région subpolaire présente une tendance au refroidissement qui diminue de SSP126 à SSP585. L'ensemble de l'océan Pacifique Nord affiche des tendances au réchauffement de la SST, s'intensifiant également de SSP126 à SSP585. Enfin, l'analyse d'ensemble des tendances au déclin de la glace de mer estivale suggère que l'année la plus précoce pour un océan Arctique libre de glace en été serait 2046 selon le scénario SSP585.

1. Introduction

The 6th iteration of the Coupled Model Intercomparison Project (CMIP6) is the latest modeling effort for simulating and projecting various aspects of climate change for which a new set of scenarios has been developed. CMIP5 used Representative Concentration Pathway (RCP) to represent greenhouse gas (GHG) concentration trajectory. In contrast, the new scenarios in CMIP6 represent different socio-economic developments as well as different pathways of atmospheric greenhouse gas concentrations (Shared Socio-economic Pathways; SSPs; from SSP1 to SSP5; Figure 1.1). The funded CSRF project of "The performance and projections of the CMIP6 Earth System Models (ESMs) for Canada's three oceans" has two goals - one is the evaluation of these models' present climate simulations, and the other one is the future projections using these models. The evaluations of the models have been addressed in the previous report (Wang et al., 2024), and this report will focus on the projections for the North Atlantic, the Arctic and the North Pacific Oceans. Multi-model climate projections represent an essential source of information for mitigation and adaptation decisions, and this report attempts to use different ensemble approaches for the projections. In this report, we focus on SSP126, SSP245, SSP370 and SSP585 (Figure 1.1).

	Shared Socioeconomic Pathways				
	SSP1 **Sustainability**	***SSP2*** **Middle of the road**	***SSP3*** **Regional Rivalry**	***SSP4*** **Inequality**	***SSP5*** **Fossil fueled development**
2100 forcing level (W/m^2) 8.5					✓
7.0			✓		
6.0					
4.5		✓			
3.4					
2.6	✓				
1.9					

Figure 1.1 SSP scenarios and forcing levels((adapted from https://www.dkrz.de/en/communication/climate-simulations/cmip6-en/the-SSP-scenarios).The scenarios investigated in this report are marked with "✓".

This report focuses on the future projection period of 2015-2059, a total of 45 years. Empirical Orthogonal Functions (EOFs), trends and relative changes are used in the analysis of the models' future climate. Details about the methodologies are presented in the Appendix 0.

2. Results & Discussion

2.1 Changes in the atmosphere over the Northern Hemisphere

2.1.1 Sea level pressure

2.1.1.1 Empirical Orthogonal Function patterns

Figures A1.1a-d and Figures A1.2a-d, respectively (Appendix 1), show the EOF1 patterns and the first Principal Component (PC1) from the 22 CMIP6 models. The general patterns of the EOF1s for the projection period from all four scenarios were similar in each model and among all the 22 models (details in Wang et al., 2024), and they were also consistent with patterns in the historical period (1955-2014; Figure 2.2.1 in Wang et al., 2024). It was noticeable that the differences among the four scenarios in each model did exist, but it was challenging to find clear changes among them, and this was also true for the EOF1s from different models. The PC1s from the four scenarios in all 22 models demonstrated variability at multiple timescales from inter-annual to decadal, and even longer. The PC1 of the SLP represented the North Pacific Oscillation (NPO; Wang et al., 2024). We investigated the PC1 changes between scenarios using the standard deviation (Table 2.1.1). The model ensemble means of the standard deviations over the 22 models were calculated and shown there as well. The ensemble means demonstrated that the standard deviations of SLP PC1s from the four climate scenarios generally increased from SSP126 to SSP585, indicating probable increasing variations of the NPO with the increasing greenhouse gas emissions. The mean standard deviation from the historical period fell between that of SSP245 and SSP370, consistent with the mean historic CO_2 emission trend which also fell between that of SSP245 and SSP370.

Table 2.1.1 Standard deviations of the SLP PC1s of the historical period (hist) and four scenarios described in Figure 1.1.

models	hist	SSP126	SSP245	SSP370	SSP585
ACCESS-CM2	69.41	60.7	72.75	73.32	69.54
ACCESS-ESM1-5	66.64	54.81	54.4	52.84	54.71
AWI-CM-1-1-MR	66.29	77.83	56.19	71.54	75.78
CAMS-CSM1-0	78.9	81.01	76.93	81.17	92.3
CanESM5	70.68	54.39	47.09	53.02	55.14
CESM2	87.01	80.13	80.11	77.75	69.47
CESM2-WACCM	84.12	69.01	83.62	81.41	59.65
CMCC-CM2-SR5	103.06	108.9	109.12	99.91	117.15
CNRM-CM6-1	48.31	61.72	56.08	67.03	44.96
CNRM-CM6-1-HR	41.87	39.58	53.15	51.49	54.45

CNRM-ESM2-1	54.31	46.08	49.57	62.91	63.07
EC-Earth3	71.27	74.43	77.75	84.53	86.67
GISS-E2-1-G	55.61	55.25	71.86	56.83	66.61
IPSL-CM6A-LR	56.95	52.32	62.59	62.55	61.56
MIROC6	90.63	85.64	95.59	82.91	91.43
MIROC-ES2L	79.64	61.10	61.03	65.10	64.56
MPI-ESM1-2-HR	66.49	75.70	71.18	63.94	70.04
MPI-ESM1-2-LR	77.88	87.72	77.03	76.34	90.38
MRI-ESM2-0	64.80	60.01	55.46	59.94	72.07
NorESM2-LM	74.25	71.47	70.45	69.15	63.84
TaiESM1	65.76	66.98	80.60	97.59	76.21
UKESM1-0-LL	56.92	54.31	50.02	50.05	66.49
Mean	69.58	67.23	68.75	70.06	71.19

Table 2.1.2 lists the variances explained by the EOF1s. The ensemble means and most individual models did not show substantial changes in the variances explained between the historical period and four scenarios, suggesting that the represented variances were not impacted by the increasing variations of NPO with the increasing GHG emissions.

Table 2.1.2 The variances explained by the EOF1s of the historical period and four scenarios.

models	hist	SSP126	SSP245	SSP370	SSP585
ACCESS-CM2	0.55	0.55	0.55	0.55	0.55
ACCESS-ESM1-5	0.59	0.60	0.60	0.61	0.60
AWI-CM-1-1-MR	0.51	0.53	0.50	0.51	0.51
CAMS-CSM1-0	0.51	0.51	0.51	0.51	0.51
CanESM5	0.59	0.59	0.60	0.60	0.61
CESM2	0.49	0.48	0.50	0.49	0.50

CESM2-WACCM	0.49	0.49	0.49	0.49	0.49
CMCC-CM2-SR5	0.57	0.57	0.55	0.55	0.55
CNRM-CM6-1	0.48	0.48	0.48	0.48	0.47
CNRM-CM6-1-HR	0.48	0.48	0.47	0.49	0.47
CNRM-ESM2-1	0.49	0.46	0.47	0.48	0.48
EC-Earth3	0.50	0.50	0.50	0.50	0.50
GISS-E2-1-G	0.43	0.43	0.45	0.43	0.44
IPSL-CM6A-LR	0.51	0.51	0.52	0.51	0.52
MIROC6	0.60	0.60	0.60	0.60	0.60
MIROC-ES2L	0.67	0.67	0.67	0.67	0.67
MPI-ESM1-2-HR	0.53	0.52	0.52	0.52	0.52
MPI-ESM1-2-LR	0.53	0.53	0.50	0.51	0.52
MRI-ESM2-0	0.52	0.51	0.51	0.53	0.52
NorESM2-LM	0.51	0.50	0.49	0.49	0.48
TaiESM1	0.57	0.58	0.57	0.57	0.58
UKESM1-0-LL	0.54	0.56	0.57	0.55	0.55
Mean	0.53	0.53	0.53	0.53	0.53

Figures A1.3a-d and Figures A1.4a-d (Appendix 1), respectively, show the EOF2 patterns and PC2s from the 22 CMIP6 models. Similar to the EOF1s described earlier, the general patterns of the EOF2s for the projection period from four scenarios were similar in each model and among the 22 models, and they were also consistent with patterns in the historical period (1955-2014; Figure 2.2.2 in Wang et al., 2024). We need to stress that the differences between the historical period and four projections do exist in each model, but they don't appear to show a clear consistent pattern. The PC2s from the four scenarios in all 22 models demonstrated variability at multiple timescales from inter-annual to decadal, and even longer. The PC2 of the SLP represented the North Atlantic Oscillation and Arctic Oscillation (NAO/AO; Wang et al., 2024). We investigated the PC2 changes among scenarios using the standard deviation (Table 2.1.3). The model ensemble means over the 22 models were calculated and shown there as well. No clear pattern of the standard deviation changes with increasing GHG emissions was noted, but the ensemble means suggested the future variations of the NAO/AO are stronger than the historical ones. Some models suggested decreasing variations of NAO/AO in future projections compared to the historical period, e.g., ACCESS-CM2, GISS-E2-1-G.

Table 2.1.3 Standard deviations of the SLP PC2s of the historical period and four scenarios

models	hist	SSP126	SSP245	SSP370	SSP585
ACCESS-CM2	154.00	109.32	143.21	137.01	133.93
ACCESS-ESM1-5	115.32	122.69	119.35	121.57	149.07
AWI-CM-1-1-MR	104.93	120.40	146.78	154.35	142.54
CAMS-CSM1-0	114.24	151.27	121.55	118.17	116.46
CanESM5	132.79	177.82	183.32	158.74	140.78
CESM2	190.67	195.80	182.55	187.03	155.35
CESM2-WACCM	152.75	137.23	158.80	139.83	164.40
CMCC-CM2-SR5	157.74	160.80	204.36	177.32	232.30
CNRM-CM6-1	144.92	169.69	152.25	170.64	160.34
CNRM-CM6-1-HR	126.06	139.96	133.30	122.40	123.77
CNRM-ESM2-1	154.19	132.24	158.27	117.49	133.89
EC-Earth3	131.23	170.38	118.12	129.15	119.91
GISS-E2-1-G	177.08	172.54	161.52	167.59	145.05
IPSL-CM6A-LR	148.21	147.43	165.26	184.55	148.58
MIROC6	107.30	107.59	120.81	115.87	93.35
MIROC-ES2L	93.52	97.45	86.72	98.70	97.58
MPI-ESM1-2-HR	113.32	152.73	124.18	135.30	121.80
MPI-ESM1-2-LR	142.21	146.82	139.13	106.72	153.05
MRI-ESM2-0	152.94	119.69	143.53	151.60	156.61
NorESM2-LM	151.02	139.97	186.99	182.13	186.41
TaiESM1	162.25	126.53	129.06	149.37	154.60
UKESM1-0-LL	152.80	112.41	108.26	126.21	133.49
Mean	139.98	141.40	144.88	143.26	143.78

Table 2.1.4 lists the variances explained by the EOF2s. The ensemble means and most individual models did not show substantial changes in the variances explained between the historical period and four scenarios, suggesting that the represented variances were not impacted by the increasing variations of NAO/AO with increasing GHG emissions, as is consistent with the EOF1s.

Table 2.1.4 The variances explained by the EOF2s of the historical period and four scenarios

Models	hist	SSP126	SSP245	SSP370	SSP585
ACCESS-CM2	0.10	0.11	0.10	0.11	0.10
ACCESS-ESM1-5	0.07	0.08	0.08	0.08	0.09
AWI-CM-1-1-MR	0.13	0.11	0.14	0.14	0.14
CAMS-CSM1-0	0.11	0.11	0.11	0.11	0.11
CanESM5	0.07	0.10	0.10	0.09	0.08
CESM2	0.12	0.14	0.12	0.12	0.11
CESM2-WACCM	0.13	0.13	0.14	0.13	0.14
CMCC-CM2-SR5	0.09	0.11	0.12	0.11	0.13
CNRM-CM6-1	0.11	0.12	0.12	0.12	0.13
CNRM-CM6-1-HR	0.10	0.12	0.12	0.10	0.12
CNRM-ESM2-1	0.10	0.12	0.13	0.11	0.11
EC-Earth3	0.12	0.13	0.13	0.13	0.14
GISS-E2-1-G	0.14	0.17	0.16	0.17	0.16
IPSL-CM6A-LR	0.12	0.12	0.11	0.12	0.11
MIROC6	0.08	0.09	0.09	0.10	0.09
MIROC-ES2L	0.06	0.06	0.05	0.06	0.05
MPI-ESM1-2-HR	0.12	0.14	0.14	0.15	0.14
MPI-ESM1-2-LR	0.12	0.14	0.14	0.13	0.14
MRI-ESM2-0	0.1	0.11	0.11	0.11	0.11
NorESM2-LM	0.12	0.12	0.13	0.11	0.13

TaiESM1	0.10	0.11	0.10	0.10	0.10
UKESM1-0-LL	0.10	0.09	0.10	0.10	0.10
Mean	0.11	0.11	0.11	0.11	0.12

2.1.2 Air temperature

2.1.2.1 Empirical Orthogonal Function patterns

The procedure of the EOF analysis for air temperature was detailed in Wang et al. [2024]. Figures A1.5a-d and Figures A1.6a-d (Appendix 1), respectively, show the EOF1 patterns and the PC1s from the 22 CMIP6 models. The generally warm pattern was the common feature of the EOF1s from all 22 models and their four climate scenarios, and the warming pattern was prominent over land areas. It is noticeable that many of the models and scenarios show a cooling pattern over the subpolar North Atlantic Ocean, e.g., CESM2, CESM2-WACCM, CNRM-CM6-1, CNRM-ESM2-1, EC-Earth3. The PC1s of these models demonstrated an increasing trend in the 2015-2059 period. The PC1 represented the variations of the northern hemisphere surface temperature (NH-ST; Wang et al., 2024). The standard deviations of the PC1s from the 22 models, including the historical and projected periods, were calculated and listed in Table 2.1.5. Many of the 22 models and the ensemble means suggested that the standard deviations for the four scenarios increased from SSP126 to SSP585, indicating the warming-associated events will have increasing variability with increasing GHG emissions. The ensemble mean of the historical period was between SSP126 and SSP245.

Table 2.1.5 Standard deviations of the PC1s of the air temperature for the historical period and four scenarios.

models	hist	SSP126	SSP245	SSP370	SSP585
ACCESS-CM2	1.59	2.29	2.78	2.65	3.25
ACCESS-ESM1-5	2.28	1.64	2.51	2.29	3.12
AWI-CM-1-1-MR	1.80	1.33	1.84	2.22	2.56
CAMS-CSM1-0	1.12	1.16	1.45	1.72	1.75
CanESM5	2.46	2.16	3.18	3.99	4.38
CESM2	1.95	2.01	2.19	2.36	2.78
CESM2-WACCM	2.10	1.58	2.09	2.31	2.91
CMCC-CM2-SR5	2.17	2.83	2.98	2.99	3.63
CNRM-CM6-1	2.12	1.57	1.90	2.56	2.88

CNRM-CM6-1-HR	1.59	1.80	2.24	2.22	2.89
CNRM-ESM2-1	2.01	1.32	1.54	1.81	2.41
EC-Earth3	3.41	1.48	2.10	2.31	3.27
GISS-E2-1-G	1.55	1.97	1.85	2.30	2.55
IPSL-CM6A-LR	1.72	2.02	2.32	3.29	3.46
MIROC6	1.53	1.94	2.38	2.77	2.95
MIROC-ES2L	1.69	1.78	2.08	2.26	3.11
MPI-ESM1-2-HR	1.36	1.21	1.51	2.03	2.15
MPI-ESM1-2-LR	1.73	1.15	1.84	1.93	2.20
MRI-ESM2-0	1.78	1.41	2.16	2.32	2.59
NorESM2-LM	2.03	1.32	1.68	1.92	2.24
TaiESM1	2.06	2.65	2.84	3.27	4.00
UKESM1-0-LL	2.59	2.88	3.55	4.05	4.81
Mean	1.94	1.80	2.23	2.53	3.00

Table 2.1.6 lists the variances explained by the EOF2s. The ensemble means and most of the individual models showed that the explained variances by the EOF1s increased from SSP126 to SSP585, suggesting that the warming signals will become more dominant with increasing GHG emissions.

Table 2.1.6 The variances explained by the EOF1s of the air temperature for the historical period and four scenarios.

models	hist	SSP126	SSP245	SSP370	SSP585
ACCESS-CM2	0.32	0.49	0.60	0.58	0.65
ACCESS-ESM1-5	0.48	0.33	0.55	0.48	0.66
AWI-CM-1-1-MR	0.36	0.24	0.39	0.49	0.54
CAMS-CSM1-0	0.18	0.21	0.27	0.37	0.35
CanESM5	0.48	0.45	0.67	0.77	0.80

CESM2	0.40	0.43	0.52	0.54	0.63
CESM2-WACCM	0.44	0.33	0.46	0.51	0.63
CMCC-CM2-SR5	0.44	0.60	0.58	0.56	0.67
CNRM-CM6-1	0.39	0.28	0.37	0.52	0.55
CNRM-CM6-1-HR	0.35	0.43	0.53	0.52	0.63
CNRM-ESM2-1	0.41	0.21	0.26	0.35	0.49
EC-Earth3	0.65	0.27	0.43	0.49	0.65
GISS-E2-1-G	0.26	0.40	0.38	0.49	0.52
IPSL-CM6A-LR	0.35	0.42	0.51	0.68	0.72
MIROC6	0.26	0.38	0.48	0.59	0.59
MIROC-ES2L	0.31	0.37	0.44	0.48	0.64
MPI-ESM1-2-HR	0.25	0.23	0.30	0.44	0.46
MPI-ESM1-2-LR	0.34	0.21	0.40	0.40	0.48
MRI-ESM2-0	0.38	0.3	0.51	0.58	0.58
NorESM2-LM	0.41	0.24	0.33	0.39	0.44
TaiESM1	0.41	0.57	0.58	0.64	0.73
UKESM1-0-LL	0.50	0.60	0.71	0.74	0.81
Mean	0.38	0.36	0.47	0.53	0.60

Figures A1.7a-d and Figures A1.8a-d (Appendix 1), respectively, show the EOF2 patterns and PC2s from the 22 CMIP6 models. The patterns of the EOF2s were more complicated than those of EOF1s, and differences among the four scenarios in each model and among the 22 models were noticeable, as well as differences between historical and projected periods. The PC2 was found to be correlated with NAO/AO (Wang et al., 2024). The PC2s showed variations at timescales from interannual to decadal and even longer. The standard deviations of the PC2s from the 22 models, including the historical and projected periods, were calculated and listed in Table 2.1.7. No clear pattern can be established for the standard deviations of the four scenarios, but many of the 22 models and the ensemble means suggested that the PC2s of the future scenarios have smaller variability than the historical period.

Table 2.1.7 Standard deviations of the PC2s of the air temperature for the historical period and four scenarios

models	hist	SSP126	SSP245	SSP370	SSP585
ACCESS-CM2	0.90	1.02	0.83	0.84	0.91
ACCESS-ESM1-5	0.84	0.94	0.85	1.03	1.00
AWI-CM-1-1-MR	0.95	0.98	0.94	0.95	1.03
CAMS-CSM1-0	0.87	0.84	0.95	0.85	0.95
CanESM5	1.13	1.10	0.97	0.98	0.95
CESM2	1.09	1.03	0.81	1.00	0.89
CESM2-WACCM	1.13	0.96	1.00	1.13	1.04
CMCC-CM2-SR5	1.23	1.19	1.48	1.55	1.54
CNRM-CM6-1	1.25	1.01	1.09	1.03	1.28
CNRM-CM6-1-HR	0.78	0.79	0.83	0.86	0.88
CNRM-ESM2-1	0.98	1.02	1.22	0.94	1.07
EC-Earth3	1.04	1.11	1.01	1.02	1.01
GISS-E2-1-G	1.32	1.25	1.10	1.19	1.15
IPSL-CM6A-LR	1.04	1.01	0.94	0.99	0.87
MIROC6	1.26	1.24	1.11	0.98	1.15
MIROC-ES2L	1.27	1.2	1.25	1.22	1.20
MPI-ESM1-2-HR	1.04	0.99	0.87	0.89	0.91
MPI-ESM1-2-LR	1.16	0.96	1.03	1.16	1.06
MRI-ESM2-0	0.98	0.87	0.89	0.74	1.09
NorESM2-LM	1.02	1.17	1.24	1.12	1.36
TaiESM1	1.05	0.98	1.17	0.98	1.01
UKESM1-0-LL	1.23	0.91	0.86	1.04	0.94
Mean	1.07	1.03	1.02	1.02	1.06

Table 2.1.8 lists the variances explained by the EOF2s. The ensemble means and most of the individual models showed that the explained variances by the EOF2s decrease from SSP126 to SSP585, suggesting that this mode will become less dominant with increasing GHG emissions.

Table 2.1.8 The variances explained by the EOF2s of the air temperature for the historical period and four scenarios

models	hist	SSP126	SSP245	SSP370	SSP585
ACCESS-CM2	0.10	0.10	0.05	0.06	0.05
ACCESS-ESM1-5	0.07	0.11	0.06	0.10	0.07
AWI-CM-1-1-MR	0.10	0.13	0.10	0.09	0.09
CAMS-CSM1-0	0.11	0.11	0.12	0.09	0.10
CanESM5	0.10	0.12	0.06	0.05	0.04
CESM2	0.13	0.11	0.07	0.10	0.06
CESM2-WACCM	0.13	0.12	0.11	0.12	0.08
CMCC-CM2-SR5	0.14	0.11	0.14	0.15	0.12
CNRM-CM6-1	0.13	0.12	0.12	0.09	0.11
CNRM-CM6-1-HR	0.09	0.08	0.07	0.08	0.06
CNRM-ESM2-1	0.10	0.13	0.16	0.09	0.10
EC-Earth3	0.06	0.15	0.10	0.10	0.06
GISS-E2-1-G	0.19	0.16	0.14	0.13	0.11
IPSL-CM6A-LR	0.13	0.11	0.08	0.06	0.05
MIROC6	0.18	0.15	0.10	0.07	0.09
MIROC-ES2L	0.18	0.17	0.16	0.14	0.09
MPI-ESM1-2-HR	0.15	0.15	0.10	0.08	0.08
MPI-ESM1-2-LR	0.15	0.14	0.13	0.14	0.11
MRI-ESM2-0	0.12	0.11	0.09	0.06	0.10

NorESM2-LM	0.11	0.18	0.18	0.13	0.16
TaiESM1	0.11	0.08	0.10	0.06	0.05
UKESM1-0-LL	0.11	0.06	0.04	0.05	0.03
Mean	0.12	0.12	0.10	0.09	0.08

2.1.2.2 Projected trends

The trends from all four scenarios in each model were calculated and shown in Figures A1.9a-d (Appendix 1). It was clear that the warming trend gets stronger from SSP126 to SSP585 in each model, which demonstrated a known fact that increasing GHG emissions will result in higher air temperatures. It was also noticeable that the air temperature over the subpolar North Atlantic Ocean had a cooling trend in many of the 22 models, and the cooling trends decreased from SSP126 to SSP585. The ensemble means and medians (Figure A1.9d) clearly showed the warming trend increases from SSP126 to SSP585, and the cooling trend of air temperature over the subpolar North Atlantic Ocean decreased from SSP126 to SSP585.

2.2 Changes in the three oceans

2.2.1 North Atlantic Ocean

2.2.1.1 Empirical Orthogonal Function patterns

We followed the EOF approach used in Wang et al. [2024] to analyze the SST for the North Atlantic Ocean. The EOF1s and PC1s are shown in Figures A2.1a-d and FiguresA2.2a-d, respectively (Appendix 2). The general patterns in the EOF1s from the four scenarios in each model were similar, though the magnitudes of the positive and/or negative portions were different. However we observed that the patterns were generally different from one model to another, indicating that large variations of the SST represented by the first mode among these models. Wang et al. [2024] suggested that the PC1 represents the AMO (Atlantic Multi-decadal Oscillation). The majority of the 22 models showed that the PC1s had increasing trends except for ACCESS-ESM1-5 and CAMS-CEMS1-0, and these two models showed strong multi-year variations for most of the four scenarios. The standard deviations of the PC1s from the 22 models, including the historical and projected periods, were calculated and listed in Table 2.2.1. The ensemble means of the standard deviation and the standard deviations of many models suggested that the standard deviation will increase with the increasing GHG emissions, and the historical ensemble mean was in between the ensemble means of SSP126 and SSP245.

Table 2.2.1 Standard deviations of the SST PC1s of the historical period and four scenarios

Models	hist	SSP126	SSP245	SSP370	SSP585
ACCESS-CM2	1.22	1.40	1.62	1.69	1.47
ACCESS-ESM1-5	1.91	1.54	1.44	1.65	1.59
AWI-CM-1-1-MR	1.42	0.93	1.24	1.55	1.82
CAMS-CSM1-0	1.61	1.58	1.48	1.90	1.51

CanESM5	1.60	1.70	1.71	2.30	2.59
CESM2	1.20	1.77	1.32	1.32	1.58
CESM2-WACCM	1.21	1.61	1.20	1.13	1.53
CMCC-CM2-SR5	1.17	1.92	2.17	2.09	2.22
CNRM-CM6-1	1.57	1.00	1.19	1.40	1.62
CNRM-CM6-1-HR	0.98	1.01	1.16	1.10	1.58
CNRM-ESM2-1	1.61	1.39	1.23	1.27	1.34
EC-Earth3	3.30	1.12	1.35	1.50	1.99
GISS-E2-1-G	0.74	1.15	1.20	1.34	1.54
IPSL-CM6A-LR	1.09	1.34	1.32	1.81	2.18
MIROC6	1.05	1.17	1.29	1.28	1.43
MIROC-ES2L	0.99	0.99	1.24	1.27	1.76
MPI-ESM1-2-HR	0.94	0.97	0.98	1.10	1.4
MPI-ESM1-2-LR	1.10	0.78	1.08	1.31	1.04
MRI-ESM2-0	0.94	1.49	1.81	1.43	1.82
NorESM2-LM	1.15	1.64	1.19	1.04	1.43
TaiESM1	1.00	1.24	1.16	1.49	1.91
UKESM1-0-LL	1.96	1.43	1.67	2.15	2.39
Mean	1.35	1.32	1.37	1.51	1.71

Table 2.2.2 lists the variances accounted for by the EOF1s. The ensemble means and most individual models showed that the variances accounted for by the EOF1s increased from SSP126 to SSP585, suggesting that this mode will become more and more dominant with the increasing GHG emissions.

Table 2.2.2 The variances explained by the SST EOF1s of the historical period and four scenarios

Models	hist	SSP126	SSP245	SSP370	SSP585
ACCESS-CM2	0.25	0.25	0.32	0.38	0.28

ACCESS-ESM1-5	0.48	0.33	0.30	0.34	0.35
AWI-CM-1-1-MR	0.38	0.22	0.32	0.44	0.52
CAMS-CSM1-0	0.32	0.35	0.29	0.41	0.28
CanESM5	0.41	0.49	0.52	0.65	0.74
CESM2	0.48	0.60	0.51	0.46	0.58
CESM2-WACCM	0.44	0.56	0.47	0.43	0.59
CMCC-CM2-SR5	0.35	0.63	0.70	0.69	0.67
CNRM-CM6-1	0.47	0.2	0.3	0.4	0.44
CNRM-CM6-1-HR	0.33	0.33	0.39	0.36	0.55
CNRM-ESM2-1	0.50	0.39	0.32	0.33	0.37
EC-Earth3	0.71	0.25	0.33	0.37	0.53
GISS-E2-1-G	0.24	0.43	0.47	0.53	0.59
IPSL-CM6A-LR	0.30	0.36	0.33	0.51	0.61
MIROC6	0.32	0.37	0.41	0.47	0.48
MIROC-ES2L	0.28	0.27	0.39	0.35	0.52
MPI-ESM1-2-HR	0.23	0.22	0.22	0.28	0.37
MPI-ESM1-2-LR	0.29	0.18	0.31	0.41	0.30
MRI-ESM2-0	0.25	0.52	0.6	0.55	0.60
NorESM2-LM	0.35	0.51	0.37	0.31	0.46
TaiESM1	0.39	0.55	0.44	0.60	0.69
UKESM1-0-LL	0.57	0.31	0.43	0.57	0.61
Mean	0.38	0.38	0.40	0.45	0.51

The EOF2s and PC2s are shown in Figures A2.3a-d and FiguresA2.4a-d (Appendix 2), respectively. Similar to the EOF1s, the general patterns in the EOF2s from the four scenarios in each model were similar, though magnitudes in positive and/or negative portions were different. The EOF2s from most of the models showed positive patterns in high and low latitudes and negative patterns in between. This tri-

polar pattern was commonly known to be the NAO-related pattern, and the PC2 was found to be correlated with NAO/AO (Wang et al. 2024). The PC2s from all the models clearly showed variations at timescales from inter-annual to decadal, and to even longer. The standard deviations of the PC2s from the 22 models, including the historical and projected periods, were calculated and listed in Table 2.2.3. No clear pattern in the standard deviation ensembles could be seen from low emission scenario SSP126 to high emission scenario SSP585, indicating the complexity of this NAO-related mode, and that the SST uncertainty associated with this mode was high. The ensemble means tended to suggest the variations of the SST from this mode will be not smaller than the historical period.

Table 2.2.3 Standard deviations of the PC2s of the historical period and four scenarios

Models	hist	SSP126	SSP245	SSP370	SSP585
ACCESS-CM2	0.94	1.31	1.23	1.07	1.35
ACCESS-ESM1-5	1.08	1.28	1.31	1.18	1.29
AWI-CM-1-1-MR	0.74	0.68	0.86	0.72	0.66
CAMS-CSM1-0	1.03	0.94	1.19	1.03	1.20
CanESM5	0.97	0.71	0.88	0.75	0.66
CESM2	0.59	0.73	0.61	0.76	0.62
CESM2-WACCM	0.73	0.74	0.59	0.6	0.63
CMCC-CM2-SR5	0.82	0.72	0.71	0.67	0.88
CNRM-CM6-1	0.73	0.91	0.81	0.69	0.93
CNRM-CM6-1-HR	0.54	0.63	0.67	0.61	0.65
CNRM-ESM2-1	0.69	0.83	0.79	0.90	0.88
EC-Earth3	1.06	0.95	0.85	1.01	0.95
GISS-E2-1-G	0.70	0.68	0.56	0.65	0.61
IPSL-CM6A-LR	0.71	0.81	0.93	0.90	0.76
MIROC6	0.71	0.77	0.71	0.57	0.71
MIROC-ES2L	0.80	0.83	0.77	1.06	0.97
MPI-ESM1-2-HR	0.69	0.80	0.77	0.78	0.81
MPI-ESM1-2-LR	0.69	0.71	0.65	0.61	0.74

MRI-ESM2-0	0.83	0.68	0.66	0.51	0.70
NorESM2-LM	0.77	0.79	0.73	0.70	0.72
TaiESM1	0.62	0.51	0.76	0.59	0.70
UKESM1-0-LL	0.91	1.27	0.94	1.03	0.96
Mean	0.79	0.83	0.82	0.79	0.83

Table 2.2.4 lists the variances accounted for by the EOF2s. The ensemble means and most of the individual models showed that the variances accounted for by the EOF2s decrease from SSP126 to SSP585, suggesting that this mode will become less dominant with increasing GHG emissions, as was opposite to the role of EOF1s. The historical variance was the same as for SSP245.

Table 2.2.4 The variances explained by the SST EOF2s of the historical period and the four scenarios

models	hist	SSP126	SSP245	SSP370	SSP585
ACCESS-CM2	0.15	0.22	0.19	0.15	0.24
ACCESS-ESM1-5	0.15	0.22	0.25	0.17	0.23
AWI-CM-1-1-MR	0.10	0.12	0.15	0.10	0.07
CAMS-CSM1-0	0.13	0.12	0.19	0.12	0.18
CanESM5	0.15	0.08	0.14	0.07	0.05
CESM2	0.12	0.10	0.11	0.15	0.09
CESM2-WACCM	0.16	0.12	0.11	0.12	0.10
CMCC-CM2-SR5	0.17	0.09	0.07	0.07	0.11
CNRM-CM6-1	0.10	0.17	0.14	0.10	0.14
CNRM-CM6-1-HR	0.10	0.13	0.13	0.11	0.09
CNRM-ESM2-1	0.09	0.14	0.13	0.16	0.16
EC-Earth3	0.07	0.18	0.13	0.17	0.12
GISS-E2-1-G	0.22	0.15	0.10	0.12	0.09
IPSL-CM6A-LR	0.13	0.13	0.16	0.13	0.07

MIROC6	0.15	0.16	0.13	0.09	0.12
MIROC-ES2L	0.18	0.19	0.15	0.25	0.16
MPI-ESM1-2-HR	0.12	0.15	0.14	0.14	0.12
MPI-ESM1-2-LR	0.11	0.15	0.11	0.09	0.15
MRI-ESM2-0	0.20	0.11	0.08	0.07	0.09
NorESM2-LM	0.16	0.12	0.14	0.14	0.11
TaiESM1	0.15	0.09	0.18	0.09	0.09
UKESM1-0-LL	0.12	0.24	0.14	0.13	0.1
Mean	0.14	0.15	0.14	0.12	0.12

2.2.1.2 Projected trends

The trends from the 22 models for the four climate scenarios in the 2015-2059 period were calculated and shown in Figures A2.5a-d (Appendix 2). Though the patterns from the four SSPs in each model were generally consistent, the differences among the 22 models were obvious, not just in their magnitudes, but also in their patterns. The most prominent difference was that some models project a general future warming in the subpolar region, while other models suggested a cooling pattern in the future. The warming patterns got stronger from SSP126 to SSP585 in each model, which was consistent with common knowledge that increasing GHG emissions can result in increasing SST, and warming patterns were shown in the low to mid-latitudes in the majority of these models.

We also calculated the means and medians of the 22 models for the SST trends (bottom two panels of Figure A2.5d [Appendix 2]), and they were consistent in pattern and magnitude. It was clear that low to mid-latitudes had warming trends, and the warming trends increased from SSP126 to SSP585. The strongest trends were in an open ocean region to the southeast of Newfoundland, and the waters on and off the Scotian Shelf had strong warming trends as well. In the subpolar region, there was a general cooling trend, however the cooling trend decreased from SSP126 to SSP585.

2.2.1.3 Projected changes

In order to provide information on SST changes from the projections in the four climate scenarios, changes in the decadal means for the 2030-2039, 2040-2049 and 2050-2059 periods relative to the 30-year climatology of the historical period of 1985 – 2014 were calculated and shown in Figure 2.2.1 in black. We also calculated those changes in the medians and these were shown in Figure 2.2.1 as well in red. In the projected changes for the three decades, the decadal mean SST warm anomalies increased from SSP126 to SSP585, as was consistent with the trends in the four scenarios. We noticed that the decadal mean cold anomalies in the subpolar region clearly got stronger from the first decade to the third decade in SSP126, and this tendency was not as clear as that in the other three scenarios. In SSP126, the cold anomaly in the eastern subpolar region reached about -1.0^{o}C in 2050-2069 period. The strongest warm anomalies were in the region to the southeast of Newfoundland, and SST anomalies were above 2^{o}C there starting from 2040-2049. The changes in medians showed similar features as those in the means, however the magnitudes in the medians were stronger than those in the means.

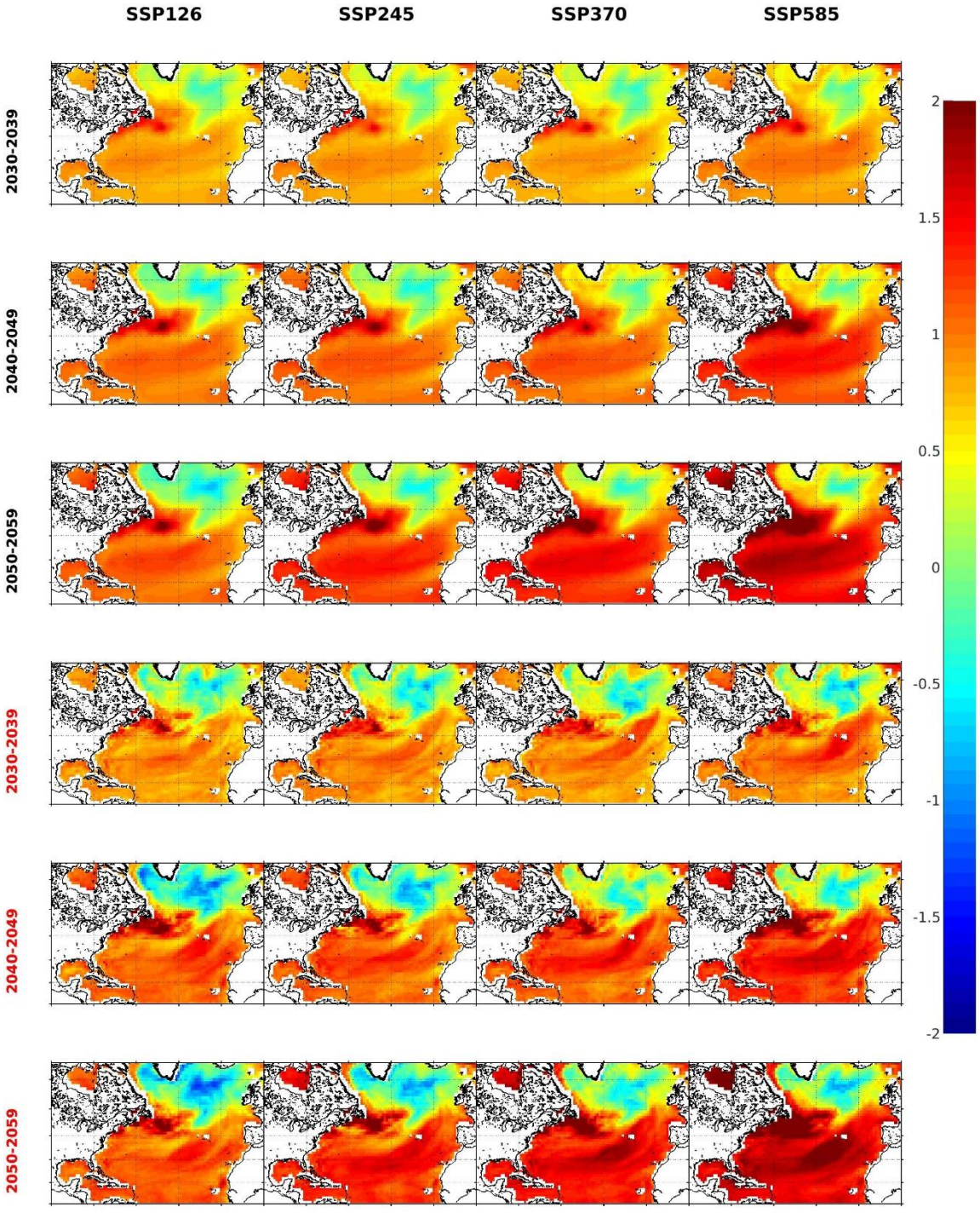

Figure 2.2.1. Changes in decadal SST between three future decades and the historical climatology of the 1985-2014 period. Periods in black for means, those in red for medians. Unit: ºC.

The evaluation of the CMIP6 models by Wang et al. [2024] ranked the 22 CMIP6 models based on their performances in the representation of the SST from HadISST. Here we attempted to project the SST changes for the three decades based on ensemble means using different numbers of the top models listed in Table 3.1 in Wang et al. [2024]. The model scores used in ranking these models there are defined as the combined normalized correlation coefficients between the modeled principal components and the observed ones. Details on this methodology can be found in Wang et al. [2024]. Figures 2.2.2a-b showed the projected changes for the four scenarios using 1 to 12 top-models means for the period of 2030-2039, Figures 2.2.3a-b for 2040-2049, and Figures 2.2.4a-b for 2050-2059. It was clear that the means from the top one model and top two models had different patterns of SST changes than other ensemble means using more than just top two models for the most of the four scenarios in the three decades. The big difference was the subpolar region, and the means from the top 1 model and the top two models showed a cooling pattern in the eastern part of the subpolar gyre, however when calculating ensemble means using top three or more models, the cooling pattern occupied most of the subpolar region. Apparently, the means of the top one and the top two model produced stronger warm anomalies than those using top three or more models. With the number of top models used in the ensemble increasing, the means started to resemble the ensemble means shown in Figure 2.2.6.

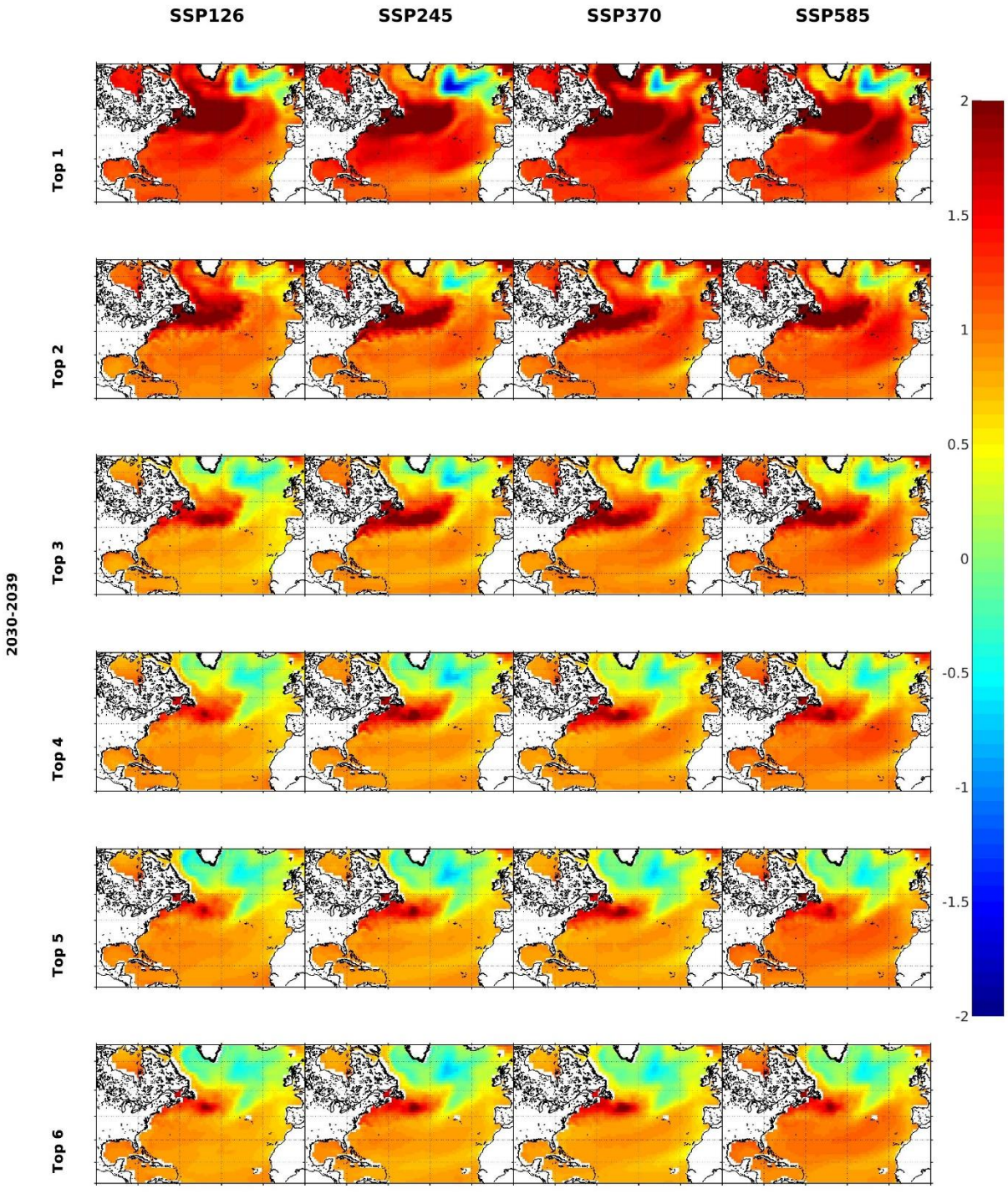

Figure 2.2.2a. Ensemble mean SST changes between period of 2030-2039 and the historical climatology of the 1985-2014 period using top number of best models. Unit: ºC.

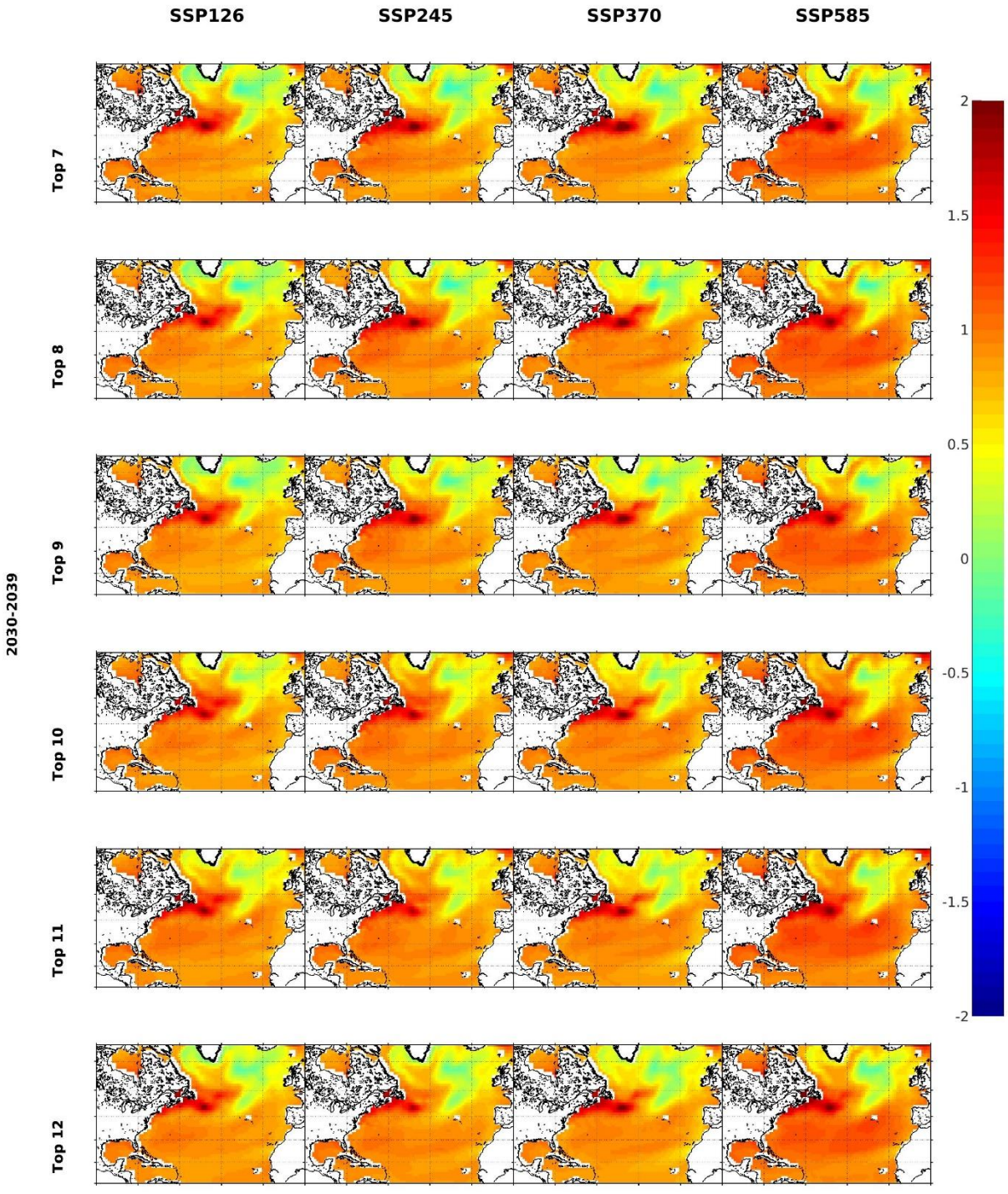

Figure 2.2.2b. Ensemble mean SST changes between period of 2030-2039 and the historical climatology of the 1985-2014 period using top number of best models. Unit: ºC.

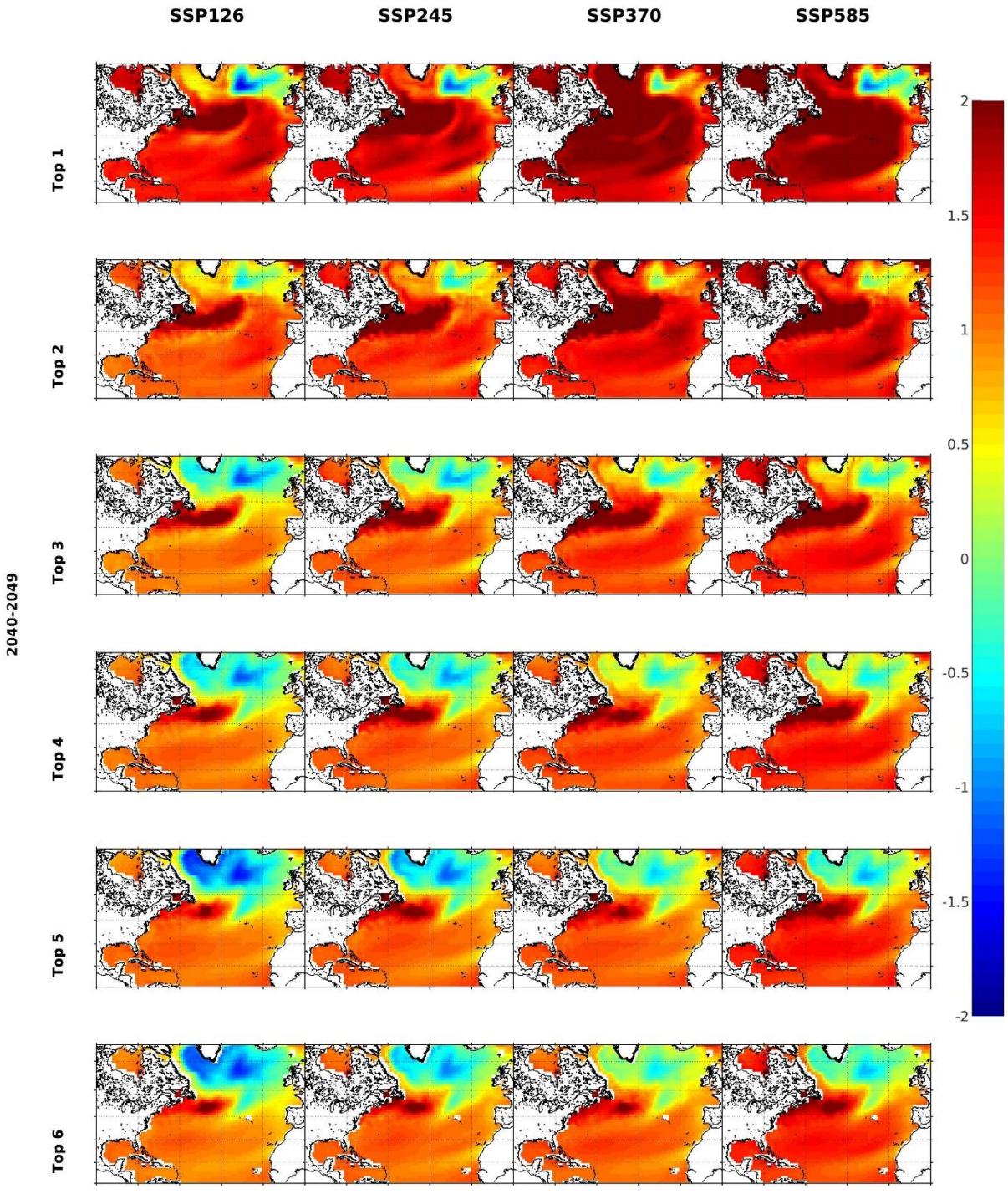

Figure 2.2.3a. Ensemble mean SST changes between the period of 2040-2049 and 1985-2014 period using top number of best models. Unit: ºC.

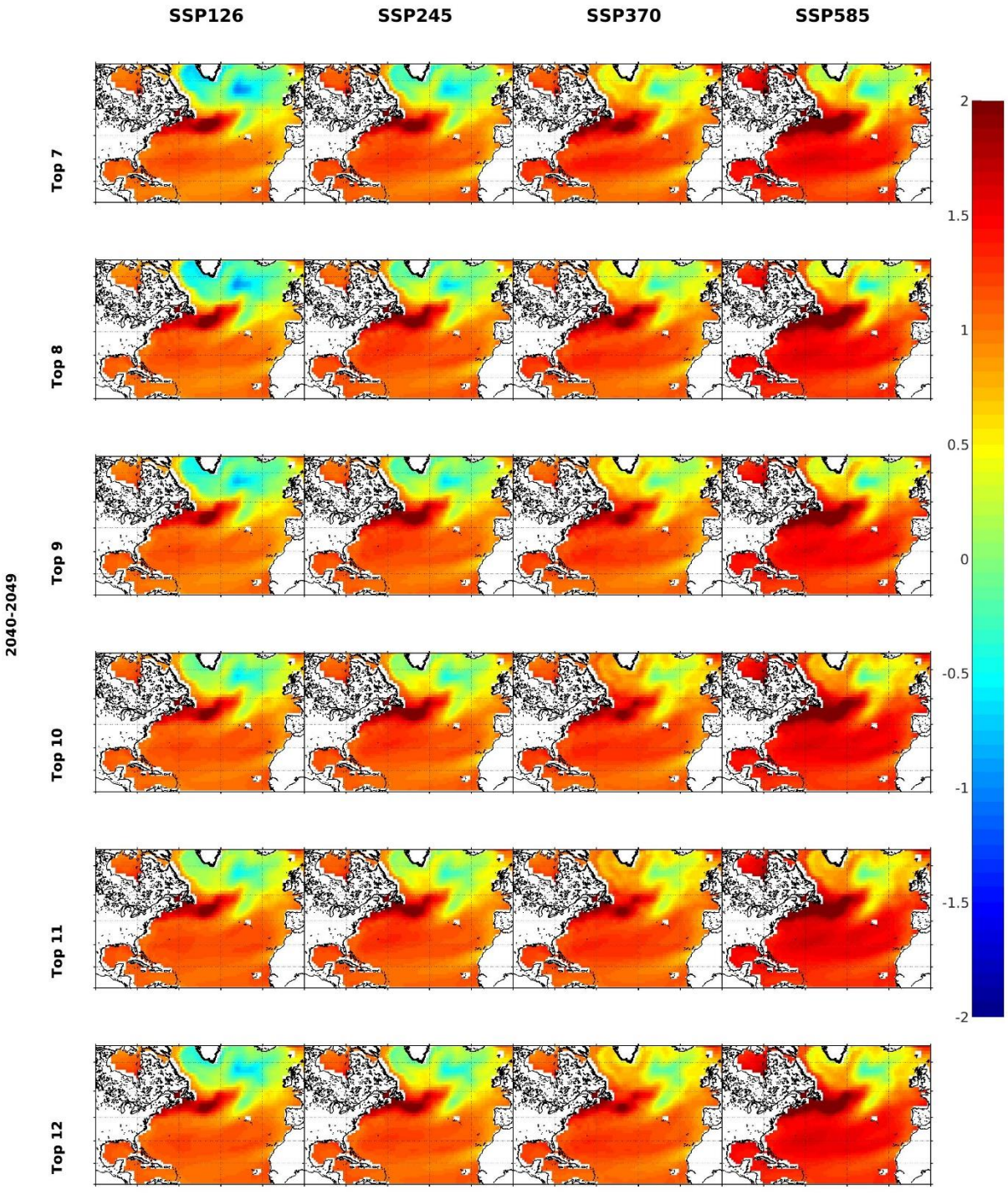

Figure 2.2.3b. Ensemble mean SST changes between period of 2040-2049 and the 1985-2014 period using top number of best models. Unit: ºC.

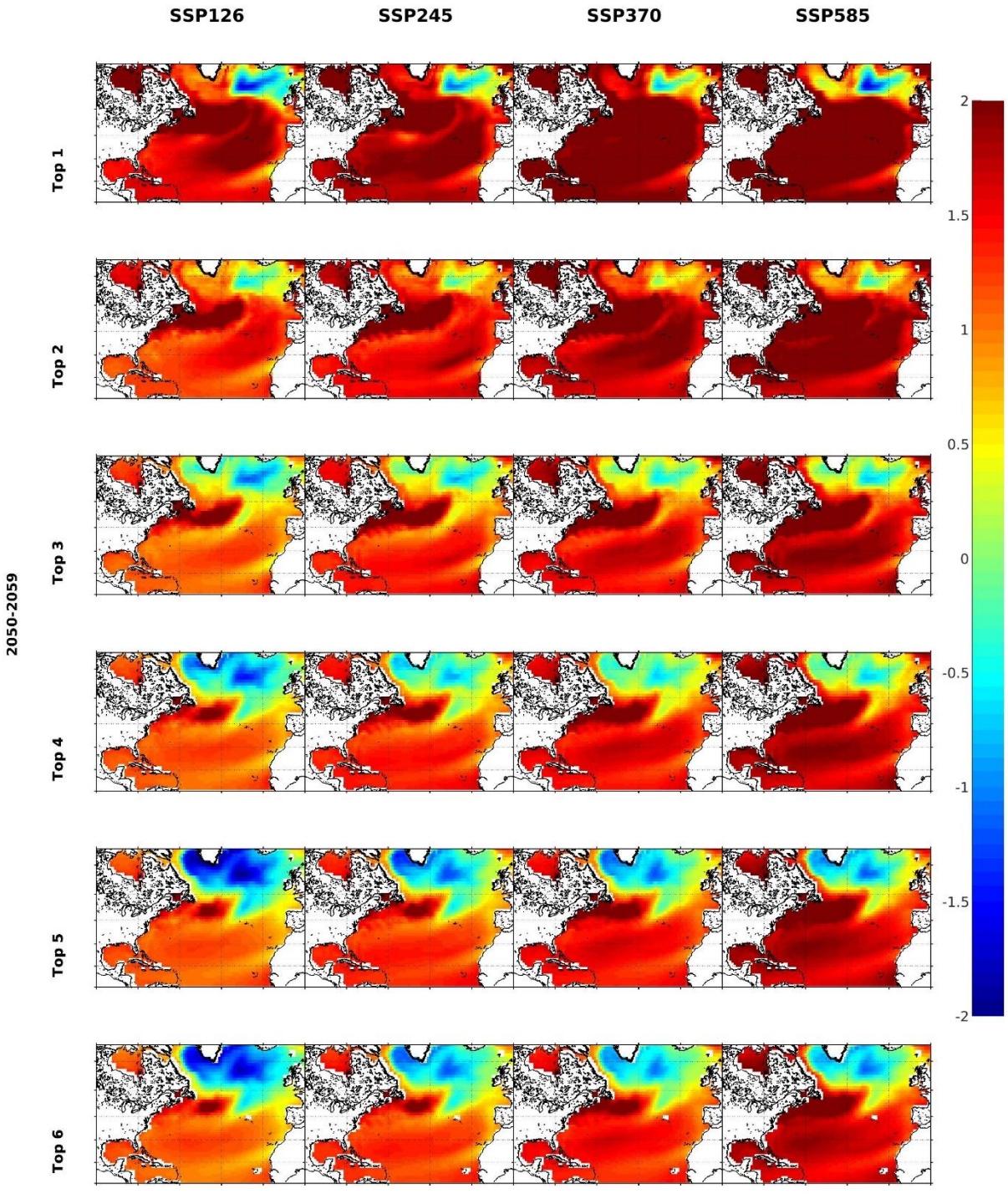

Figure 2.2.4a. Ensemble mean SST changes between period of 2050-2059 and the 1985-2014 period using top number of best models. Unit: ºC.

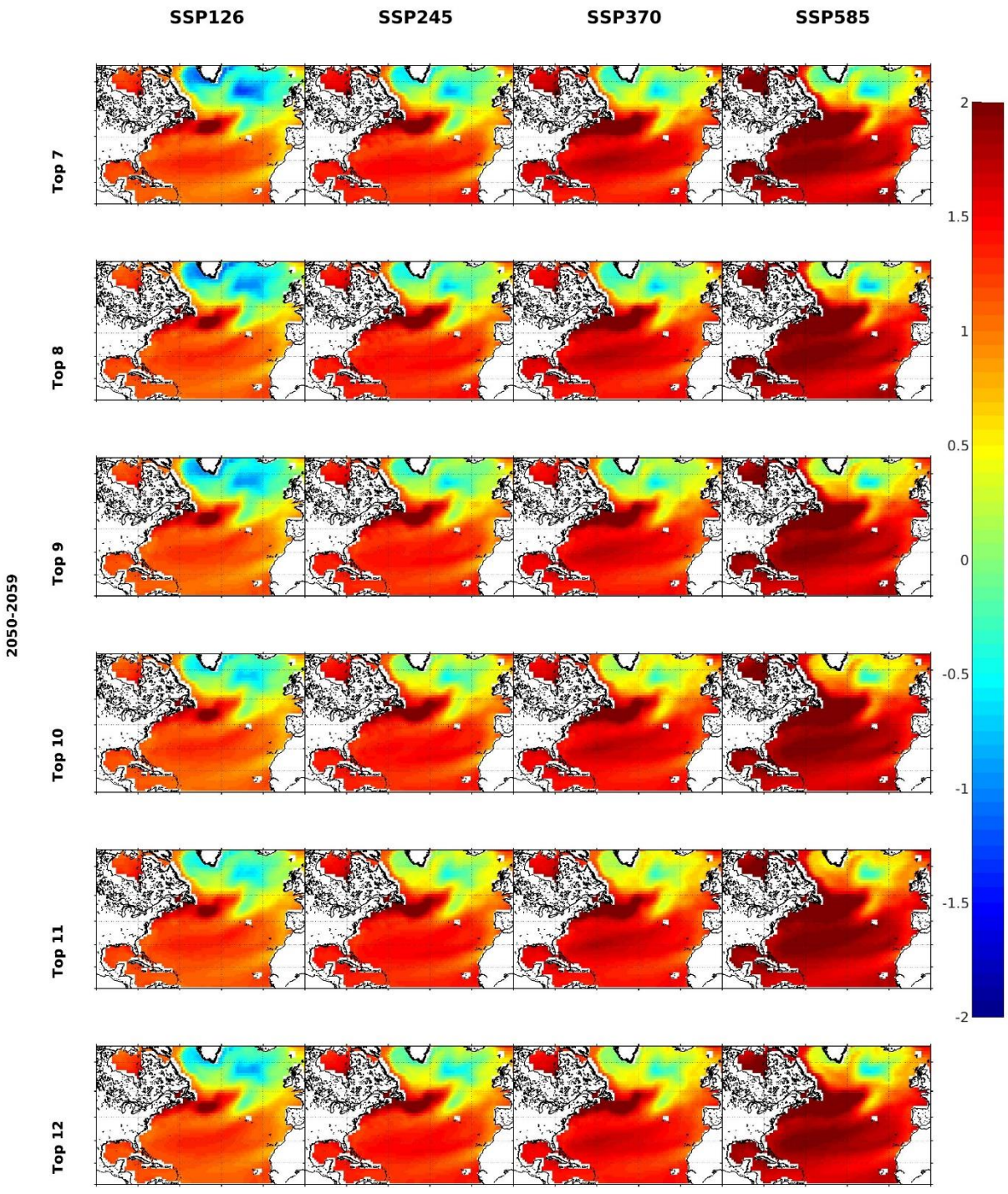

Figure 2.2.4b. Ensemble mean SST changes between period of 2050-2059 and the 1985-2014 period using top number of best models. Unit: ºC.

2.2.2 North Pacific Ocean

2.2.2.1 Empirical Orthogonal Function patterns

We followed the EOF approach used in Wang et al. [2024] to analyze the SST for the North Pacific Ocean. It was demonstrated that the CMIP6 models overestimate the warming events in the North Pacific Ocean (Wang et al., 2024), and this warming mode was in the EOF2 of the HadISST, however it was in the EOF1 of the CMIP6 models. The EOF1 of HadISST was the PDO (Pacific Decadal Oscillation) mode, and this mode became the EOF2 in the CMIP6 models' solutions. In order to compare the SST from HadISST and SST from CMIP6 models, the EOF1 and EOF2 from CMIP6 models were switched in Wang et al. [2024], while we kept the original order of the EOFs in this analysis for simplicity.

The EOF1s and PC1s from the CMIP6 models are shown in Figures A2.6a-d and Figures A2.7a-d, respectively (Appendix 2). The general patterns in the EOF1s from the four scenarios in each model were mostly similar, and differences were visible in some models, such as, AWI-CM-1-1-MR, MPI-ESM1-2-HR. Wang et al. [2024] suggested that the warming events in the SST from HadISST were represented in the PC2 and PC1 in CMIP6 models, and this warming signal was consistent with NH-ST (northern hemisphere land-ocean temperature index). The majority of the 22 models showed that the PC1s had increasing trends. The standard deviations of the PC1s from the 22 models, including the historical and projected periods, were calculated and listed in Table 2.2.5. The ensemble means of the standard deviation and the standard deviations of many models suggested that the standard deviation will increase with increasing GHG emissions. The historical ensemble mean was smaller than SSP126, which suggested the variability of the SST in its first mode (which reflects the NH-ST) will increase in response to increasing GHG emissions.

Table 2.2.5 Standard deviations of the PC1s of the historical period and four scenarios

Models	hist	SSP126	SSP245	SSP370	SSP585
ACCESS-CM2	0.94	1.54	1.79	1.60	2.02
ACCESS-ESM1-5	1.30	1.39	1.70	1.64	1.91
AWI-CM-1-1-MR	1.32	1.36	1.31	1.41	1.75
CAMS-CSM1-0	0.89	1.01	0.99	1.19	1.45
CanESM5	1.31	1.41	2.02	2.74	2.89
CESM2	1.33	1.48	1.55	1.20	1.85
CESM2-WACCM	1.57	1.22	1.50	1.43	1.85
CMCC-CM2-SR5	1.62	2.02	2.02	2.3	2.64
CNRM-CM6-1	1.35	1.16	1.14	1.36	1.68

CNRM-CM6-1-HR	0.99	1.26	1.44	1.46	1.90
CNRM-ESM2-1	1.04	0.90	0.84	1.01	1.42
EC-Earth3	1.56	1.15	1.20	1.39	1.88
GISS-E2-1-G	1.33	1.53	1.31	1.68	1.53
IPSL-CM6A-LR	1.04	1.24	1.44	1.73	1.87
MIROC6	1.33	1.35	1.21	1.55	1.54
MIROC-ES2L	1.55	1.24	1.38	1.19	1.66
MPI-ESM1-2-HR	1.11	1.03	1.20	1.09	1.21
MPI-ESM1-2-LR	1.32	1.19	1.34	1.12	1.40
MRI-ESM2-0	0.90	1.06	1.36	1.38	1.45
NorESM2-LM	1.56	1.14	1.21	1.55	2.13
TaiESM1	1.38	2.05	1.99	1.93	2.71
UKESM1-0-LL	1.59	1.61	2.01	2.53	2.98
Mean	1.29	1.33	1.45	1.57	1.90

Table 2.2.6 lists the variances accounted for by the EOF2s. The ensemble means and most individual models showed that the EOF2 variance increases from SSP126 to SSP585, suggesting that this mode will become more and more dominant with increasing GHG emissions. The ensemble variance in the historical period was smaller than that of SSP126.

Table 2.2.6 The variances explained by the EOF1s of the historical period and four scenarios

models	hist	SSP126	SSP245	SSP370	SSP585
ACCESS-CM2	0.23	0.48	0.51	0.48	0.54
ACCESS-ESM1-5	0.35	0.43	0.51	0.51	0.60
AWI-CM-1-1-MR	0.33	0.37	0.32	0.34	0.44
CAMS-CSM1-0	0.26	0.31	0.29	0.39	0.46
CanESM5	0.37	0.41	0.60	0.76	0.76

CESM2	0.39	0.41	0.46	0.37	0.6
CESM2-WACCM	0.50	0.40	0.43	0.41	0.53
CMCC-CM2-SR5	0.40	0.55	0.47	0.54	0.64
CNRM-CM6-1	0.42	0.34	0.33	0.41	0.50
CNRM-CM6-1-HR	0.34	0.47	0.48	0.51	0.59
CNRM-ESM2-1	0.34	0.25	0.21	0.30	0.48
EC-Earth3	0.46	0.33	0.39	0.45	0.55
GISS-E2-1-G	0.42	0.46	0.39	0.50	0.46
IPSL-CM6A-LR	0.31	0.35	0.47	0.56	0.59
MIROC6	0.41	0.40	0.32	0.49	0.42
MIROC-ES2L	0.43	0.37	0.37	0.34	0.47
MPI-ESM1-2-HR	0.27	0.31	0.31	0.26	0.34
MPI-ESM1-2-LR	0.33	0.36	0.35	0.27	0.38
MRI-ESM2-0	0.30	0.35	0.47	0.49	0.50
NorESM2-LM	0.41	0.30	0.32	0.42	0.59
TaiESM1	0.45	0.62	0.59	0.53	0.71
UKESM1-0-LL	0.42	0.51	0.61	0.70	0.75
Mean	0.37	0.40	0.42	0.46	0.54

The EOF2s and PC2s are shown in Figures A2.8a-d and FiguresA2.9a-d (Appendix 2), respectively. Similar to the EOF1s, the general patterns in the EOF2s from the four scenarios in each model were similar. The EOF2s from most of the models showed positive patterns in western part and negative patterns in the eastern part. This feature was the PDO pattern, and the PC2 (PC1 in Wang et al. 2024) was found to represent PDO (Wang et al. 2024). The PC2s from all the models clearly showed variations at timescales from inter-annual, to decadal and to even longer timescales. The standard deviations of the PC2s from the 22 models, including the historical and projected periods, were calculated and listed in Table 2.2.7. It was clear that the standard deviations increased from low emission scenario SSP126 to high emission scenario SSP585. The historical ensemble mean was in between SSP126 and SSP245.

Table 2.2.7 Standard deviations of the PC2s of the historical period and four scenarios

Models	Hist	SSP126	SSP245	SSP370	SSP585
ACCESS-CM2	0.74	0.86	0.89	0.86	1.00
ACCESS-ESM1-5	1.05	0.84	0.86	0.92	0.91
AWI-CM-1-1-MR	0.87	0.91	0.98	1.12	1.15
CAMS-CSM1-0	0.71	0.67	0.92	0.81	0.81
CanESM5	0.98	0.96	1.02	0.92	0.95
CESM2	1.05	1.25	1.06	1.00	0.92
CESM2-WACCM	0.96	0.87	1.26	1.20	1.21
CMCC-CM2-SR5	1.48	1.31	1.68	1.57	1.51
CNRM-CM6-1	0.85	0.96	0.80	0.82	0.89
CNRM-CM6-1-HR	0.67	0.61	0.75	0.73	0.81
CNRM-ESM2-1	0.73	0.76	0.79	0.77	0.86
EC-Earth3	1.15	1.00	0.74	0.81	1.02
GISS-E2-1-G	0.91	1.03	0.92	0.87	0.89
IPSL-CM6A-LR	0.75	0.95	0.78	0.91	0.73
MIROC6	0.79	0.97	1.10	1.02	1.12
MIROC-ES2L	1.13	0.90	1.02	1.00	1.02
MPI-ESM1-2-HR	0.86	0.59	0.83	1.04	0.78
MPI-ESM1-2-LR	1.07	0.73	1.05	0.97	1.06
MRI-ESM2-0	0.78	0.76	0.75	0.72	0.84
NorESM2-LM	1.06	1.03	0.98	1.04	0.91
TaiESM1	0.95	0.96	1.01	1.29	1.15
UKESM1-0-LL	1.22	0.90	0.99	0.89	0.99
Mean	0.94	0.90	0.96	0.97	0.98

Table 2.2.8 lists the variances accounted for by the EOF2s. The ensemble means and most individual models showed that the variances explained by the EOF2s decreased from SSP126 to SSP585, suggesting that this mode will become less dominant with increasing GHG emissions, opposite to the role of the EOF1s. The historical scenario was larger than SSP126.

Table 2.2.8 The variances explained by the EOF2s of the historical period and four scenarios

models	hist	SSP126	SSP245	SSP370	SSP585
ACCESS-CM2	0.15	0.15	0.13	0.14	0.13
ACCESS-ESM1-5	0.23	0.16	0.13	0.16	0.14
AWI-CM-1-1-MR	0.15	0.16	0.18	0.21	0.19
CAMS-CSM1-0	0.17	0.14	0.25	0.18	0.15
CanESM5	0.21	0.19	0.15	0.09	0.08
CESM2	0.25	0.29	0.22	0.26	0.15
CESM2-WACCM	0.19	0.20	0.30	0.28	0.22
CMCC-CM2-SR5	0.34	0.23	0.32	0.25	0.21
CNRM-CM6-1	0.17	0.23	0.17	0.15	0.14
CNRM-CM6-1-HR	0.15	0.11	0.13	0.13	0.11
CNRM-ESM2-1	0.17	0.18	0.19	0.17	0.18
EC-Earth3	0.25	0.25	0.15	0.15	0.16
GISS-E2-1-G	0.19	0.21	0.20	0.13	0.16
IPSL-CM6A-LR	0.16	0.21	0.14	0.15	0.09
MIROC6	0.15	0.21	0.27	0.21	0.22
MIROC-ES2L	0.23	0.19	0.20	0.24	0.18
MPI-ESM1-2-HR	0.16	0.10	0.15	0.24	0.14
MPI-ESM1-2-LR	0.21	0.13	0.21	0.20	0.22
MRI-ESM2-0	0.22	0.18	0.14	0.14	0.17
NorESM2-LM	0.19	0.24	0.21	0.19	0.11

TaiESM1	0.21	0.14	0.15	0.24	0.13
UKESM1-0-LL	0.25	0.16	0.15	0.09	0.08
Mean	0.20	0.19	0.19	0.18	0.15

2.2.2.2 Projected trends

The trends from the 22 models for the four climate scenarios for the 2015-2059 period were calculated and shown in Figures A2.10a-d (Appendix 2). The patterns of the trends for the four SSPs in each model were generally consistent, and warming trends were consistent in all 22 models. Each model showed generally gradual increasing trends from SSP126 to SSP585. No cooling trends were observed from the 22 models, though some models showed close-to-zero trends in SSP126 for the most of the North Pacific Ocean, such as CAMS-CSM1-0, MPI-ESM1-2-HR and MPI-ESM1-2-LR.

We also calculated the means and medians over the 22 models for the SST trends (bottom two panels of Figure A2.10d [Appendix 2]). Consistent warming trends in the whole North Pacific Ocean were the feature of the ensemble means, and the trends increased from SSP126 to SSP585. The patterns and magnitude of the medians of the trends from the 22 models were close to the means of the 22 models.

2.2.2.3 Projected changes

In order to provide information on the SST changes in the four climate scenarios, changes in the decadal ensemble means for the 2030-2039, 2040-2049 and 2050-2059 periods relative to the 30-year ensemble mean climatology of the historical period of 1985 – 2014 were calculated and shown in Figure 2.2.5. We also calculated ensemble medians and they are shown in Figure 2.2.5 as well. In the projected changes for the three decades, the decadal mean SST warm anomalies increased from SSP126 to SSP585, as was consistent with the trends in the four scenarios. In the 2030-2039 period, the decadal means for all four SSPs had warm anomalies less than 1.5^{o}C. A band with a large warm anomaly above 2^{o}C in the western part of the mid-North Pacific Ocean was shown in SSP245 in the period 2040-2049, and it continued to expand in SSP370 and SSP585. In 2050-2059 period, most of the North Pacific Ocean had warm anomalies above 1.5^{o}C for all four climate scenarios, and in SSP585 most of the region showed warm anomalies above 2^{o}C. The spatial pattern of the SST changes in the medians showed larger variations, but the general patterns were similar to the patterns in the means.

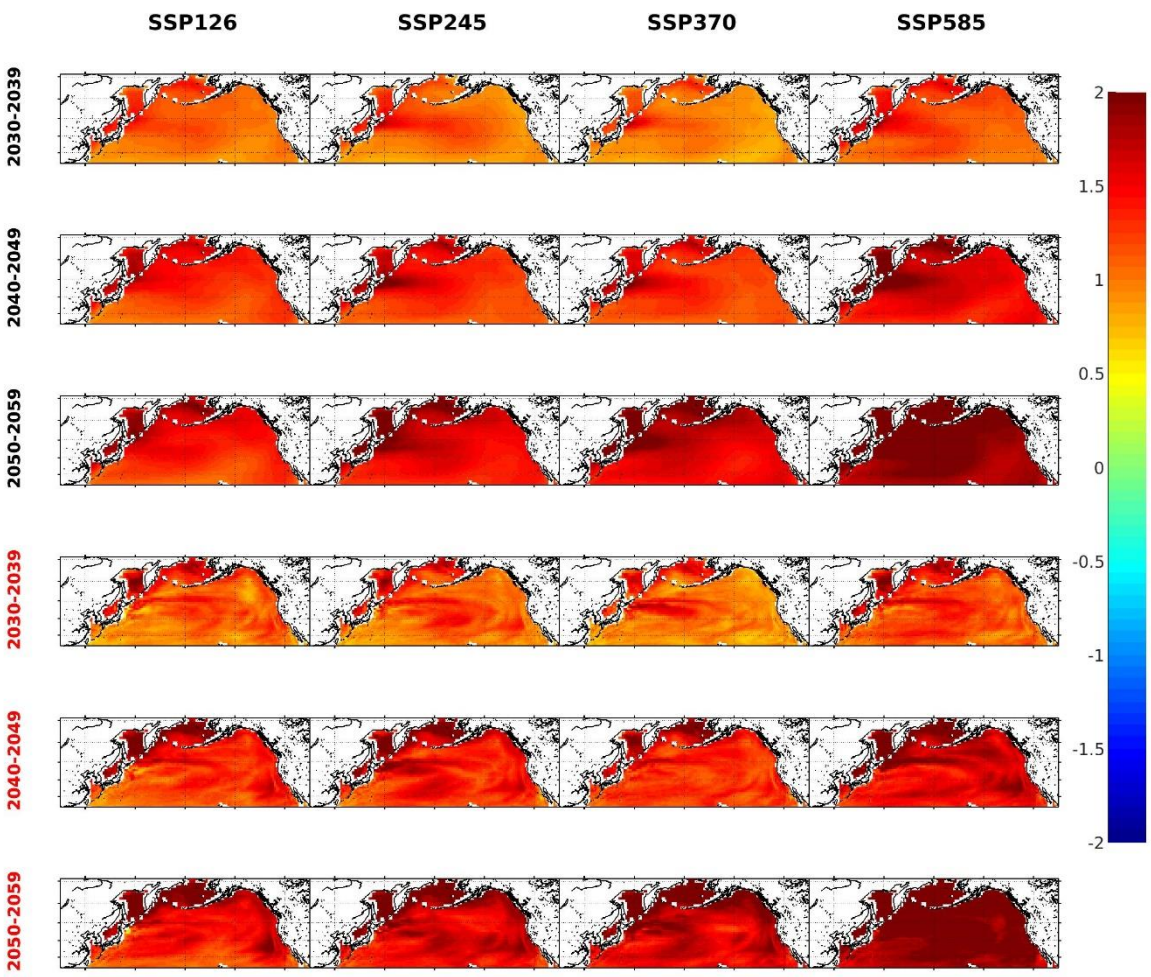

Figure 2.2.5. Changes in decadal SST ensemble means between three future decades and the historical climatology of the 1985-2014 period. Periods in black for means, those in red for medians. Unit: ºC.

The evaluation of the CMIP6 models by Wang et al. [2024] ranked the 22 CMIP6 models based on their performances in the representation of SST from the HadISST. Here we attempted to project the SST changes for the three decades based on ensemble means using different numbers of the top models listed in Table 3.1 in Wang et al. [2024]. Figures 2.2.6a-b showed the projected changes for the four scenarios using 1 to 12 top-models means for the period of 2030-2039, Figures 2.2.7a-b for 2040-2049, and Figures 2.2.8a-b for 2050-2059.

Unlike those for the North Atlantic Ocean, the ensemble means using different numbers of the top models are very similar, though the warm anomalies appeared to be slightly larger when the number of the models used was small, for the all the three decades. When the number of the models used in the ensemble increased to six, the means for all four scenarios in all three decades were similar to the means shown in Figure 2.2.5.

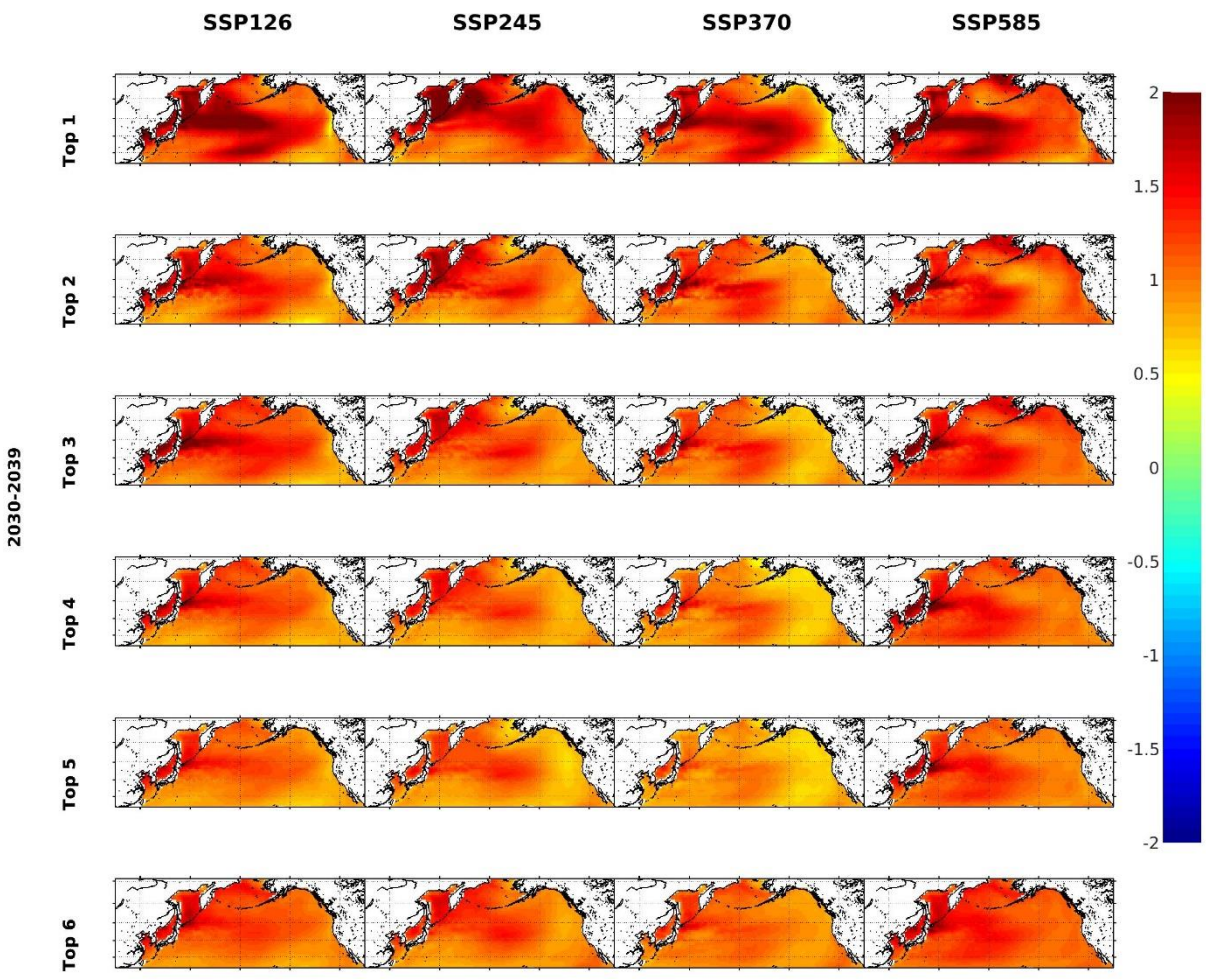

Figure 2.2.6a. Ensemble mean SST changes between period of 2030-2039 and the historical climatology of the 1985-2014 period using top number of best models. Unit: ºC.

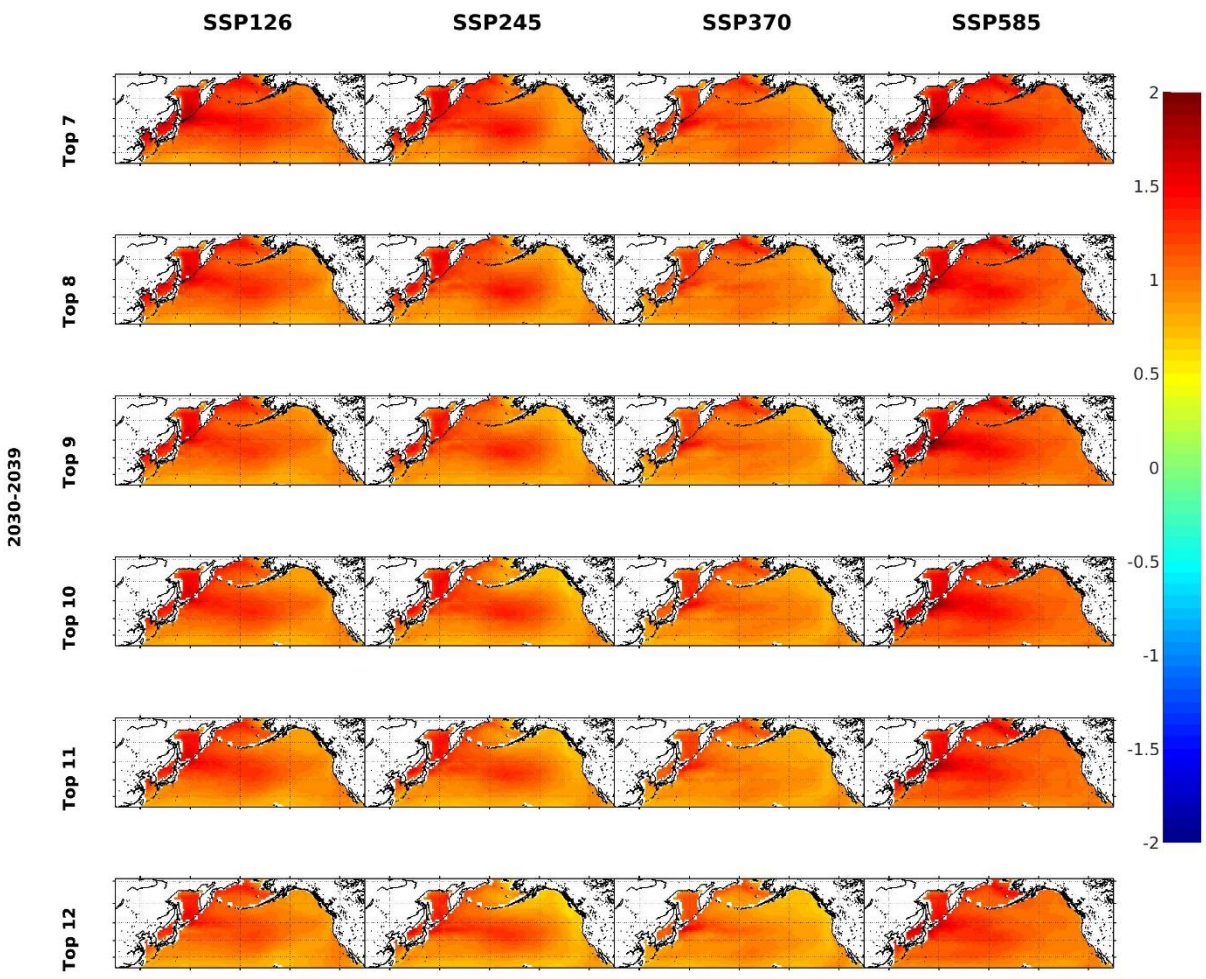

Figure 2.2.6b. Ensemble mean SST changes between period of 2030-2039 and the historical climatology of the 1985-2014 period using top number of best models. Unit: ^{o}C.

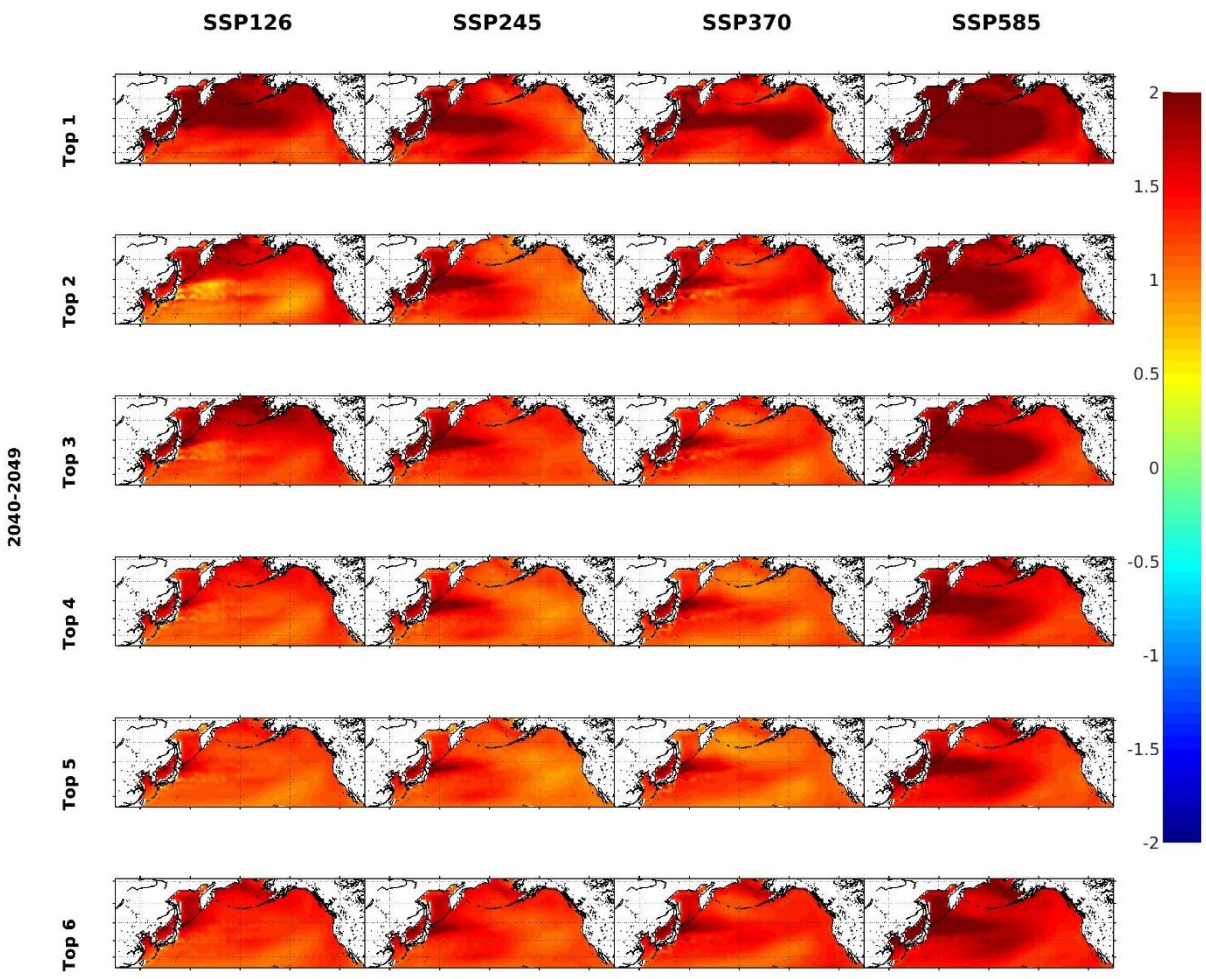

Figure 2.2.7a. Ensemble mean SST changes between period of 2040-2049 and the historical climatology of the 1985-2014 period using top number of best models. Unit: ºC.

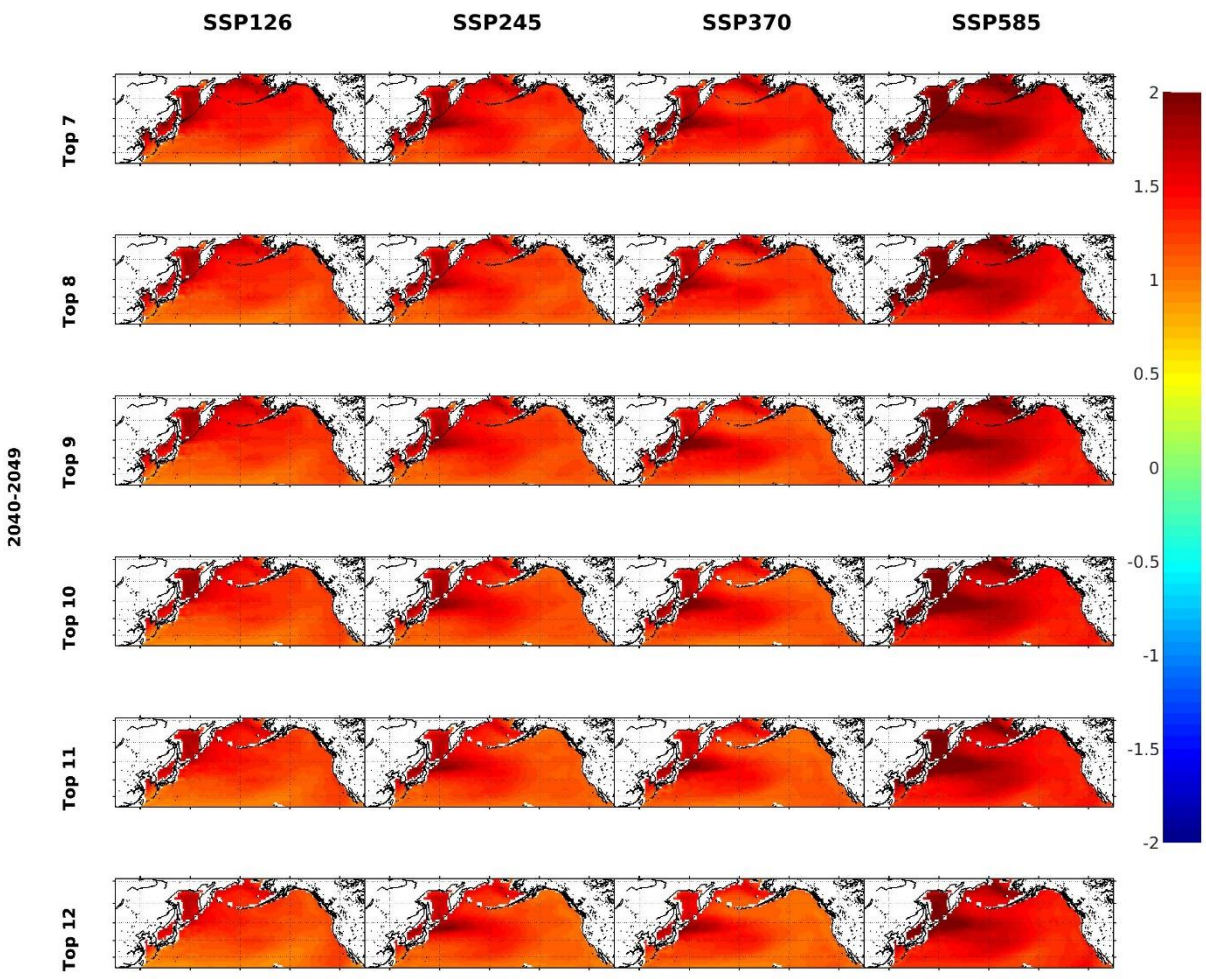

Figure 2.2.7b. Ensemble mean SST changes between period of 2040-2049 and the historical climatology of the 1985-2014 period using top number of best models. Unit: ºC.

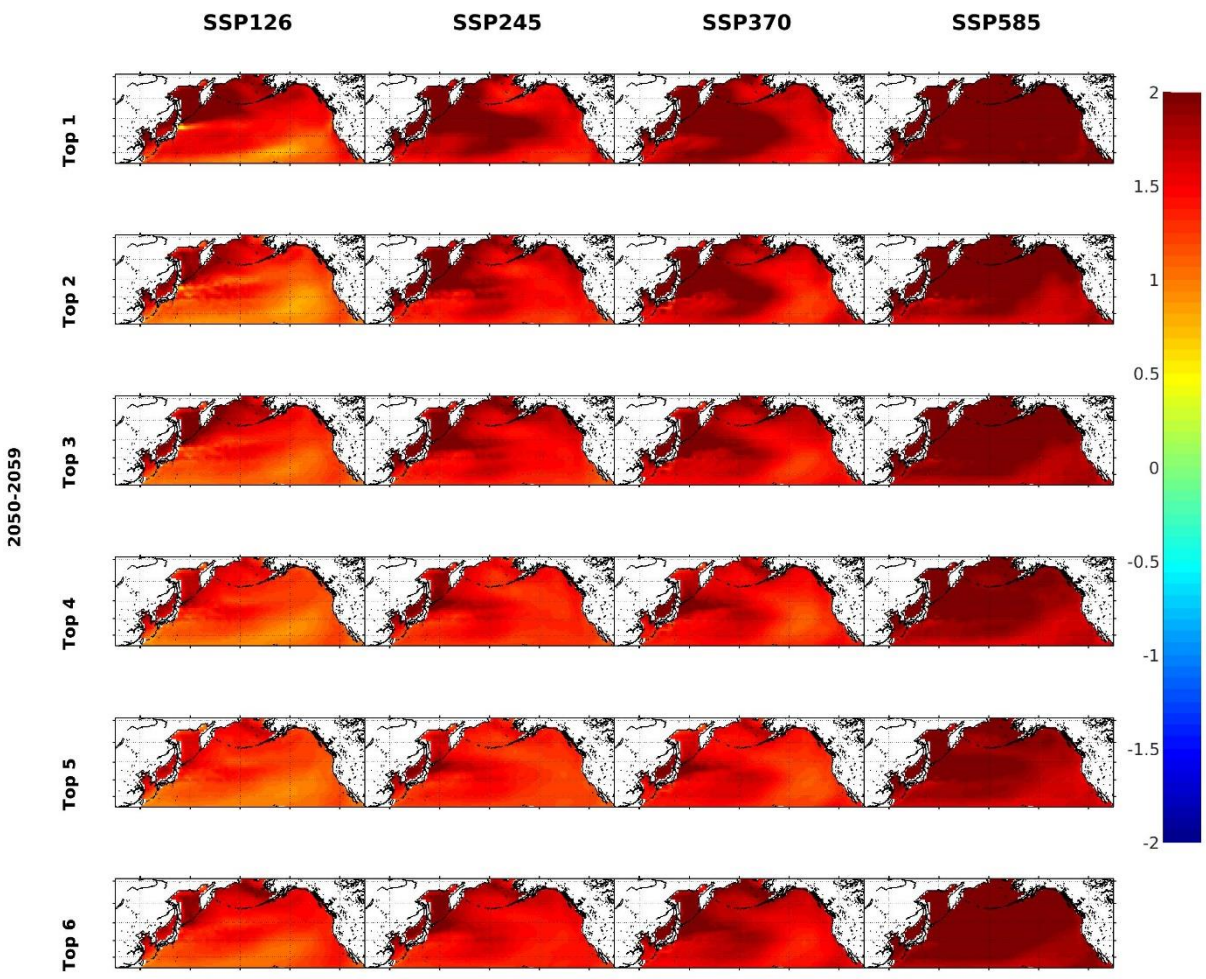

Figure 2.2.8a. Ensemble mean SST changes between period of 2050-2059 and the historical climatology of the 1985-2014 period using top number of best models. Unit: ºC.

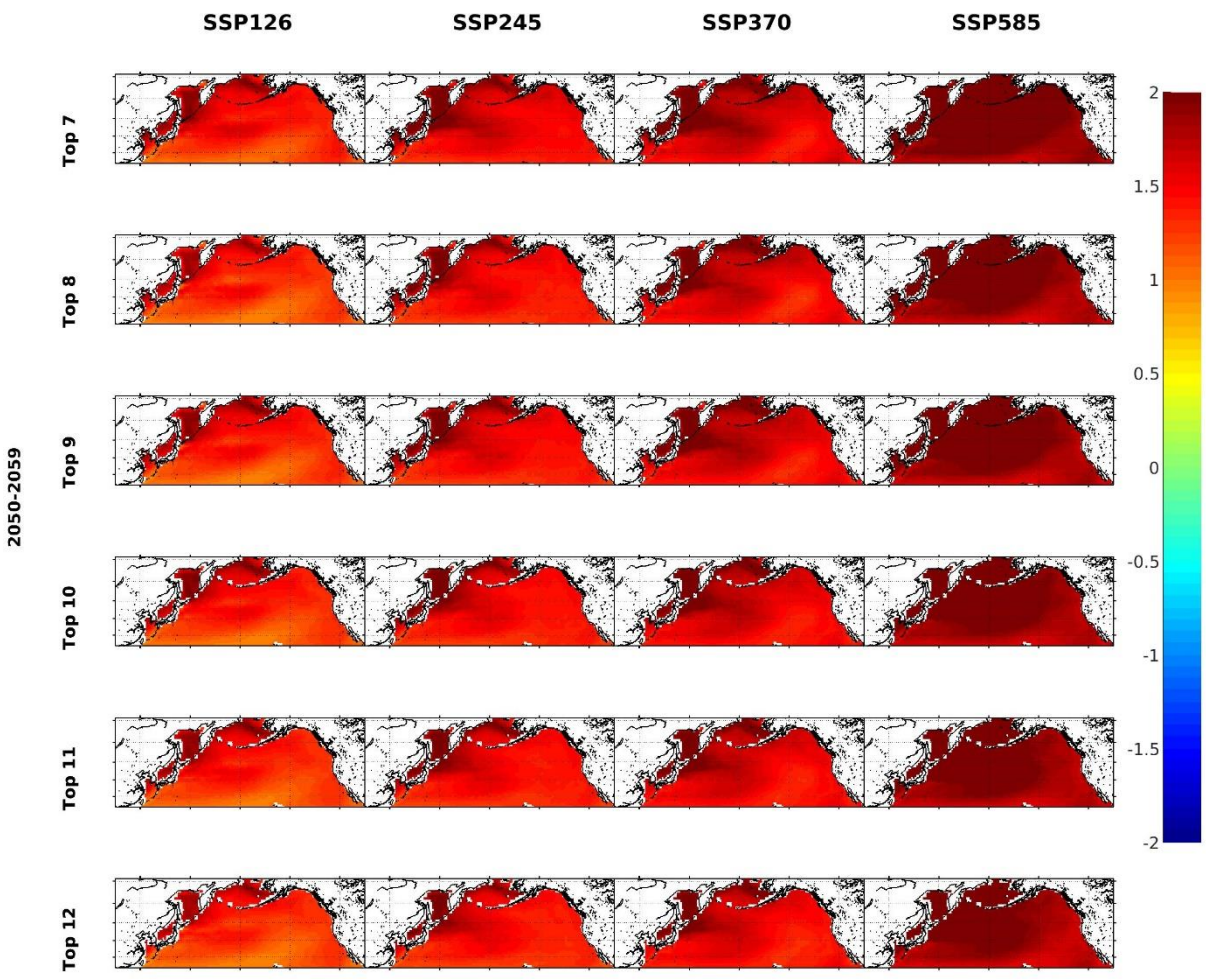

Figure 2.2.8b. Ensemble mean SST changes between period of 2050-2059 and the historical climatology of the 1985-2014 period using top number of best models. Unit: ^{o}C.

2.2.3 Arctic Ocean

2.2.3.1 Projected Ice Area Trends

Wang et al. [2024] investigated several metrics to evaluate the model performance for Arctic sea ice. The decreasing ice cover in the summertime is one of the most serious consequences associated with global warming. In this analysis, we focused mostly on the summer trend of the sea ice area in the Arctic Ocean.

Table 2.2.9 lists the summer trends of sea ice area in the Arctic Ocean for the 2015-2059 period, and it was expected that the declining trends would increase from SSP126 to SSP585, as can be seen from individual models and also from the ensemble means and the medians. The historical ensemble mean was between SSP370 and SSP585, indicating the Arctic Ocean had been probably undergoing a warming scenario between SSP370 and SSP585.

Table 2.2.9 The summer trends of sea ice area of the historical period and four scenarios (unit: $10^3 km^2$/year). The trend from HadISST ice: $-53.7 \times 10^3 km^2$/year.

Models	hist	SSP126	SSP245	SSP370	SSP585
ACCESS-CM2	-25.6	-22.6	-38.0	-33.0	-52.7
ACCESS-ESM1-5	-39.3	-6.4	-31.0	-23.1	-48.8
AWI-CM-1-1-MR	-36.3	-21.6	-36.0	-38.8	-53.7
CAMS-CSM1-0	-18.1	-2.3	14.0	-26.9	2.7
CanESM5	-49.6	-27.5	-69.0	-90.6	-104.0
CESM2	-76.6	6.7	-12.0	-23.5	-14.2
CESM2-WACCM	-62.3	-6.7	-24.0	-15.9	-36.8
CMCC-CM2-SR5	-2.4	-116.7	-100.7	-63.8	-137.0
CNRM-CM6-1	-45.4	2.3	-7.0	-20.5	-15.4
CNRM-ESM2-1	-39.5	42.4	24.0	15.5	-1.6
EC-Earth3	-86.6	13.0	-16.0	-28.2	-46.3
GISS-E2-1-G	-17.7	-19.4	-15.0	-17.8	-32.3
IPSL-CM6A-LR	-57.4	-37.4	-25.0	-61.8	-56.0
MIROC6	-21.1	-23.3	-47.0	-59.8	-39.7
MIROC-ES2L	-15.7	-26.3	-29.0	-37.0	-57.0
MPI-ESM1-2-HR	-37.1	-21.1	-12.0	-45.3	-38.9
MPI-ESM1-2-LR	-36.3	-9.4	-33.0	-33.2	-25.3
MRI-ESM2-0	-49.0	-29.5	-53.0	-56.7	-42.6
NorESM2-LM	-34.4	-1.1	-4.0	-0.4	-25.1

TaiESM1	-53.0	-18.3	-18.0	-39.9	-49.7
UKESM1-0-LL	-50.0	-29.3	-38.0	-42.3	-67.0
Median	-39.3	-19.4	-25.0	-33.2	-42.6
Mean	-40.6	-16.9	-27.0	-35.4	-44.8

Table 2.2.10 lists the winter trends of sea ice area in the Arctic Ocean for the 2015-2059 period, and the declining trends increased from SSP126 to SSP585, as can be seen from the most of the individual models and also from ensemble means and medians, as was consistent with the summer trends. The historical ensemble mean was significantly smaller than SSP126, which was the weakest in the four scenarios, suggesting the evolution of sea ice in winter time in the four climate scenarios was substantially different from that in the summer time.

Table 2.2.10 The winter trends of sea ice area in the Arctic of the historical period and four scenarios (unit: $10^3 km^2$/year). The trend from HadISST ice: $-14.3 \times 10^3 km^2$/year.

models	hist	SSP126	SSP245	SSP370	SSP585
ACCESS-CM2	-1.1	-77.7	-99.9	-74.9	-94.6
ACCESS-ESM1-5	-28.3	-46.6	-91.7	-72.3	-100.0
AWI-CM-1-1-MR	-23.9	-39.9	-51.0	-51.8	-67.6
CAMS-CSM1-0	1.7	-26.5	-30.9	-50.8	-38
CanESM5	-15.0	-83.3	-105.6	-101.0	-91.3
CESM2	-16.0	-48.6	-77.0	-62.8	-40.0
CESM2-WACCM	-11.0	-71.2	-88.4	-98.1	-106
CMCC-CM2-SR5	-25.0	-0.3	-0.4	-0.5	-0.3
CNRM-CM6-1	-18.0	-31.5	-49.3	-69.3	-53.3
CNRM-ESM2-1	-25.8	20.7	-17.8	-24.1	-67.1
EC-Earth3	-65.3	-47.6	-89.2	-118	-122
GISS-E2-1-G	-5.3	-70.8	-54.4	-76.3	-80.9
IPSL-CM6A-LR	-2.0	-53.3	-50.2	-70.3	-60.1
MIROC6	-14.5	-59.9	-88.4	-98.6	-92.7
MIROC-ES2L	-13.4	-48.3	-66.8	-60.0	-84
MPI-ESM1-2-HR	-5.4	-35.9	-48.9	-48.7	-78.3
MPI-ESM1-2-LR	-19.1	-29.4	-67.3	-55.4	-69.5

MRI-ESM2-0	-10.8	-35.7	-55.8	-66.5	-57.1
NorESM2-LM	-19.	-39.5	-58.6	-37.1	-82.0
TaiESM1	-9.6	-90.9	-102.6	-114.0	-86.7
UKESM1-0-LL	-31.3	-133.4	-139.2	-141	-139
Median	-15.0	-47.6	-66.8	-69.3	-80.9
Mean	-17.1	-50.0	-68.3	-71.0	-76.7

To provide a clear picture of the ice trends in the summer time and winter time from all the models and also the statistics, violin plots were used to show these trends, and they were shown in Figures 2.2.9 and 2.2.10 for summer trends and winter trends, respectively.

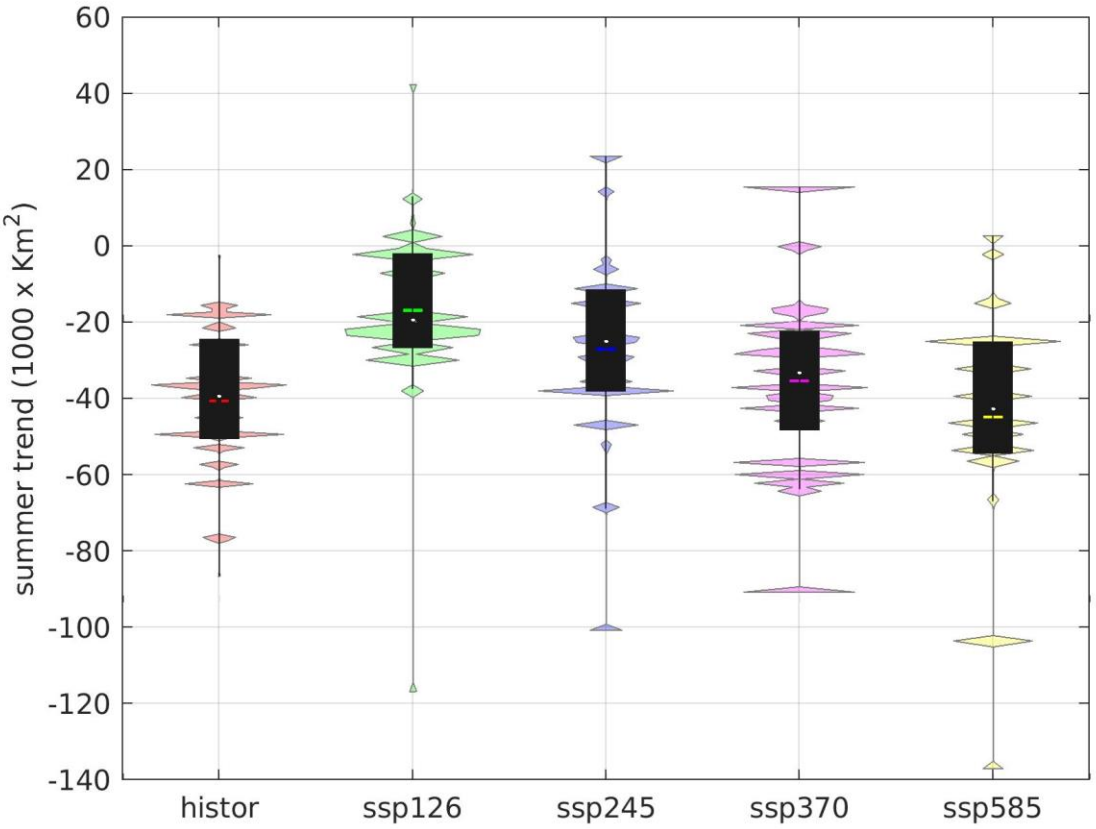

Figure 2.2.9 The violin plot of the summer trends of sea ice area from the historical period and 2015-2059 period from four climate scenarios. The boxes indicate the interquartile range (IQR), and whiskers are 1.5 IQR. Horizontal line indicates the mean value, and white circle indicates the median value. The width of each curve corresponds to the approximate frequency of data points in each region.

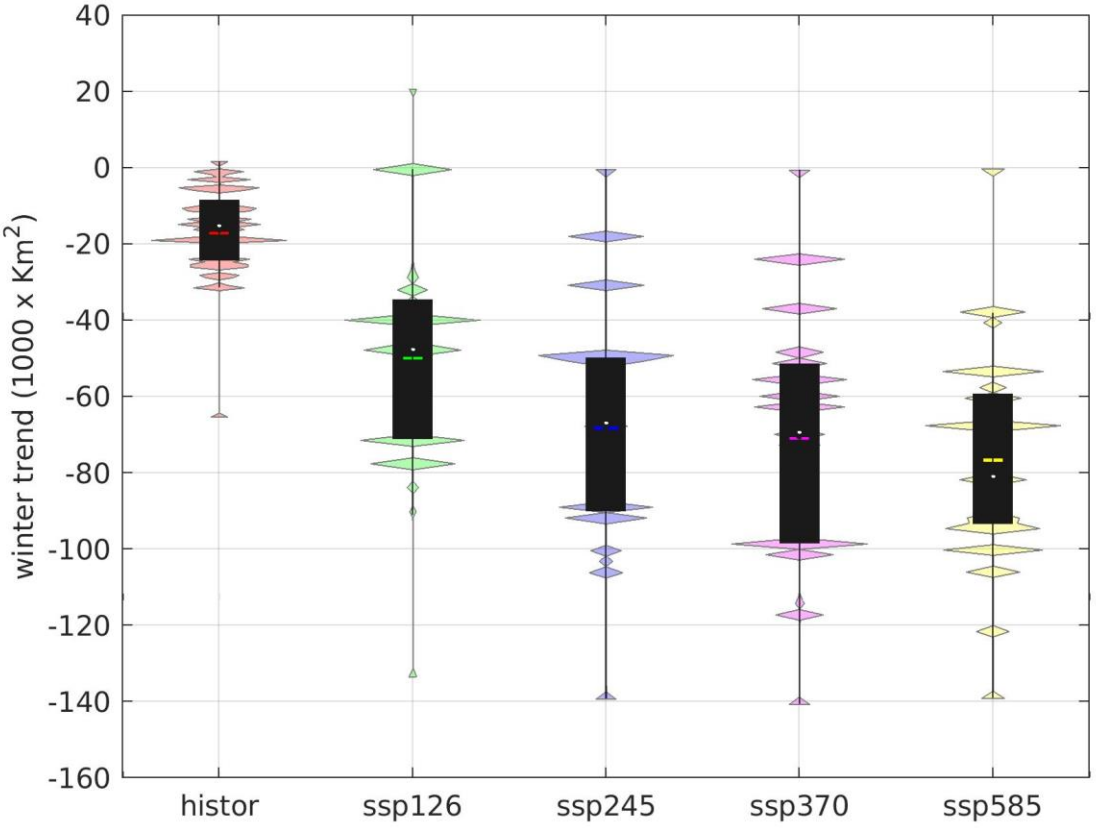

Figure 2.2.10 The violin plot of the winter trends of sea ice area from the historical period and 2015-2059 period from four climate scenarios. The boxes indicate the interquartile range (IQR), and whiskers are 1.5 IQR. Horizontal line indicates the mean value, and white circle indicates the median value. The width of each curve corresponds to the approximate frequency of data points in each region.

The ranks of the 21 CMIP6 models (missing data in one of the 22 CMIP6 model; Wang et al., 2024) representing the observed summer ice trend are listed in Table 3.1 in Wang et al. [2024]. We investigated the summer trends for the four SSPs using the ensemble means of the top CMIP6 models. The TaiESM1 was the best model among the 21 models in terms of representing the summer ice declining trend. We calculated the trends using a different number of the top models for each climate scenario and also the trend for the historical period, and they were shown in Figure 2.2.11. It was clear that the four scenarios showed that the ensemble means continued to decrease (stronger declining trend) when only using a small number of the top models, and they started to increase after reaching the minimum. SSP126 and SSP245 showed that the projected ensemble means all had weaker declining trends than the historical trend, with the SSP126 being the weakest. However, SSP370 and SSP585 demonstrated that some projected ensemble means showed stronger trends than historical trend, and apparently historical trend was close to SSP585.

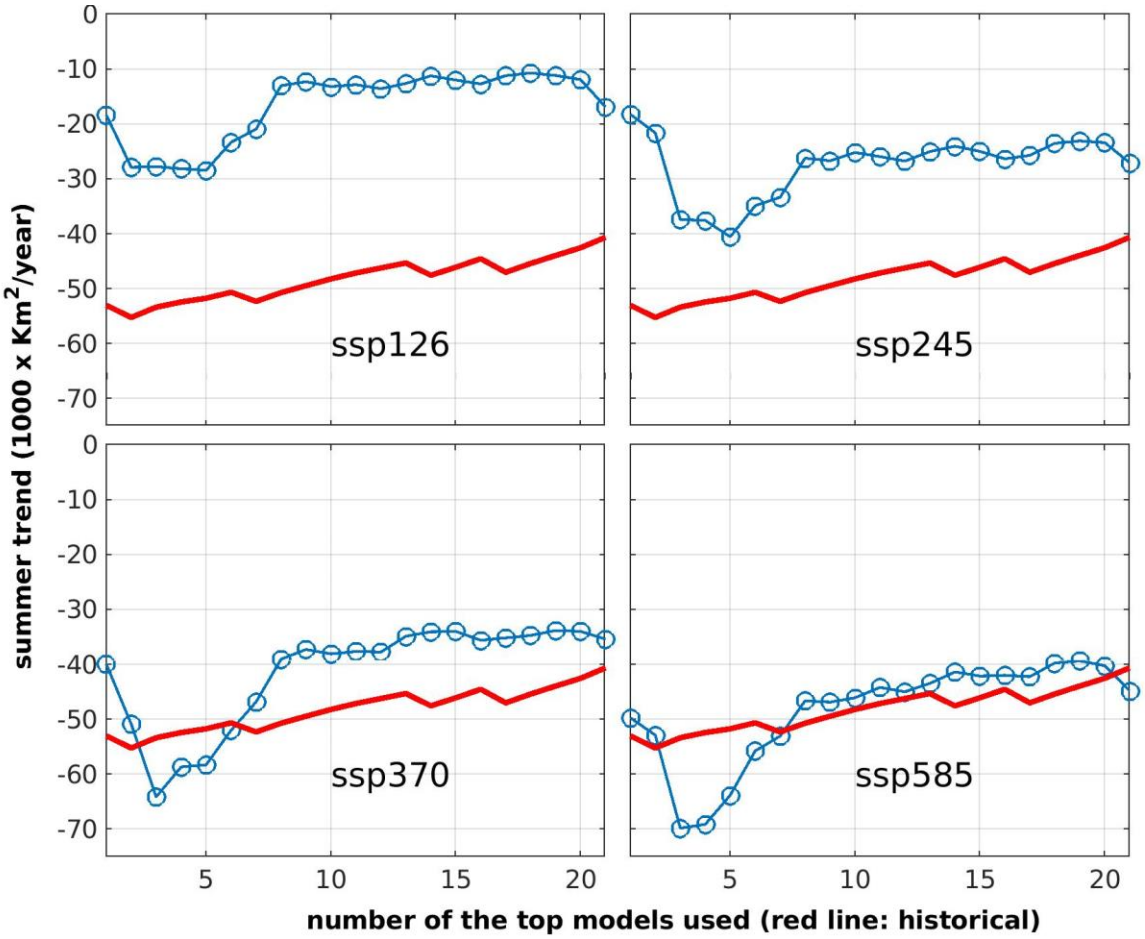

Figure 2.2.11 Ensemble mean summer ice trend for the period of 2015-2059 (blue line with circles) and the historical period of 1955-2014 (red line).

2.2.3.2 Projected earliest years of the summer-ice-free Arctic Ocean

Here we attempt to estimate the possible years of an ice-free Arctic Ocean in summer (Appendix 0). Figure 2.2.12 shows the estimated ice-free years for the four scenarios. The SSP126 and SSP245 had a very large range compared to SSP370 and SSP585. SSP370 and SSP585 showed a possibility of an ice-free Arctic Ocean ~2050, and the earliest year of 2046 was estimated in SSP585.

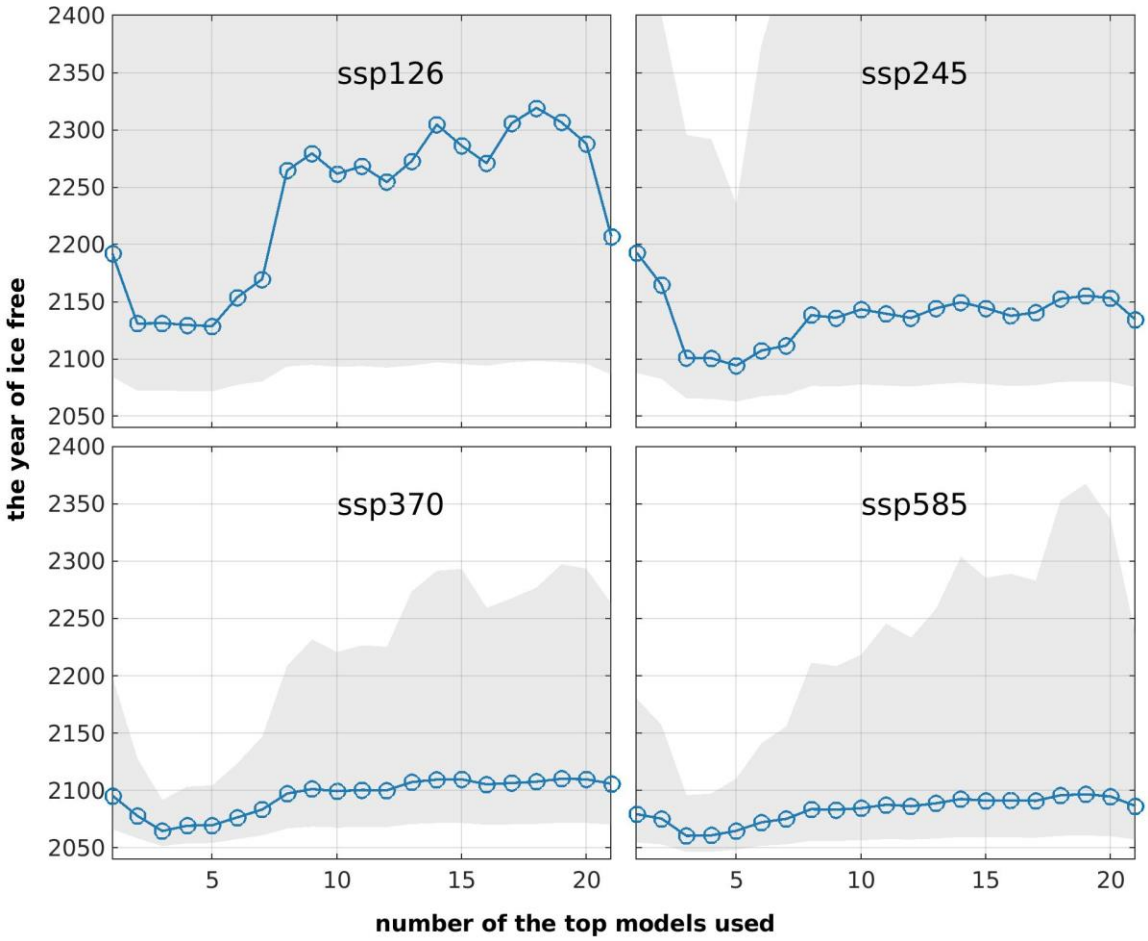

Figure 2.2.12 The years of ice-free summer Arctic Ocean using the ensemble trends calculated from top CMIP6 models for the four climate scenarios. Shaded areas are for the range of ice-free years, and solid lines with circles are the years using the ensemble means of the summer trends.

3. Summary

(1) This report investigated changes of SLP and air T over the Northern Hemisphere, and changes of SST in the North Atlantic and North Pacific Oceans, and sea ice in the Artic under four climate scenarios, SSP126, SSP245, SSP370 and SSP585, for the period of 2015 to 2059. The SST changes relative to the historical period of 1985 to 2014 were investigated as well.

(2) EOF analysis of the sea level pressure from the four SSPs suggested the NPO variability increased with increasing GHG emissions. However, the projected NAO/AO (North Atlantic Oscillation/Arctic Oscillation) did not have a clear pattern of changing variability with the increasing GHG emissions, though the four projected NAO/AO appeared to have stronger variations than the historical one (1955 to 2014). The variances explained by the EOF1s and EOF2s in the four SSPs were close to those of the historical ones.

(3) EOF analysis of the near-surface air temperature suggested warming-associated events had increasing variations with increasing GHG emissions from SSP126 to SSP585, and the warming mode became more and more dominant with stronger GHG emissions. The

AO/NAO related mode became less important with stronger GHG emissions. The air temperature over the Northern Hemisphere had dominant warming trends for all SSPs, and the warming trends increased from SSP126 to SSP585. However, the subpolar North Atlantic region would experience a cooling trend, and this trend decreased from SSP126 to SSP585.

(4) EOF analysis of the SST of the North Atlantic Ocean suggests that the AMO mode increased in variability from SSP126 to SSP585, and this mode would become more and more dominant with stronger GHG emissions. However, the NAO associated mode did not show an obvious pattern related to the changing GHG emissions, while the SSPs showed stronger variations than the historical one, and this mode became less dominant with increasing GHG emissions. Trend analysis suggested the SST of the North Atlantic Ocean from the low to mid latitudes had warming trends, and the warming trends increased from SSP126 to SSP585. The subpolar area had a general cooling trend, and this cooling trend decreased from SSP126 to SSP585. The largest warm anomalies were shown in the region to the southeast of Newfoundland, and on and off the Scotian Shelf.

(5) EOF analysis of the SST for the North Pacific Ocean suggested that variations of the SST associated with the warming trend increase from SSP126 to SSP585, and the mode reflecting the warming mode increase its variance with increasing GHG emissions. The PDO mode increased its variations from SSP126 to SSP585; however, this mode had less represented variance with increasing GHG emissions. Trend analysis suggested that the whole North Pacific Ocean experience warming trends for all SSPs, and the warming trends increase from SSP126 to SSP585. In the 2050-2059 period, the North Pacific Ocean had warm anomalies above 1.5^{o}C in all four scenarios, and most of the region had anomalies above 2^{o}C.

(6) The summer declining trends of sea ice area in the Arctic Ocean increased from SSP126 to SSP585, and the historical trend was close to that of SSP585. The declining trends in winter ice area increased from SSP126 to SSP585; however, these trends were all significantly stronger than the historical period. Our analysis showed that SSP370 and SSP585 predicted an ice-free Arctic Ocean as early as the summer of ~2060, and the earliest year of 2046 was projected by SSP585.

(7) Lotze et al. (2019) projected a decline in global marine animal biomass across all emission scenarios, primarily due to rising temperatures. Our analysis of sea surface temperature (SST) under four climate scenarios confirms the rising trend, hence biomass reductions across the three major oceans are likely.

Acknowledgements

This study is supported by the Fisheries and Oceans Canada (DFO) Competitive Science Research Fund (CSRF) through the project “The performance and projections of the CMIP6 Earth System Models (ESMs) for Canada’s three oceans” (CC-22-05-01). DFO colleagues Dr. Li Zhai and Adam Drozdowski internally reviewed this report and provided helpful comments, which helped improve the quality of this report. Section Head of the Ocean Stressors and Modeling Section, Dr. Marc Skinner, carefully reviewed the report and provided useful comments, which helped further improve the quality of the report.

References

Notz, D., & SIMIP Community (2020). Arctic sea ice in CMIP6. *Geophysical Research Letters*, 47, e2019GL086749. https://doi.org/10.1029/2019GL086749.

Lotze, H. K, et al.(2019). Global ensemble projections reveal trophic amplification of ocean biomass declines with climate change, Proc. Natl. Acad. Sci. U.S.A. 116 (26) 12907-12912, https://doi.org/10.1073/pnas.1900194116.

Wang, Z., DeTracey, B. Greenan, B., Brickman, D., Cyr, F., Galbraith, P., Steiner, N. and Christian, J. 2024. Examination of the performance of 22 CMIP6 ESMs on large scale changes in the atmosphere and oceans (North Atlantic, Arctic and North Pacific). Can. Tech. Rep. Hydrogr. Ocean. Sci. 376: v + 49 p.

Appendix 0

Methodologies

This study employs statistical analyses to investigate projected changes in the climate system. The methodology is centered on two main approaches: Empirical Orthogonal Function (EOF) analysis to identify dominant patterns of variability and trend analysis to quantify long-term changes.

a. Spatiotemporal Variability Analysis

To investigate large-scale phenomena in the atmosphere and ocean, we use Empirical Orthogonal Function (EOF) analysis. This technique is applied to model projections of future climate to identify the dominant modes of spatiotemporal variability. The analysis is performed on the following variables:

- Sea Level Pressure (SLP)
- Near-surface Air Temperature (AirT)
- Sea Surface Temperature (SST)

b. Trend and Anomaly Analysis

Long-term trends are calculated to assess projected changes in SST, AirT, and total Arctic sea ice area. To quantify regional warming, we analyze future decadal mean SST anomalies for the North Atlantic and North Pacific Oceans. These anomalies are calculated as the difference between projected future values and the historical climatological mean from the 1985–2014 baseline period.

c. Arctic Sea Ice Projection

By analyzing the projected rate of decline in Arctic sea ice area, we estimate the earliest potential year for the occurrence of an ice-free Arctic summer. The ice area in 2015 from the HadISST ice is $4.26 \times 10^6\ km^2$, and Notz & SIMIP community [2020] used $1.0 \times 10^6\ km^2$ as the ice area when the Arctic Ocean is considered to be ice-free. We also used the standard deviation of all ensemble means for each scenario to calculate the maximum and minimum of the trends

Appendix 1

Figures for the atmosphere changes in the Northern Hemisphere

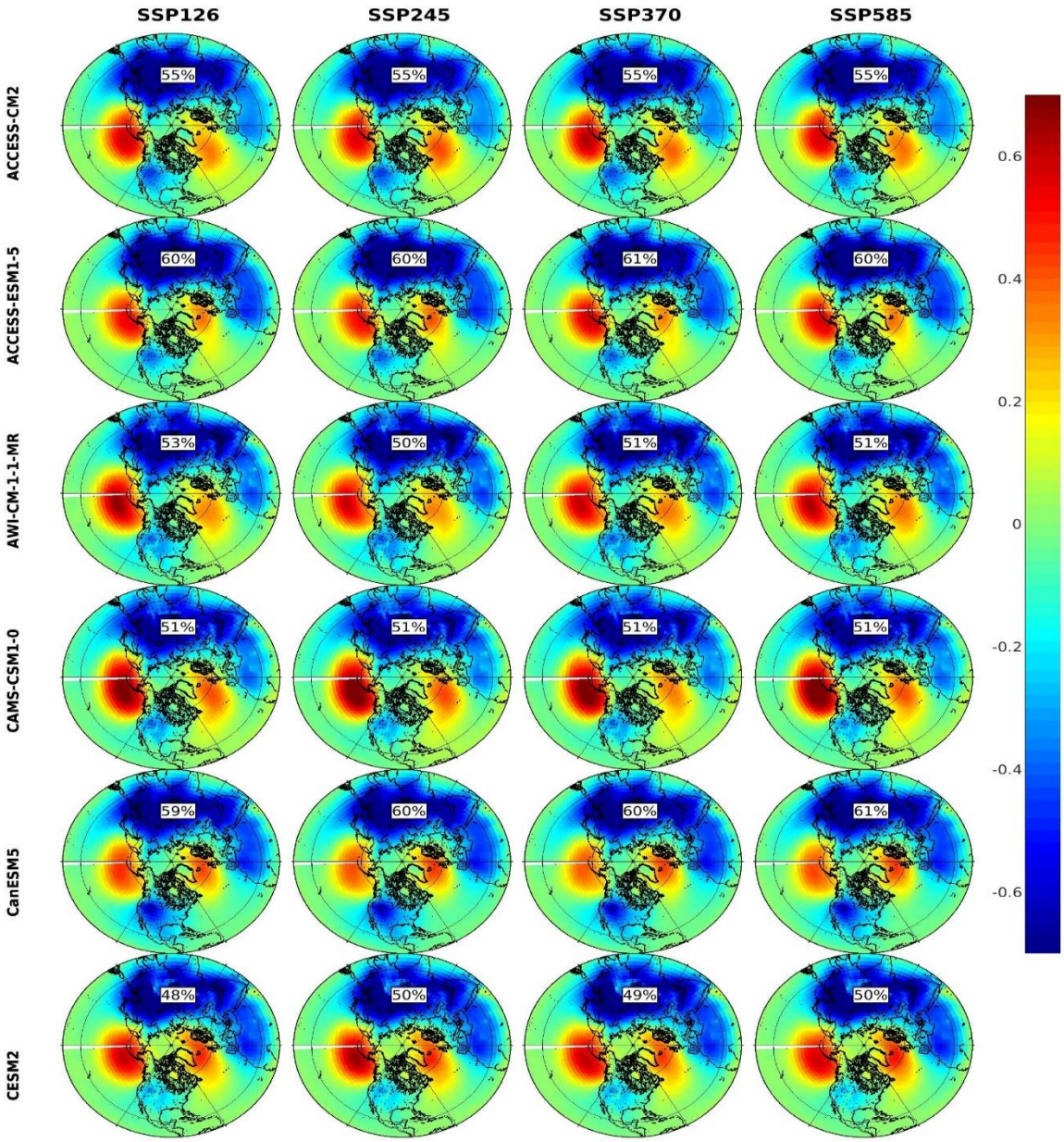

Figure A1.1a. EOF1s of the SLP for the 2015-2059 period.

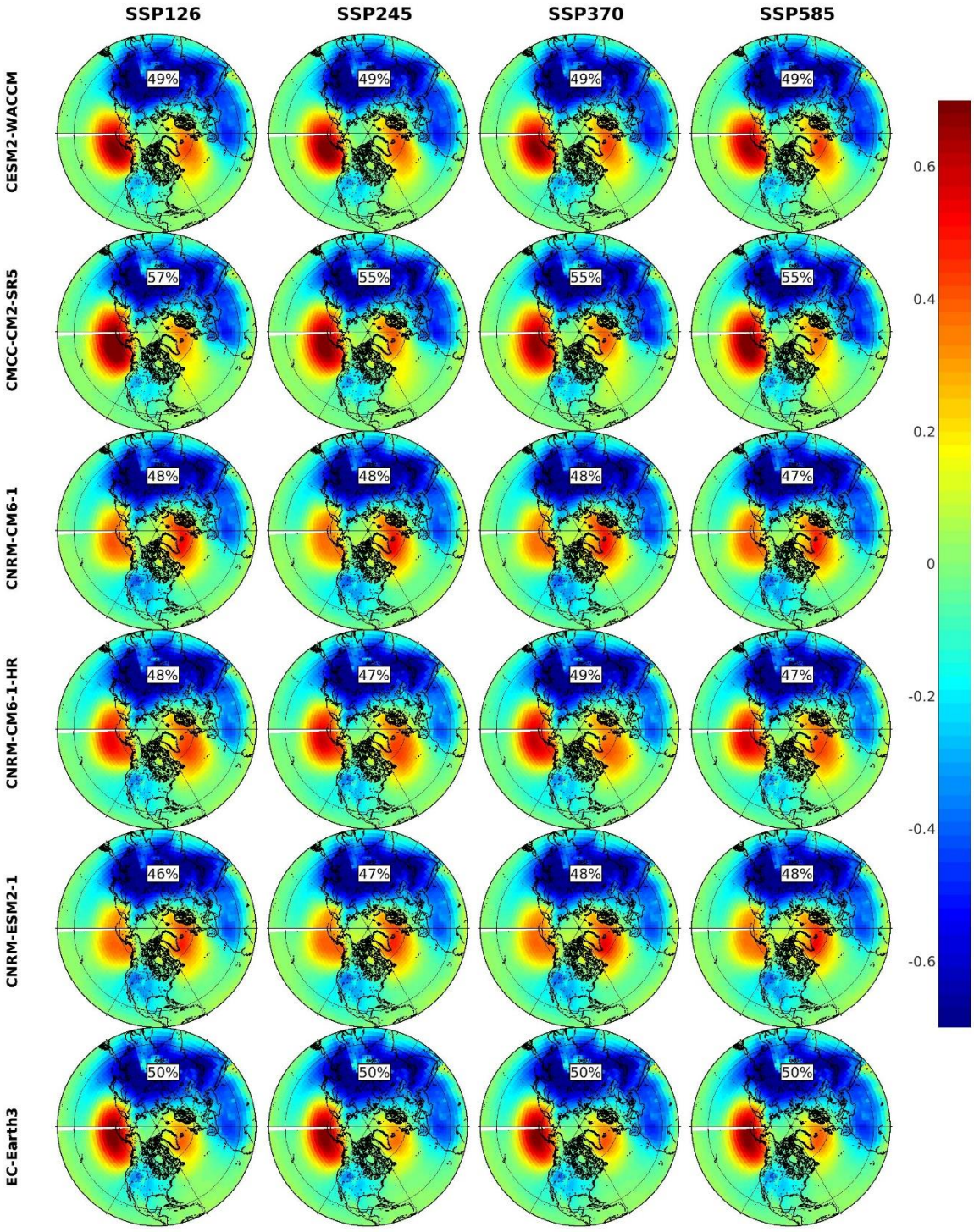

Figure A1.1b. EOF1s of the SLP for the 2015-2059 period.

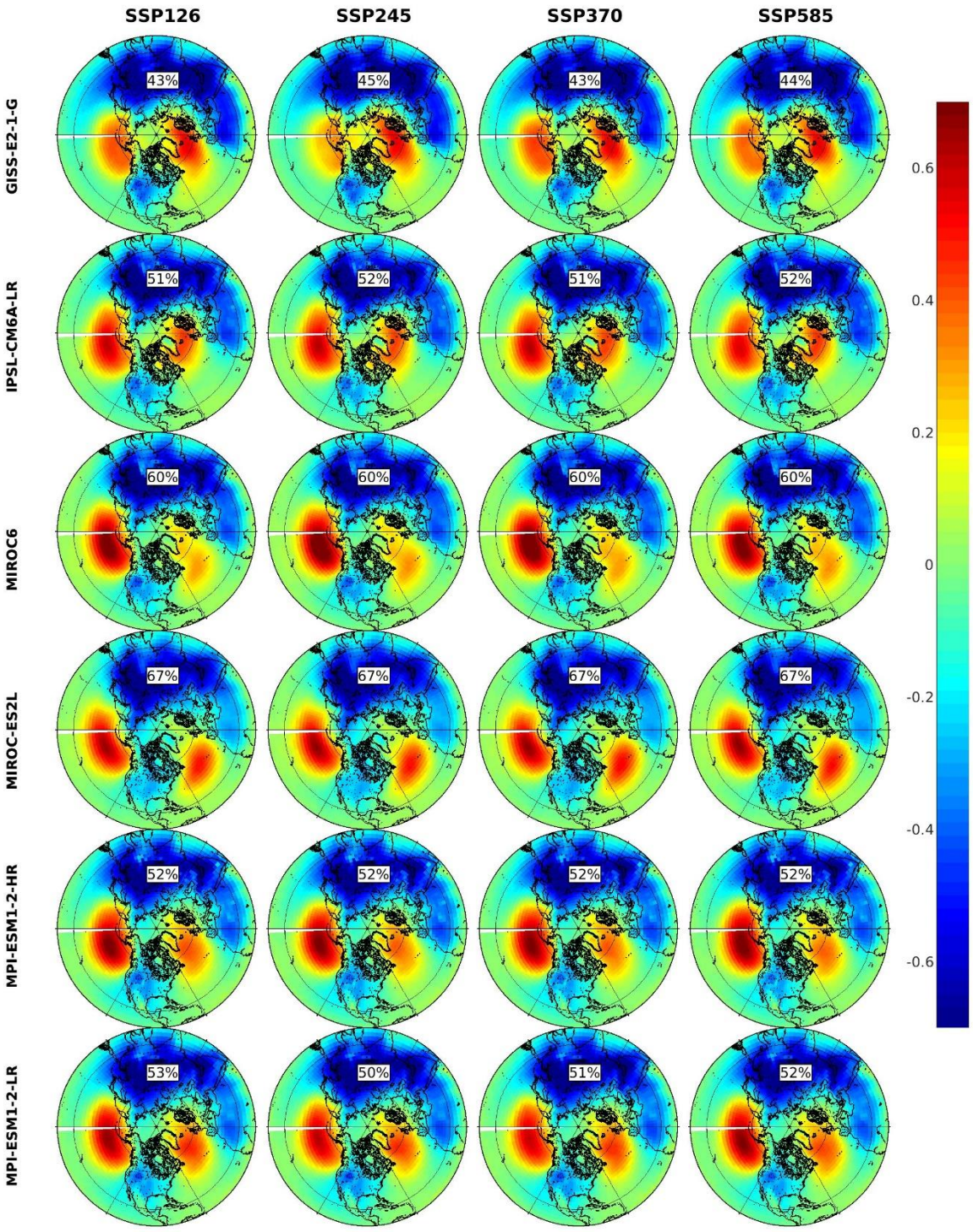

Figure A1.1c. EOF1s of the SLP for the 2015-2059 period.

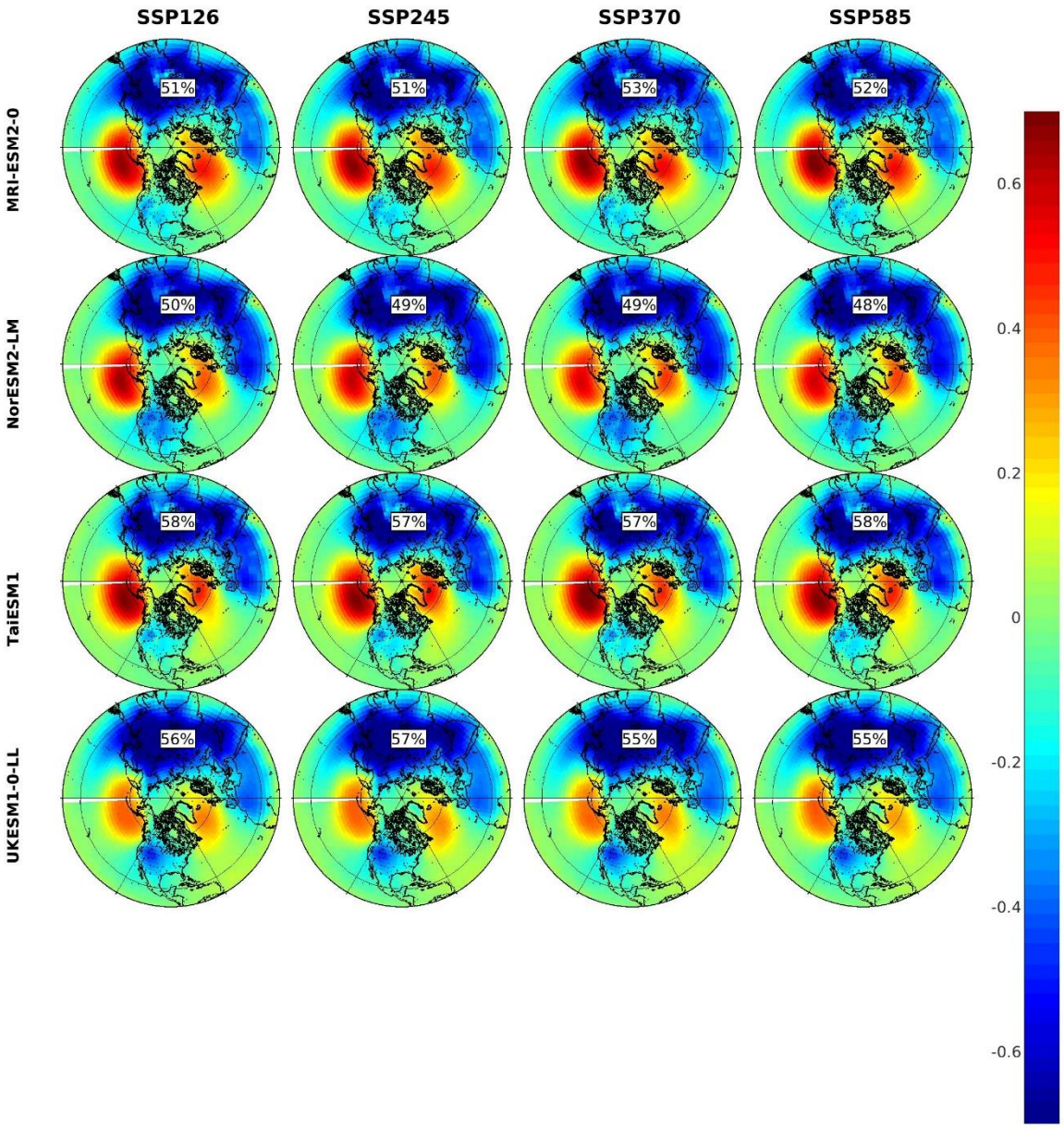

Figure A1.1d. EOF1s of the SLP for the 2015-2059 period.

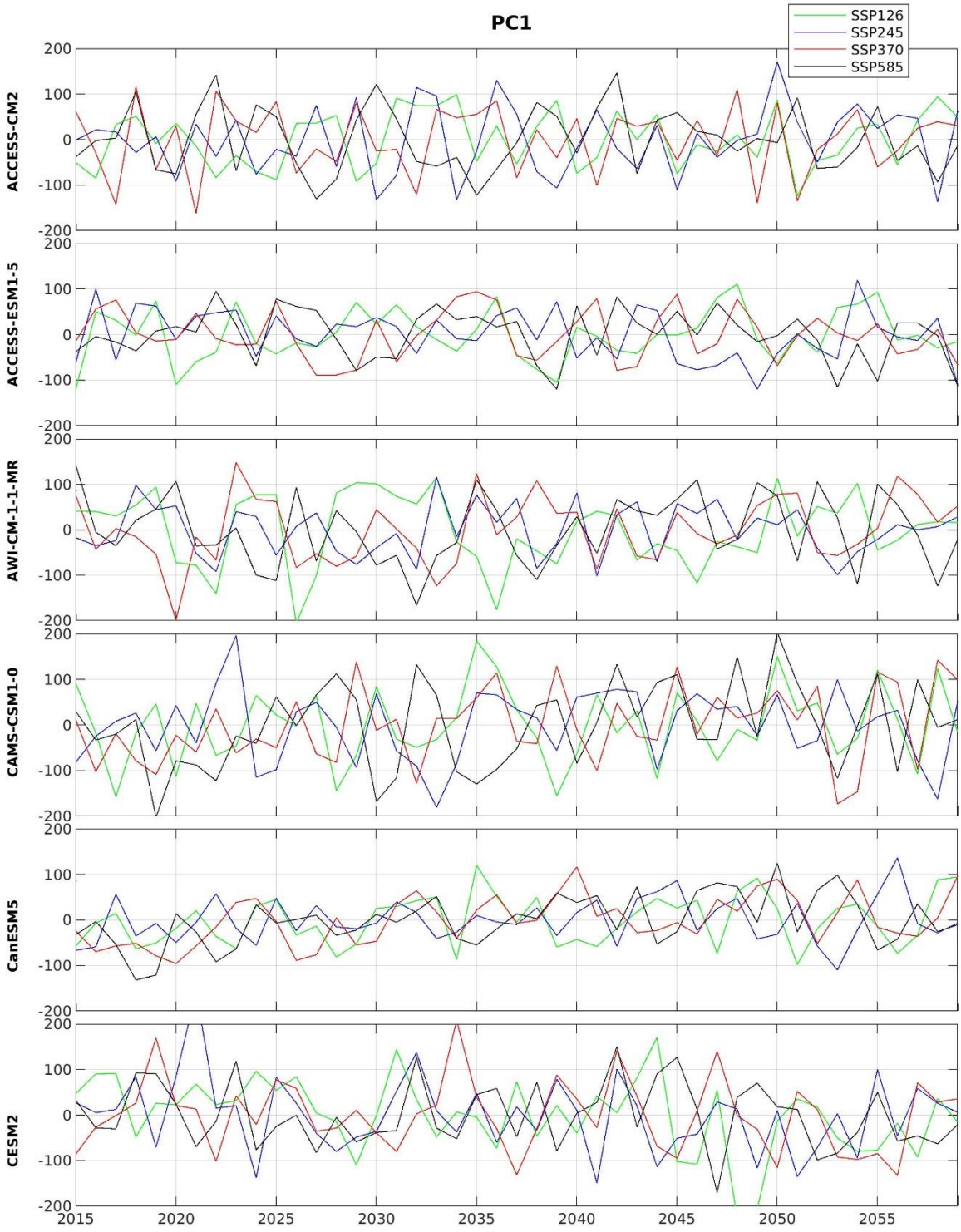

Figure A1.2a. PC1s of the SLP for the 2015-2059 period. Unit: Pa.

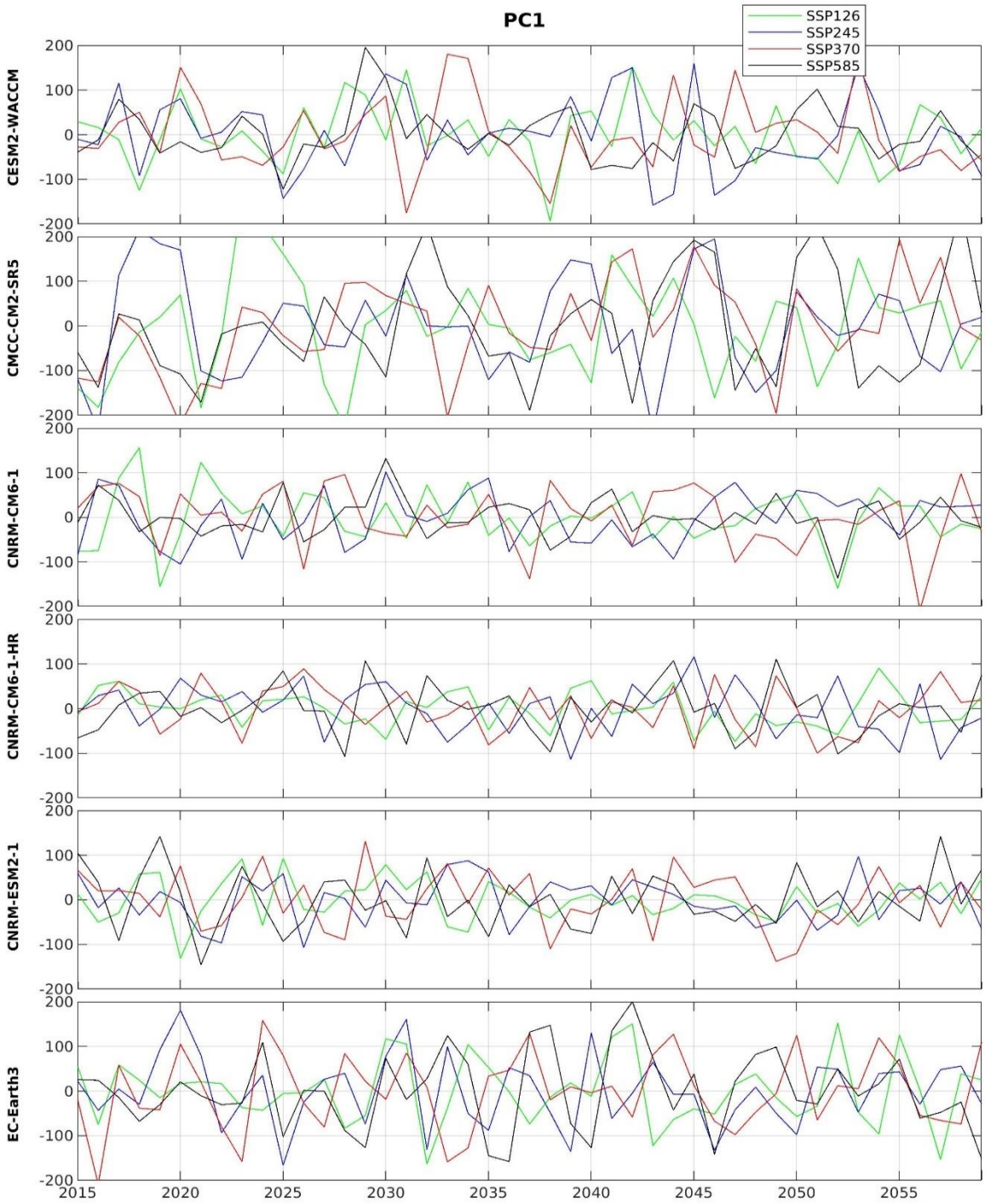

Figure A1.2b. PC1s of the SLP for the 2015-2059 period. Unit: Pa.

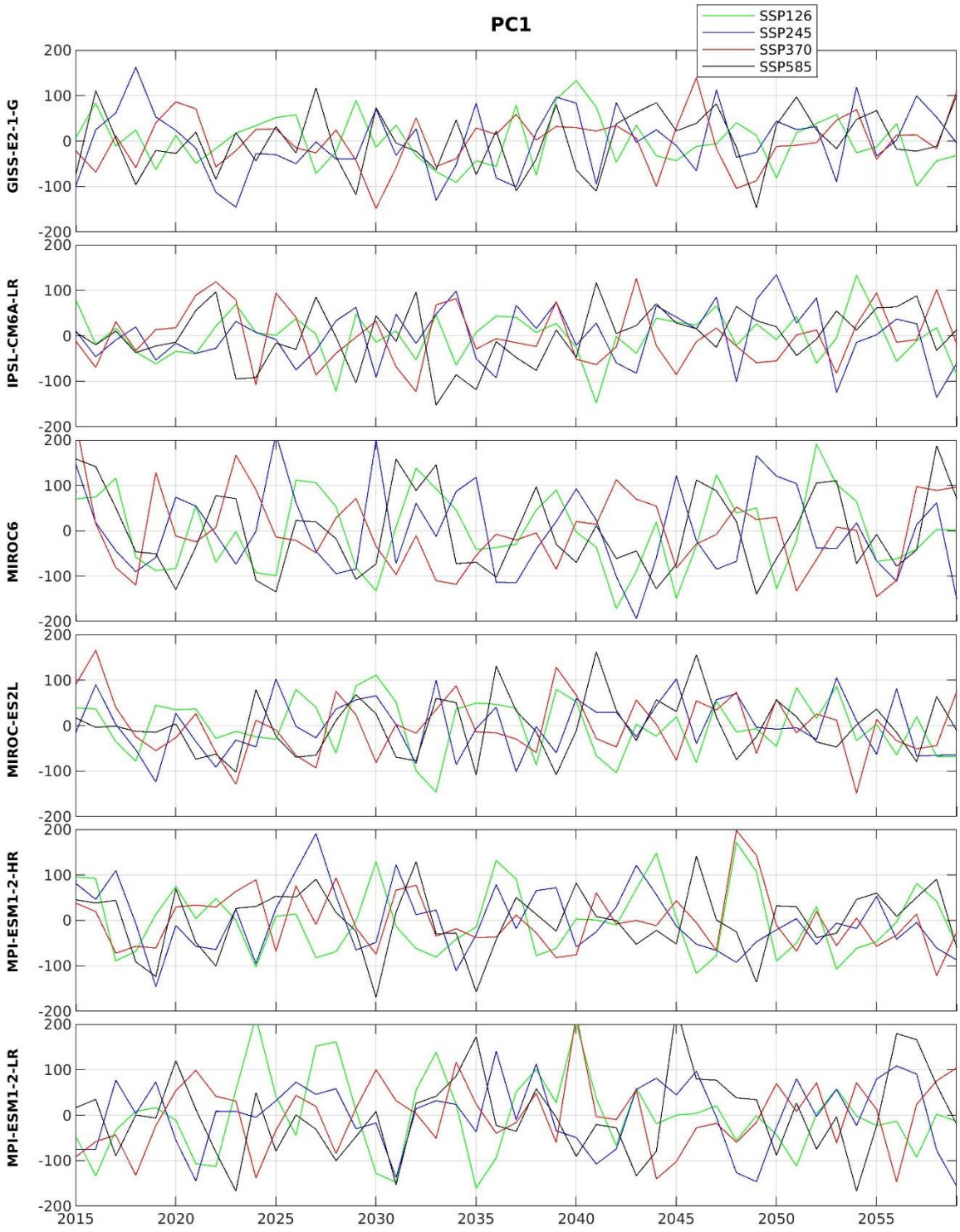

Figure A1.2c. PC1s of the SLP for the 2015-2059 period. Unit: Pa.

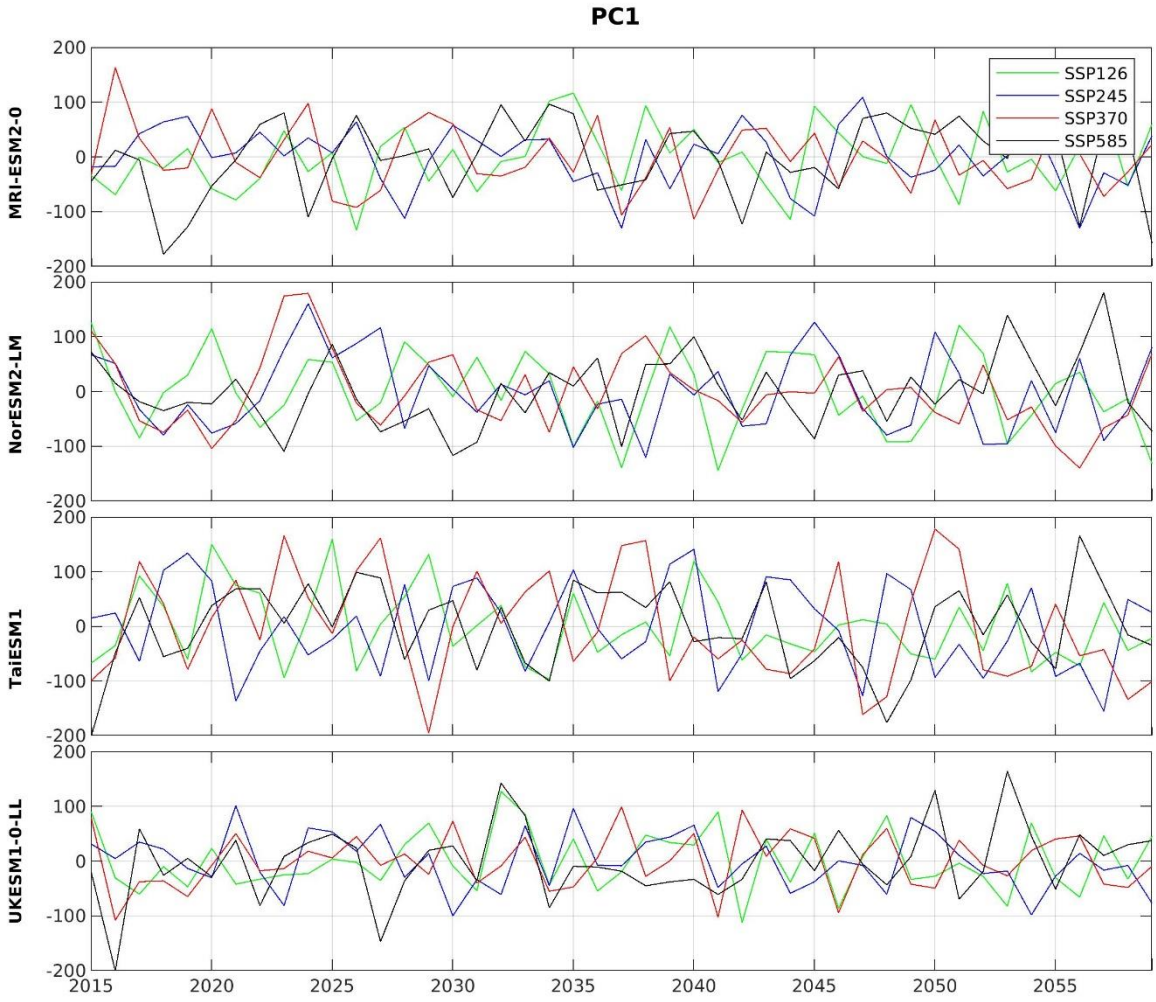

Figure A1.2d. PC1s of the SLP for the 2015-2059 period. Unit: Pa.

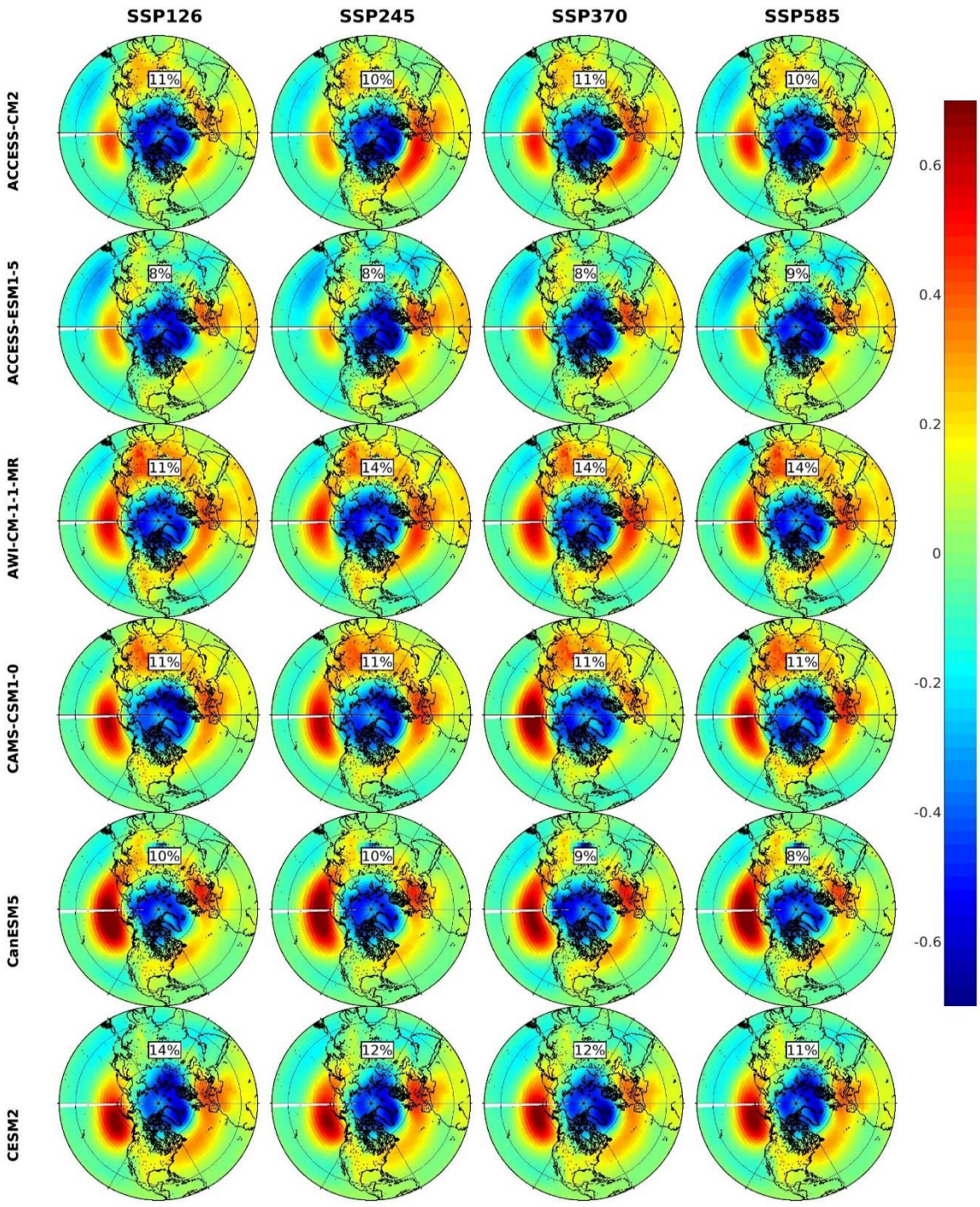

Figure A1.3a. EOF2s of the SLP for the 2015-2059 period.

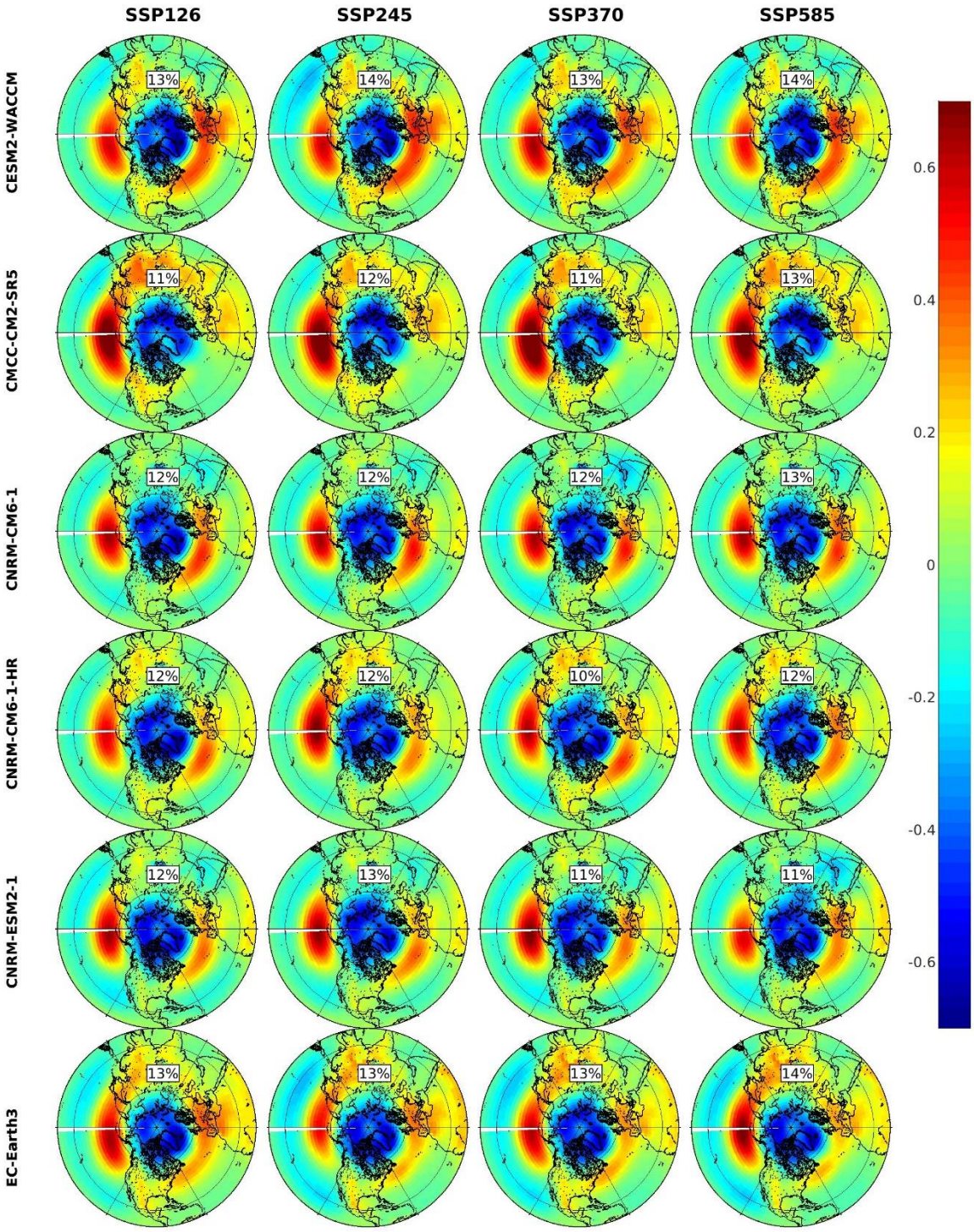

Figure A1.3b. EOF2s of the SLP for the 2015-2059 period.

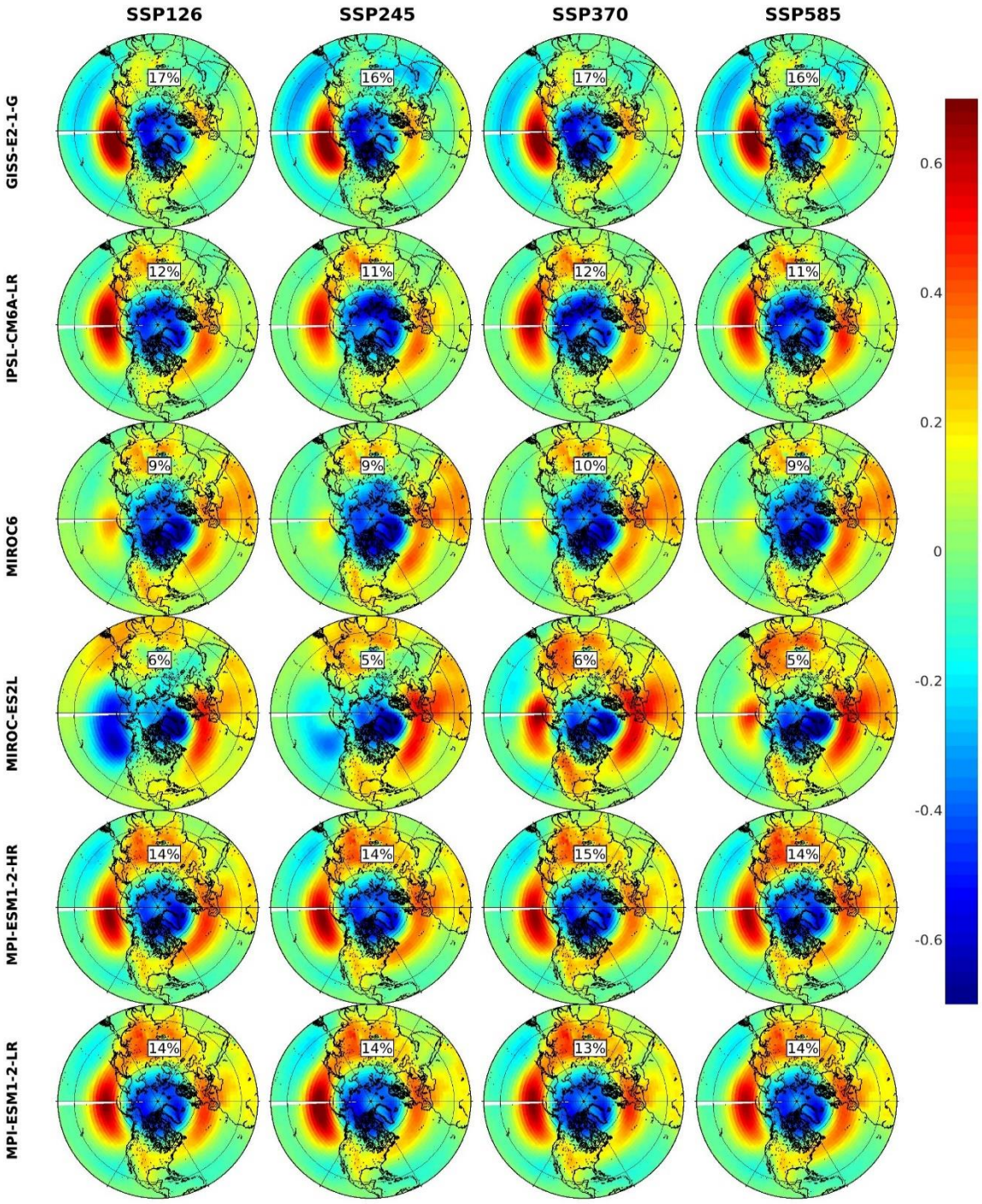

Figure A1.3c. EOF2s of the SLP for the 2015-2059 period.

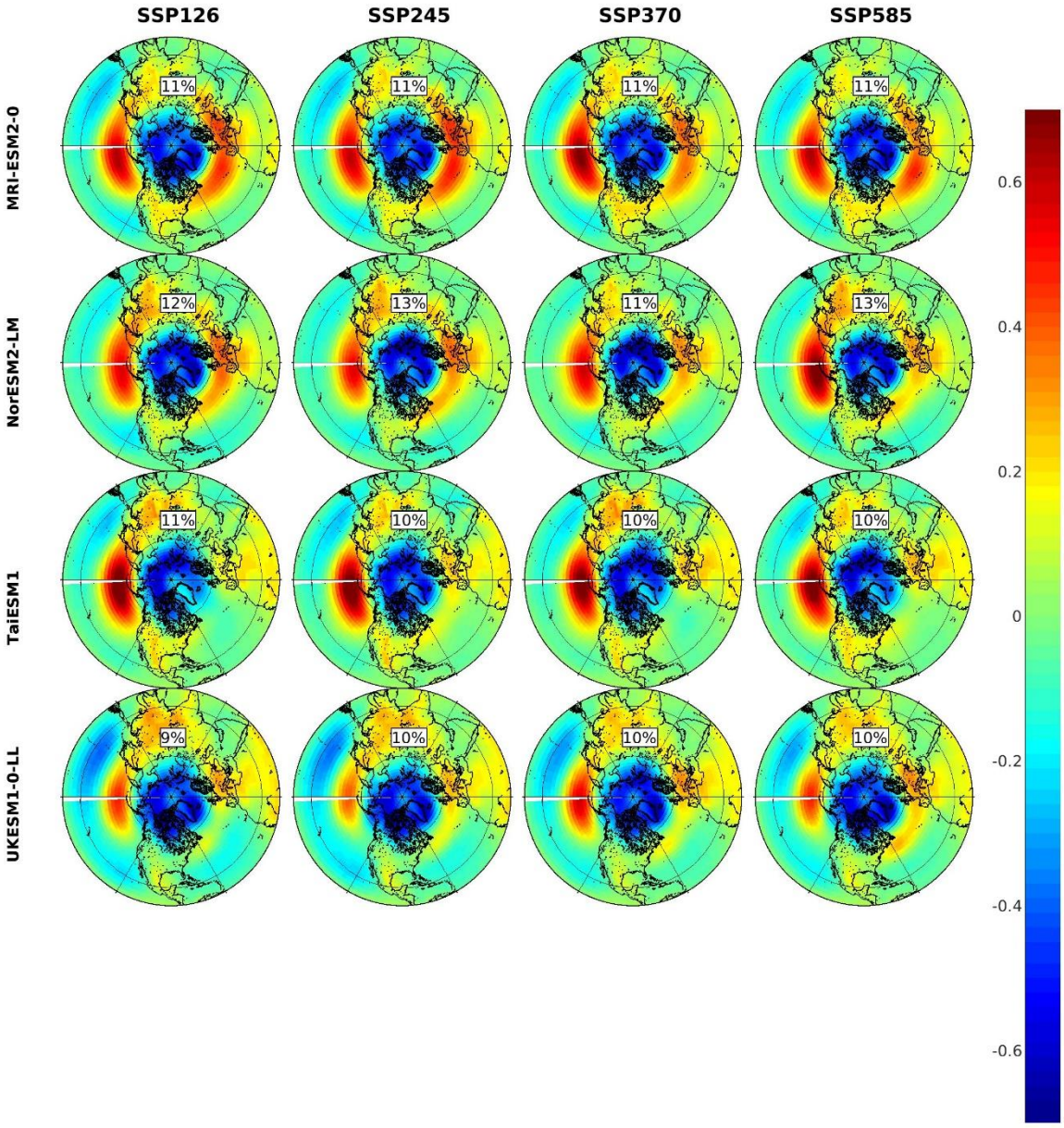

Figure A1.3d. EOF2s of the SLP for the 2015-2059 period.

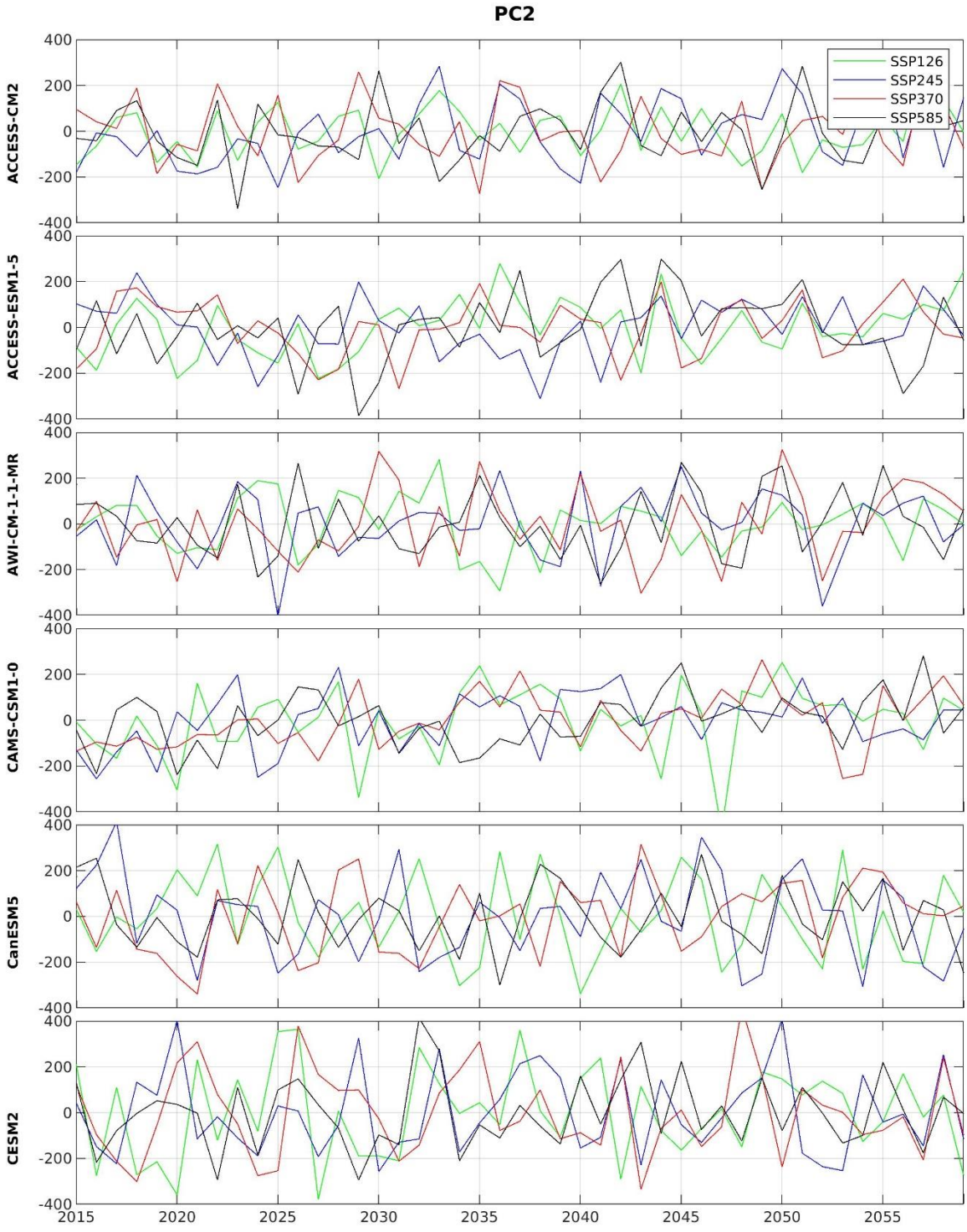

Figure A1.4a. PC2s of the SLP for the 2015-2059 period. Unit: Pa.

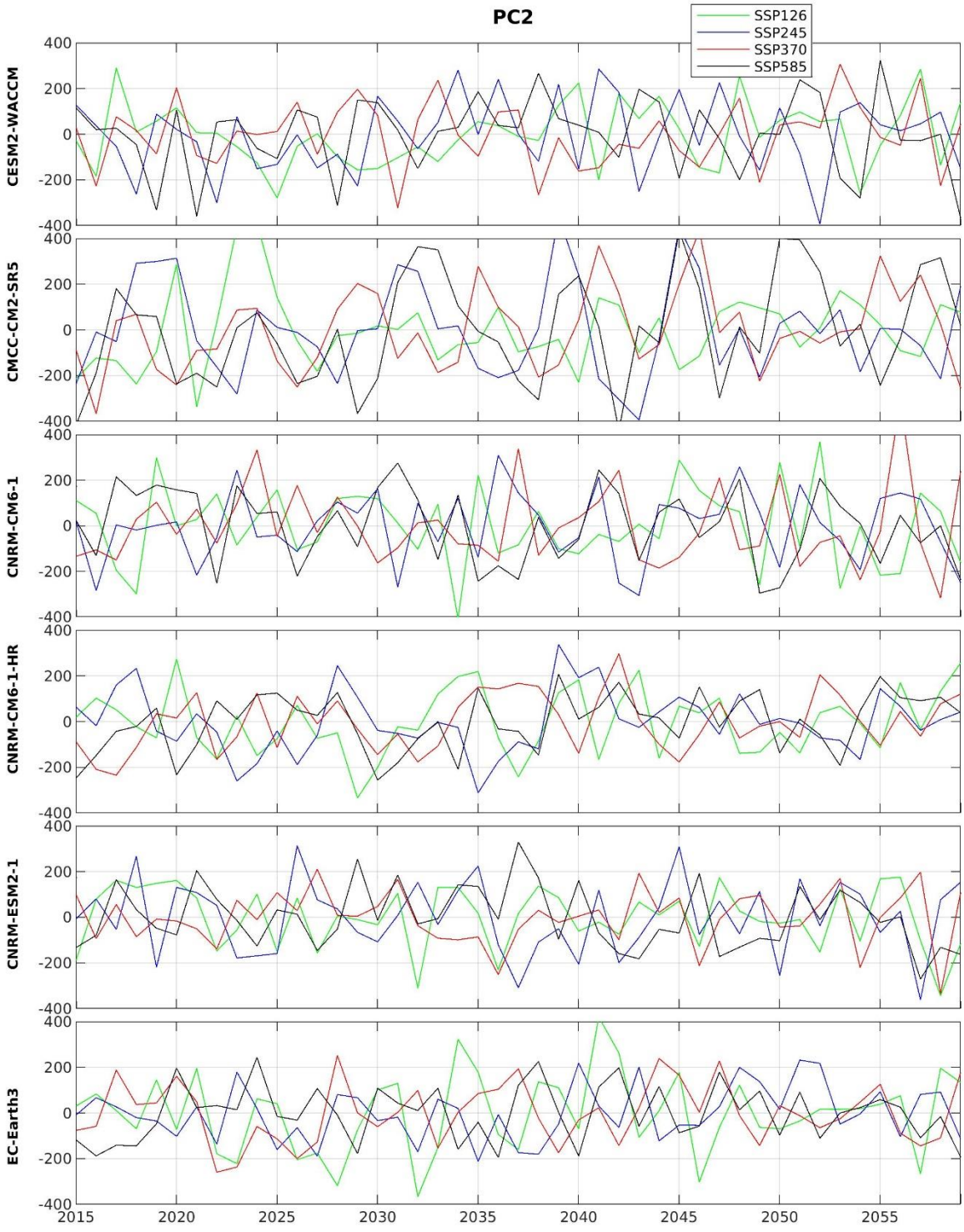

Figure A1.4b. PC2s of the SLP for the 2015-2059 period. Unit: Pa.

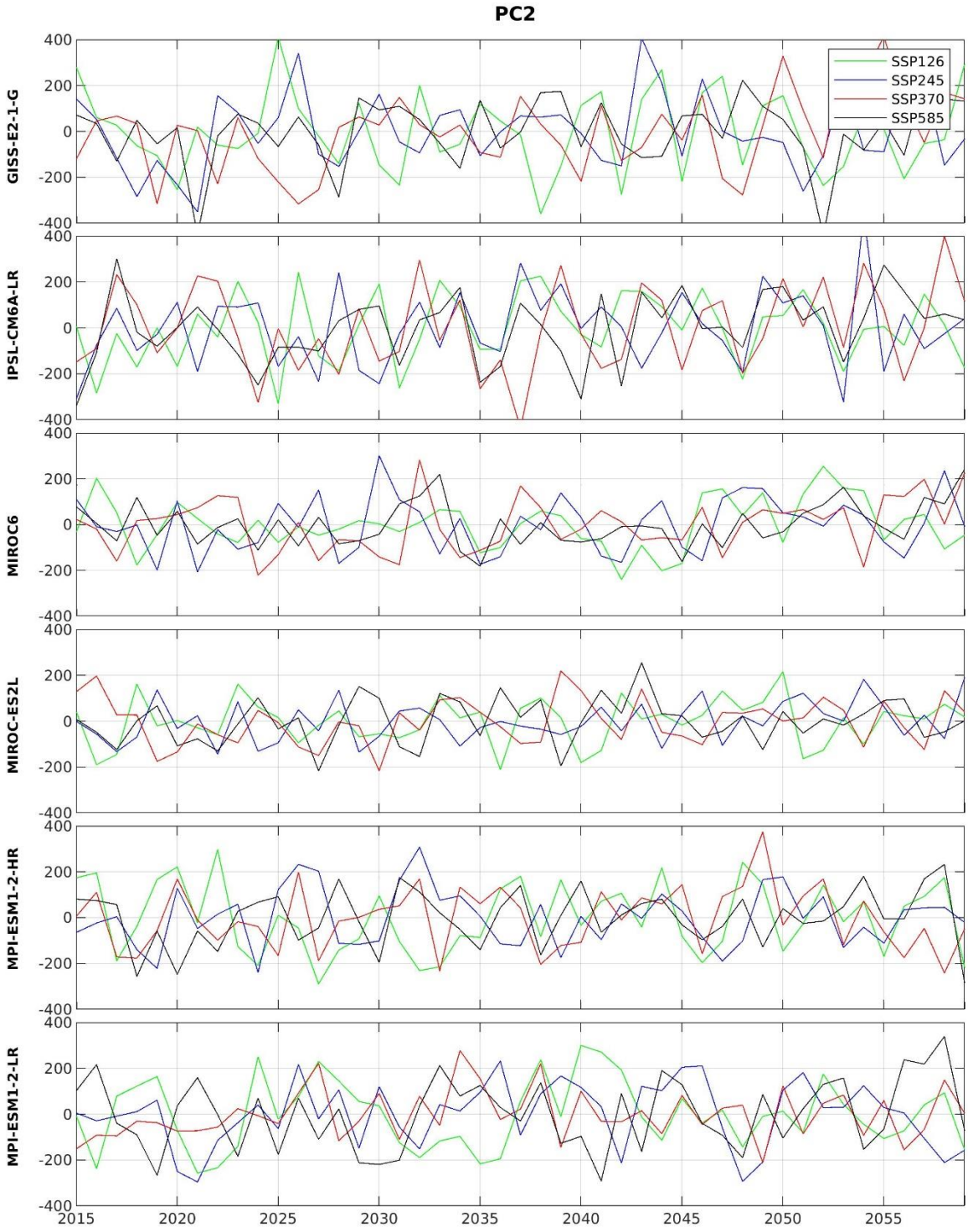

Figure A1.4c. PC2s of the SLP for the 2015-2059 period. Unit: Pa.

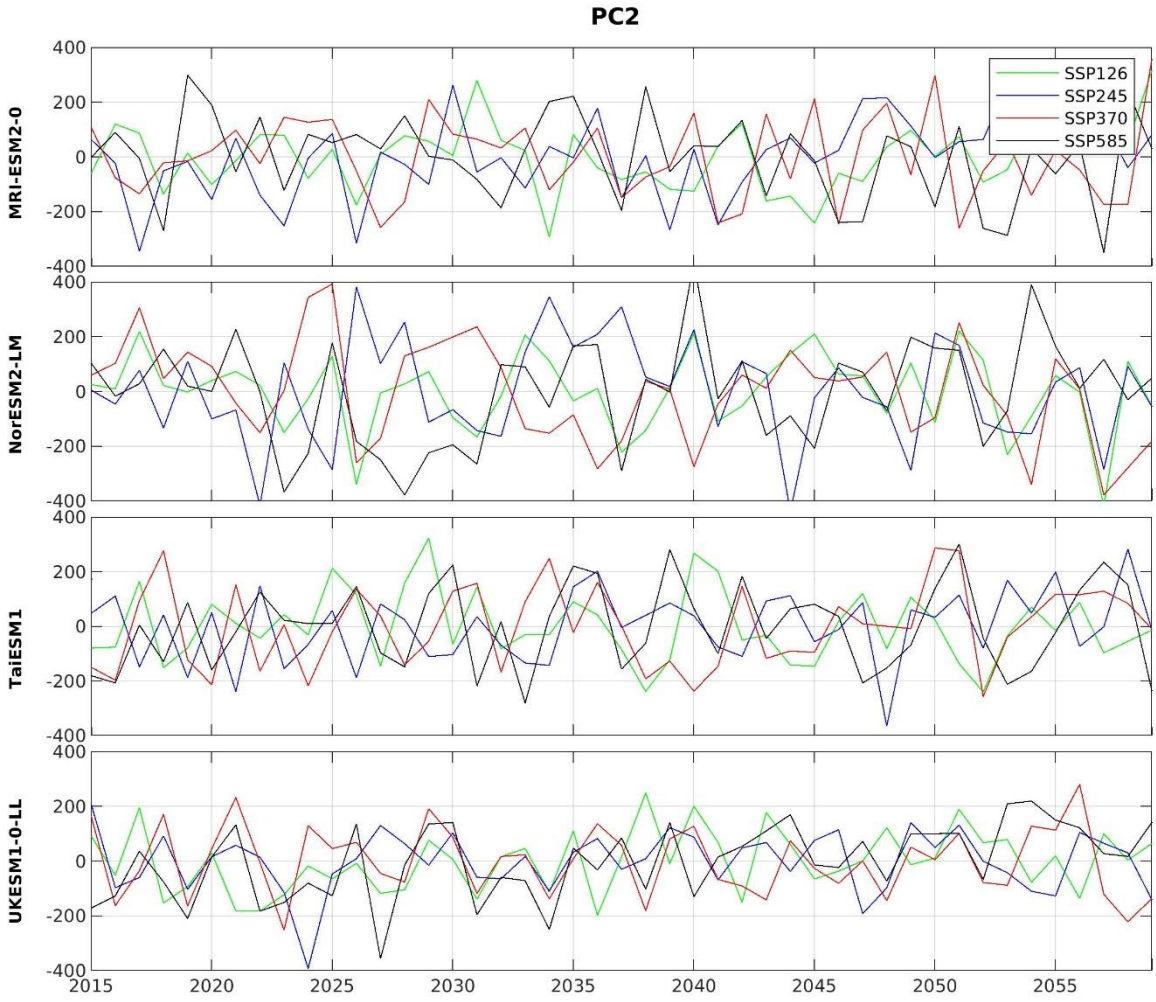

Figure A1.4d. PC2s of the SLP for the 2015-2059 period. Unit: Pa.

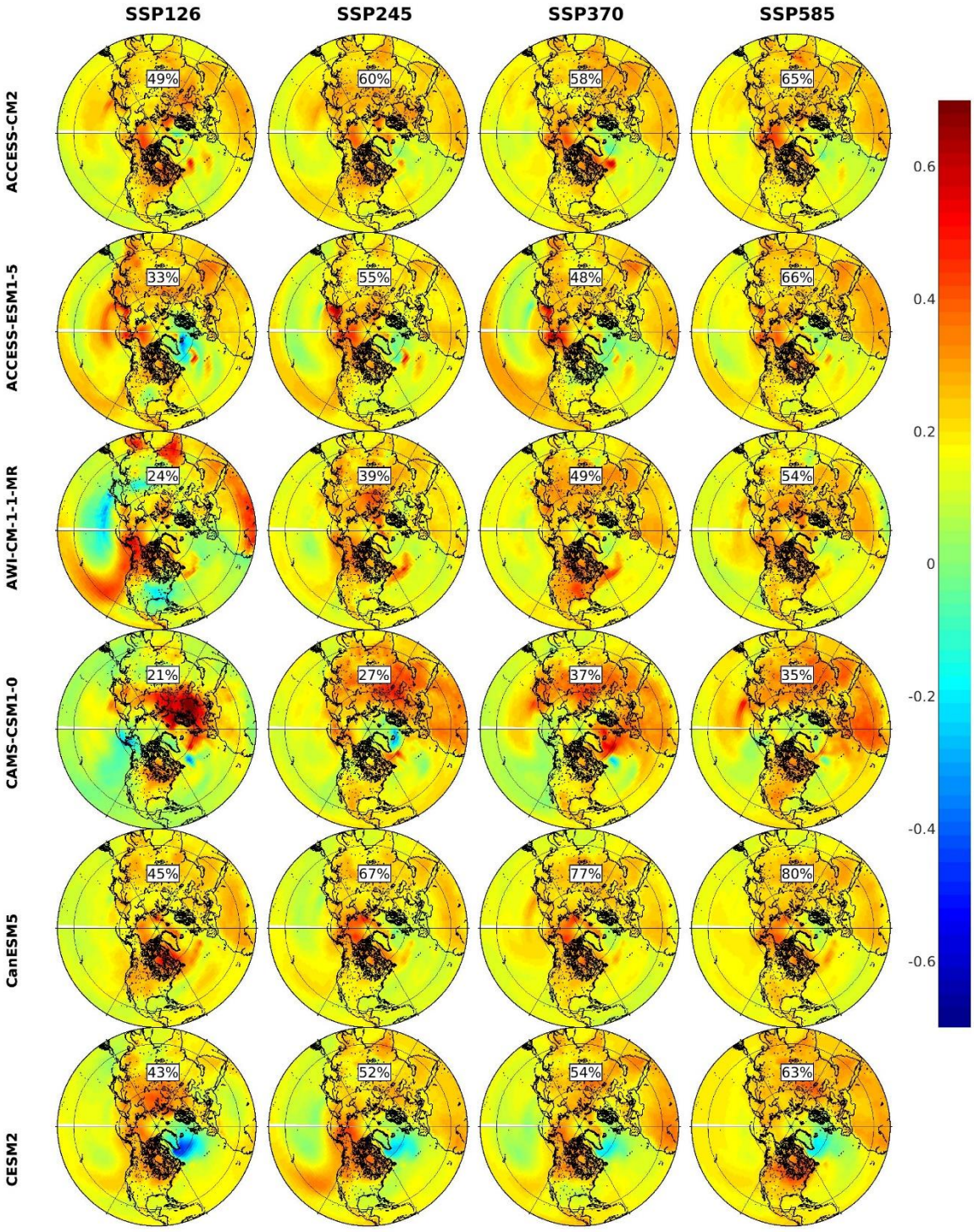

Figure A1.5a. EOF1s of the AirT for the 2015-2059 period.

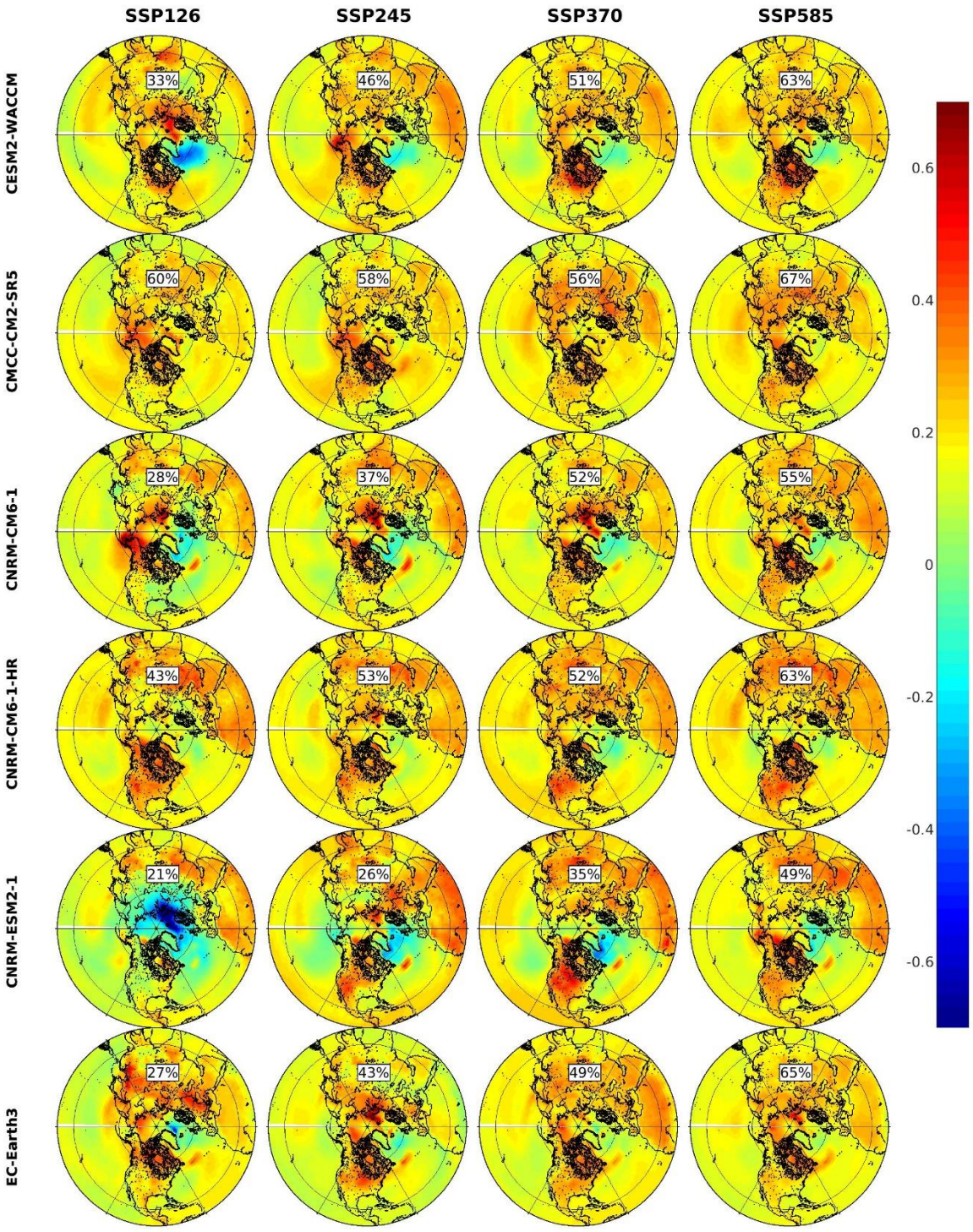

Figure A1.5b. EOF1s of the AirT for the 2015-2059 period.

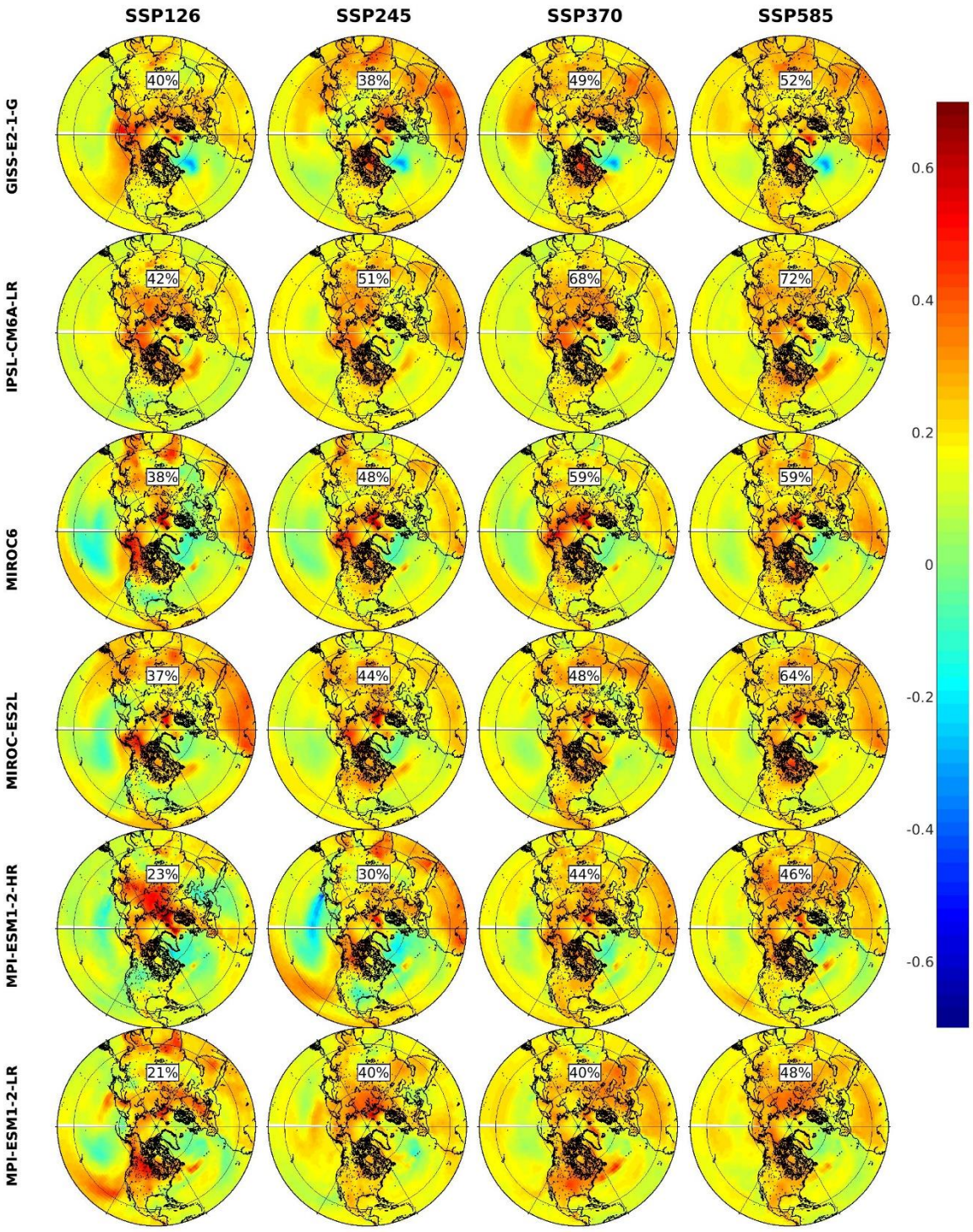

Figure A1.5c. EOF1s of the AirT for the 2015-2059 period.

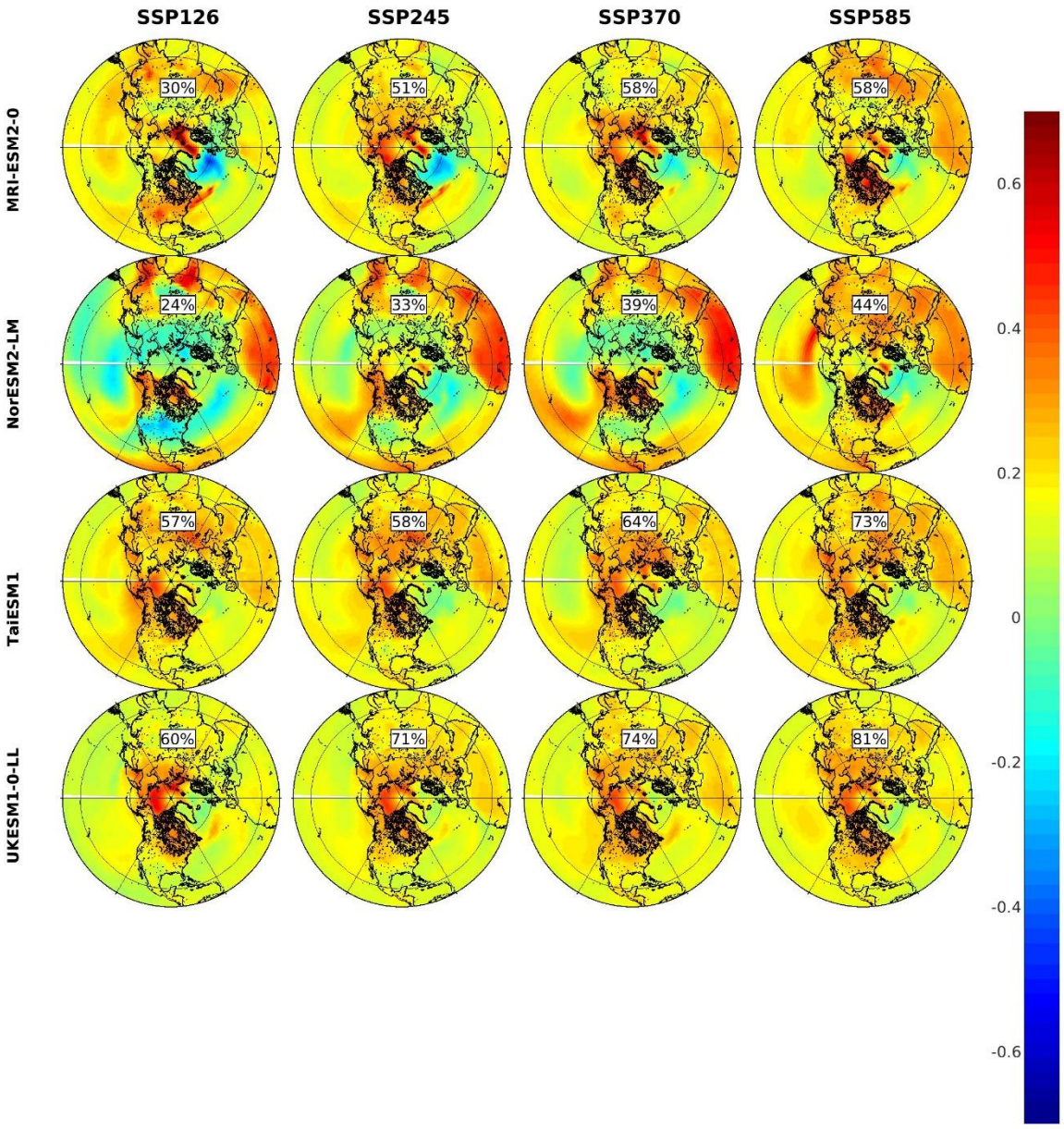

Figure A1.5d. EOF1s of the AirT for the 2015-2059 period.

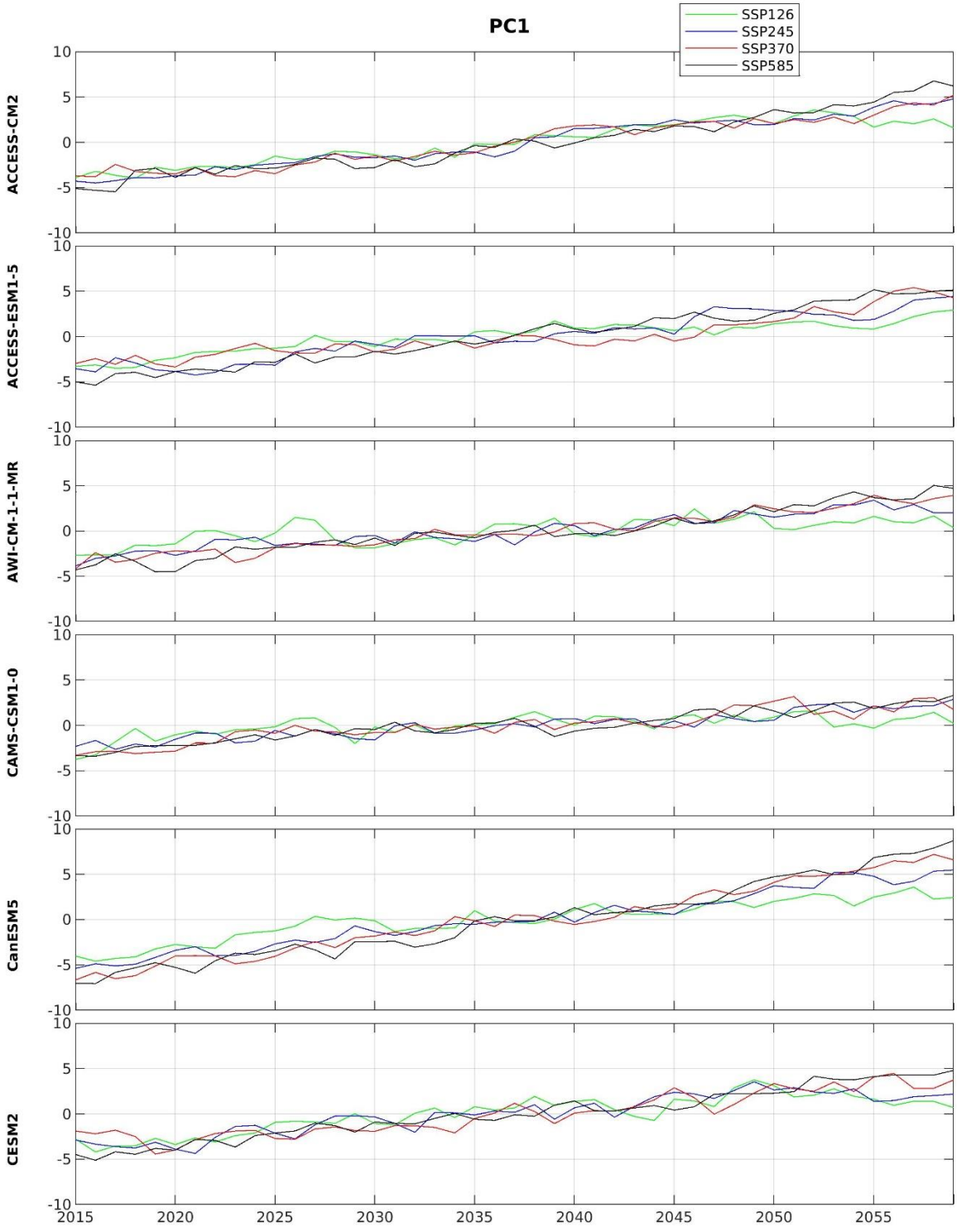

Figure A1.6a. PC1s of the AirT for the 2015-2059 period. Unit: ºC.

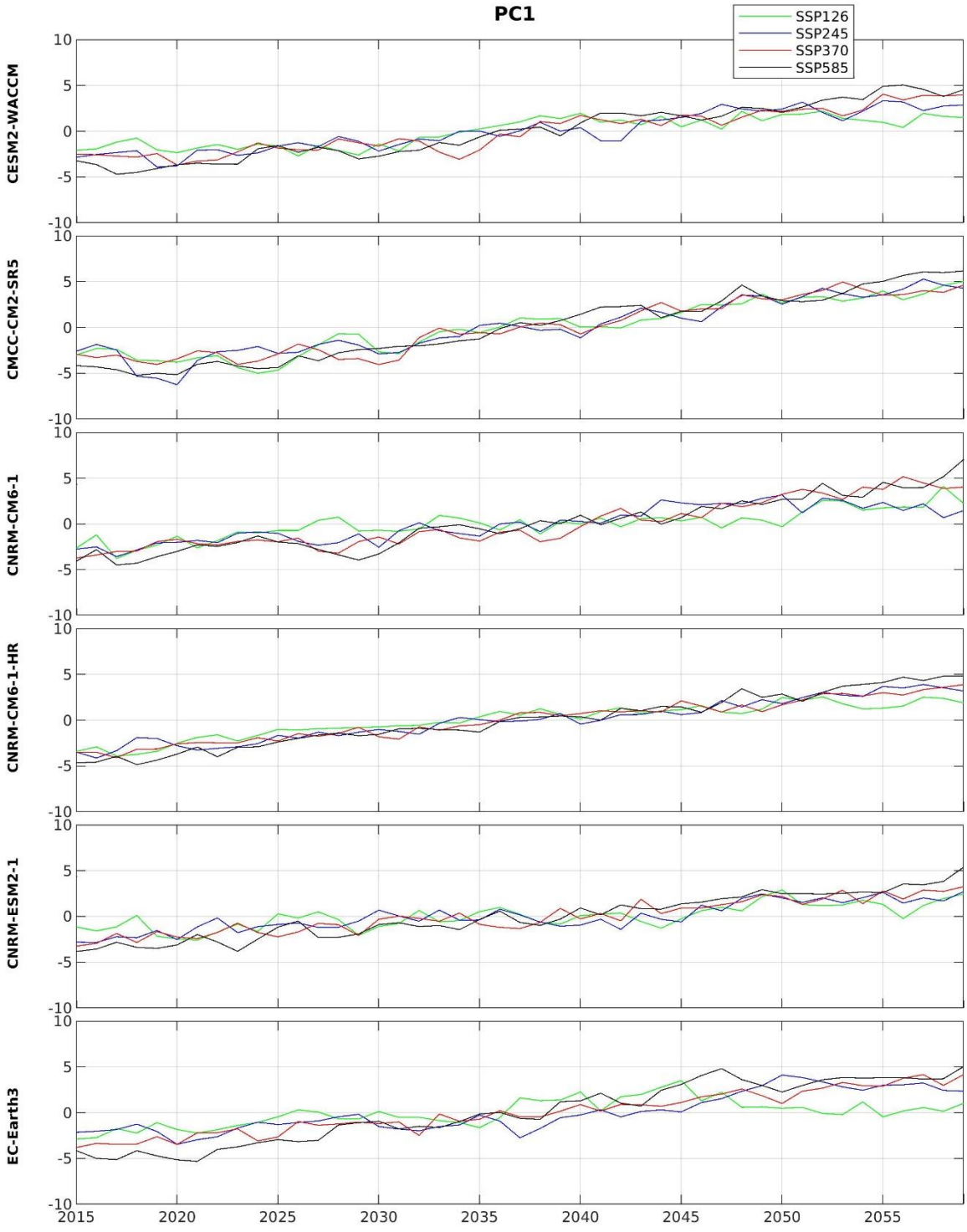

Figure A1.6b. PC1s of the AirT for the 2015-2059 period. Unit: ºC.

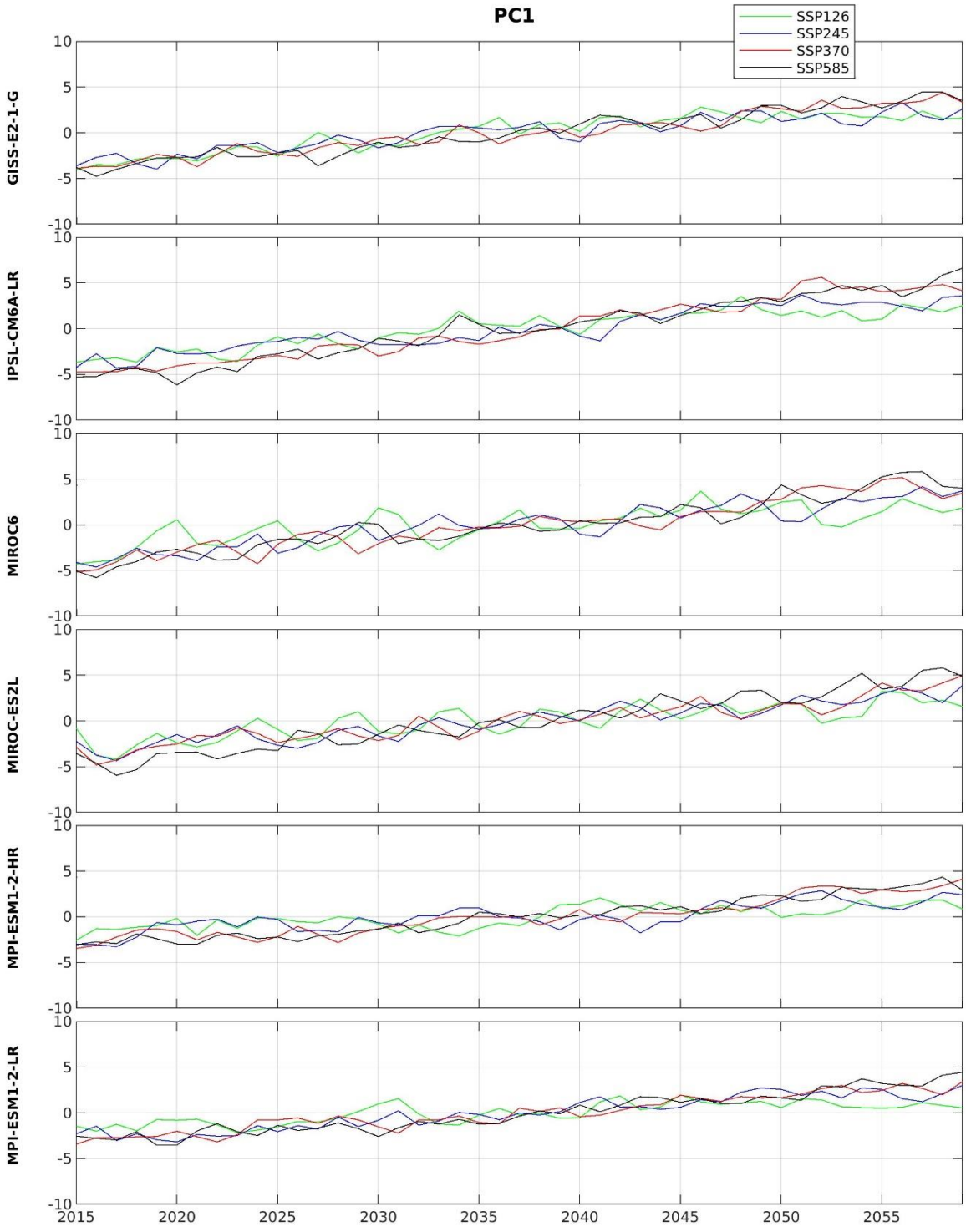

Figure A1.6c. PC1s of the AirT for the 2015-2059 period. Unit: ºC.

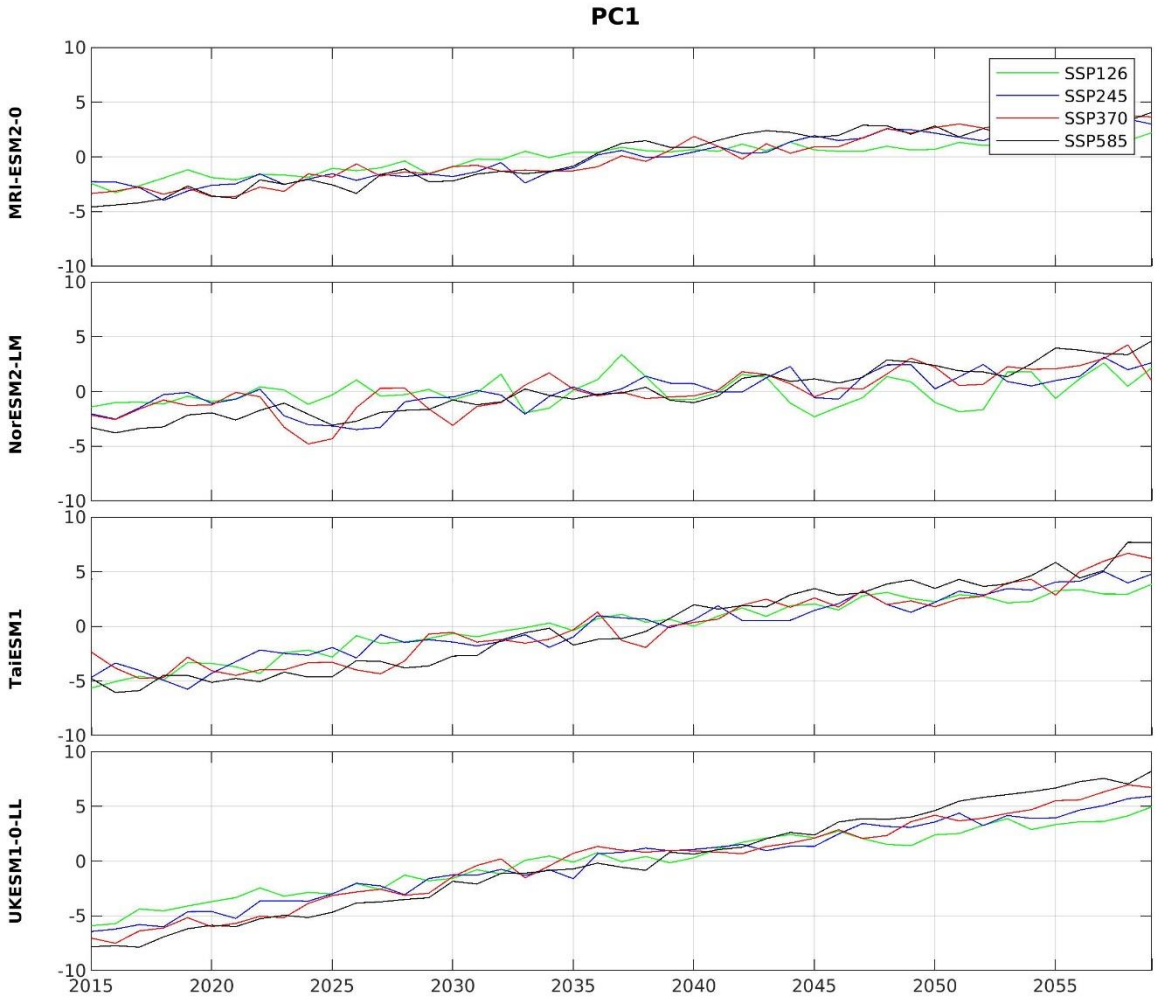

Figure A1.6d. PC1s of the AirT for the 2015-2059 period. Unit: ºC.

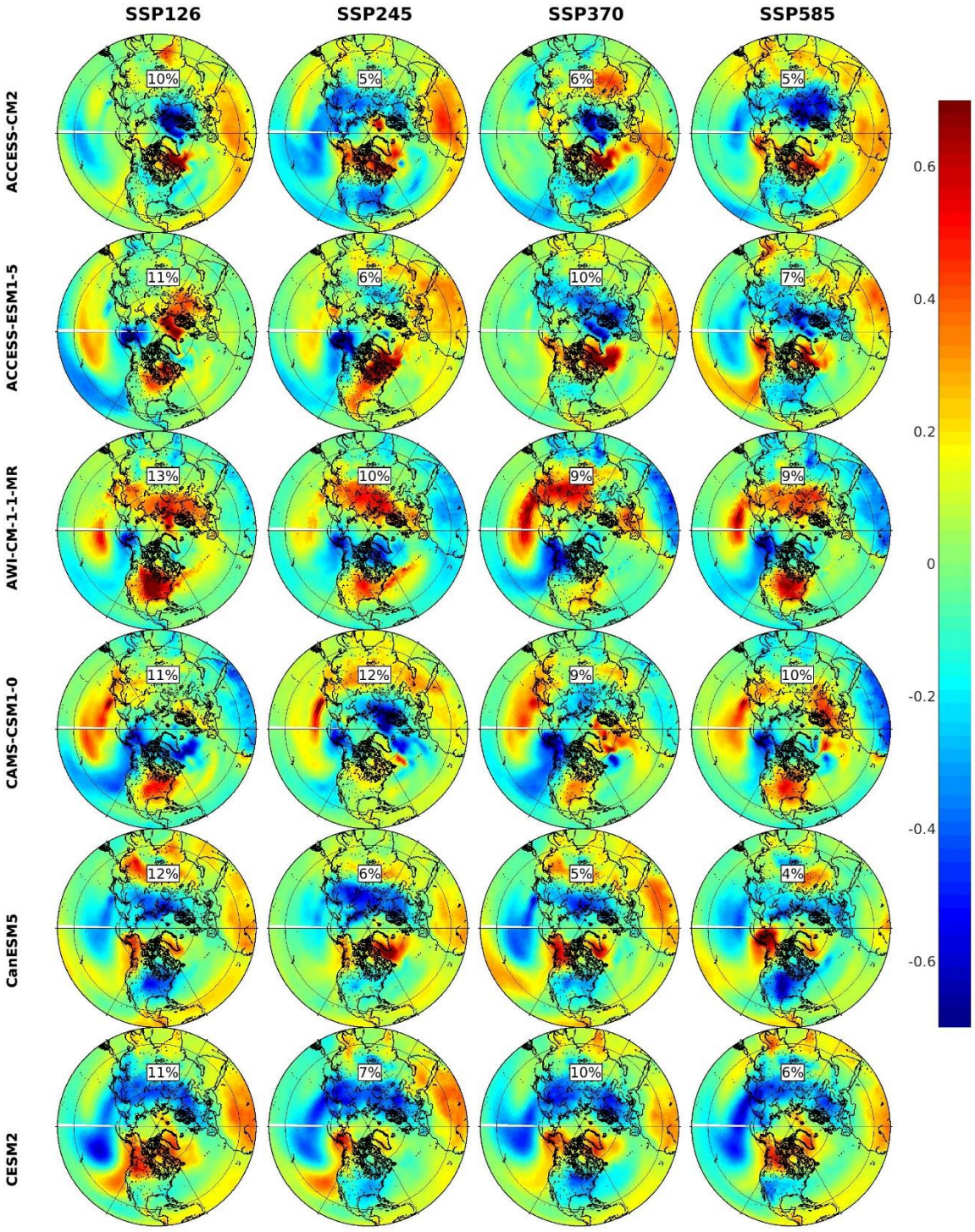

Figure A1.7a. EOF2s of the AirT for the 2015-2059 period.

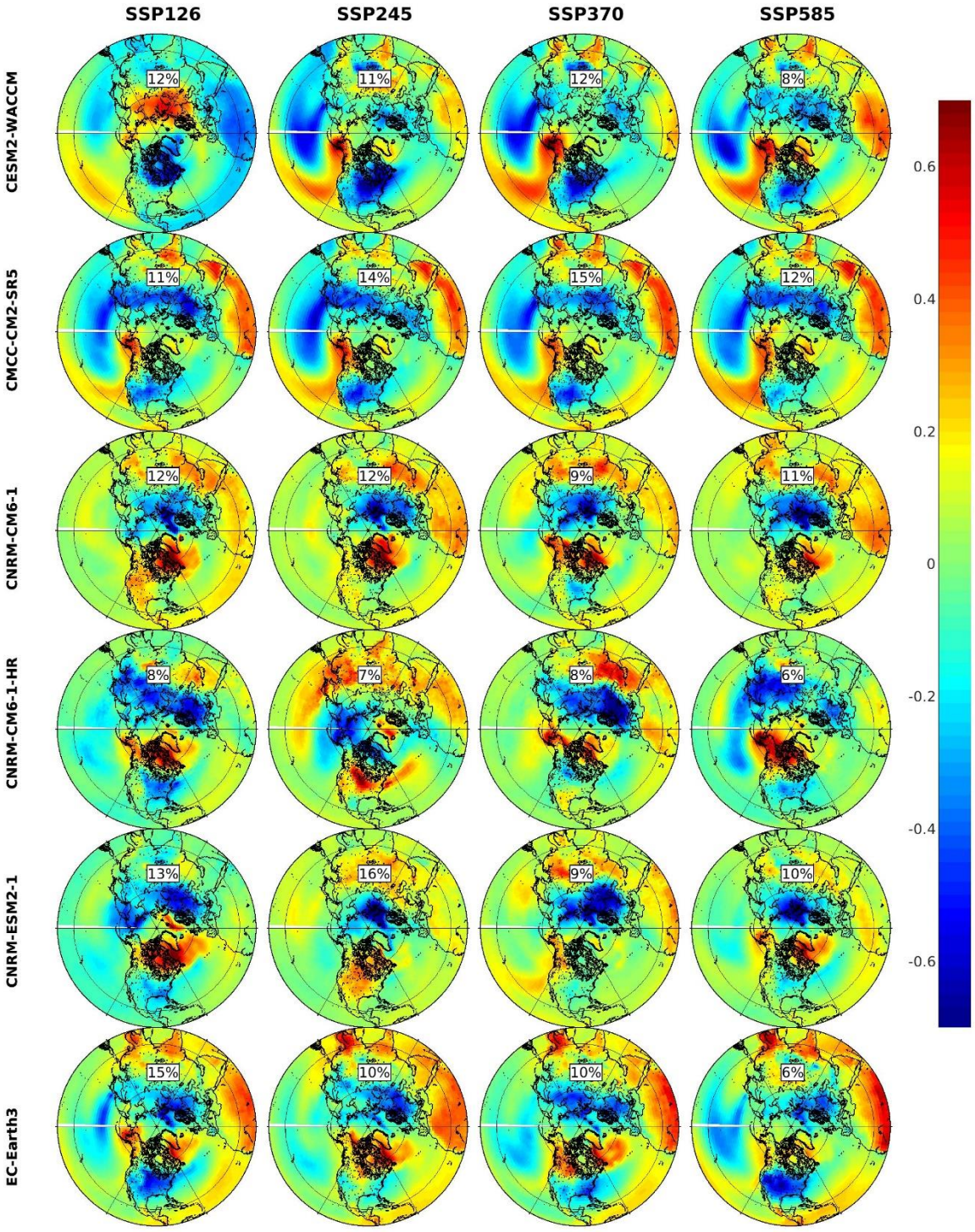

Figure A1.7b. EOF2s of the AirT for the 2015-2059 period.

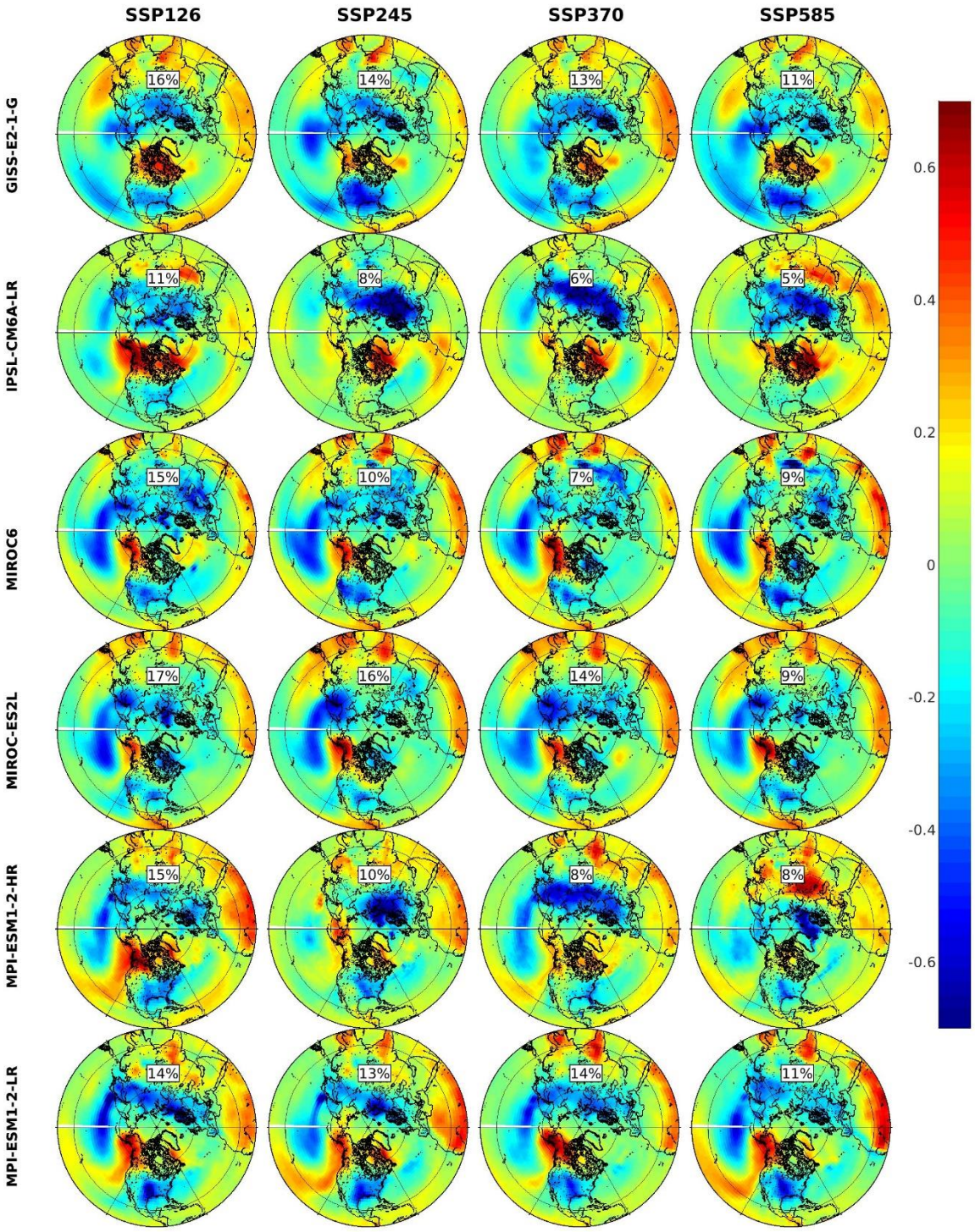

Figure A1.7c. EOF2s of the AirT for the 2015-2059 period.

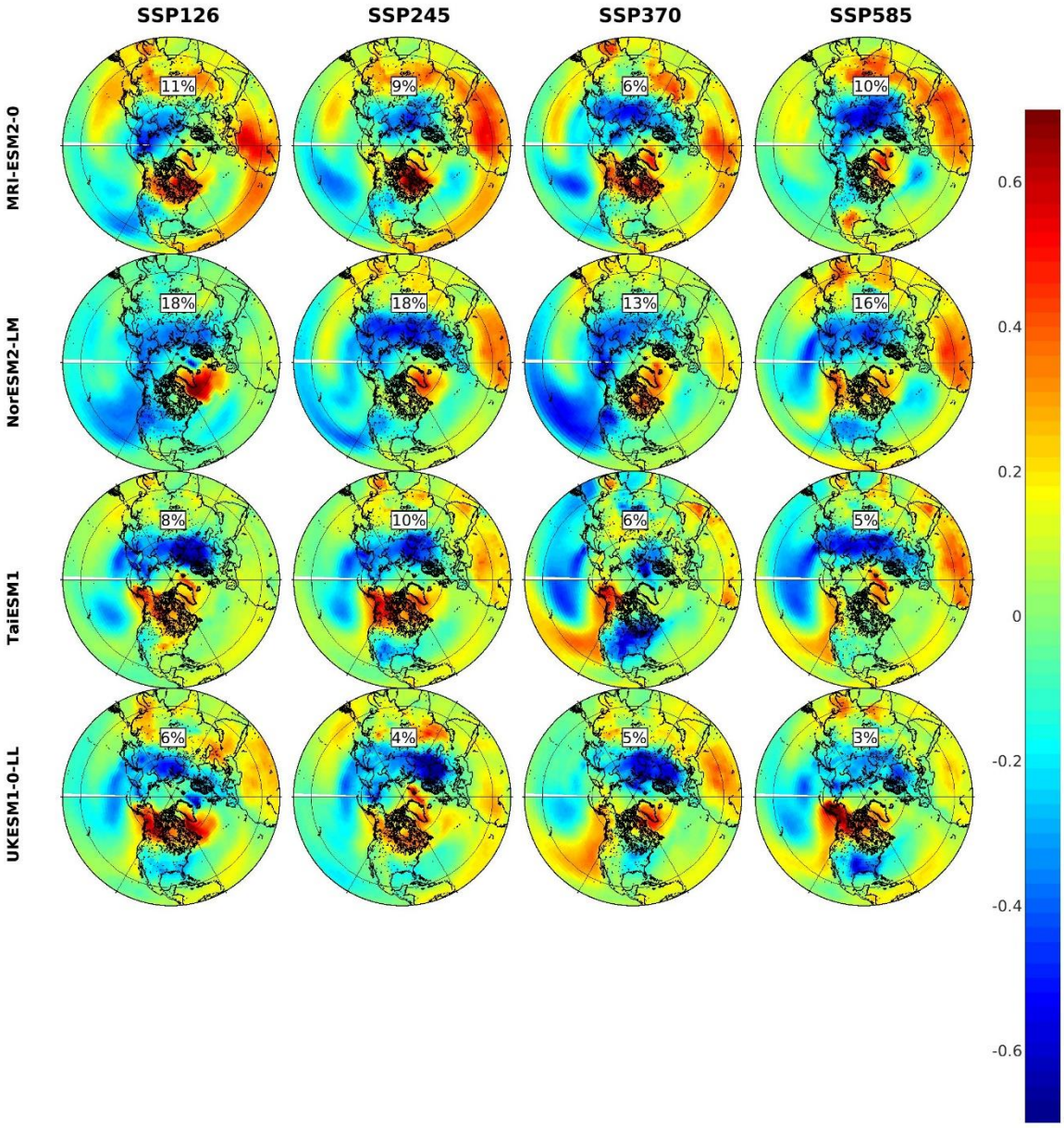

Figure A1.7d. EOF2s of the AirT for the 2015-2059 period.

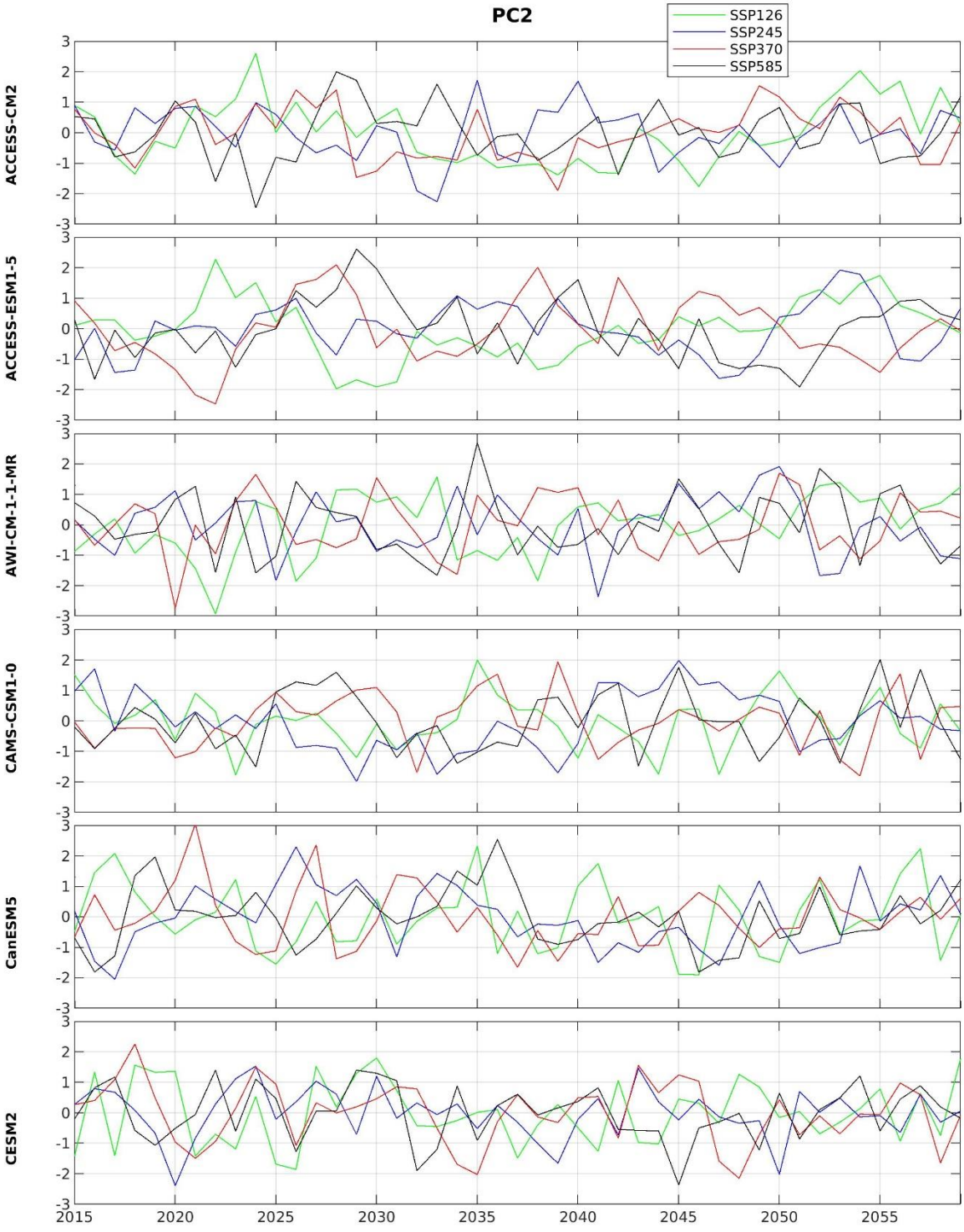

Figure A1.8a. PC2s of the AirT for the 2015-2059 period. Unit: ºC.

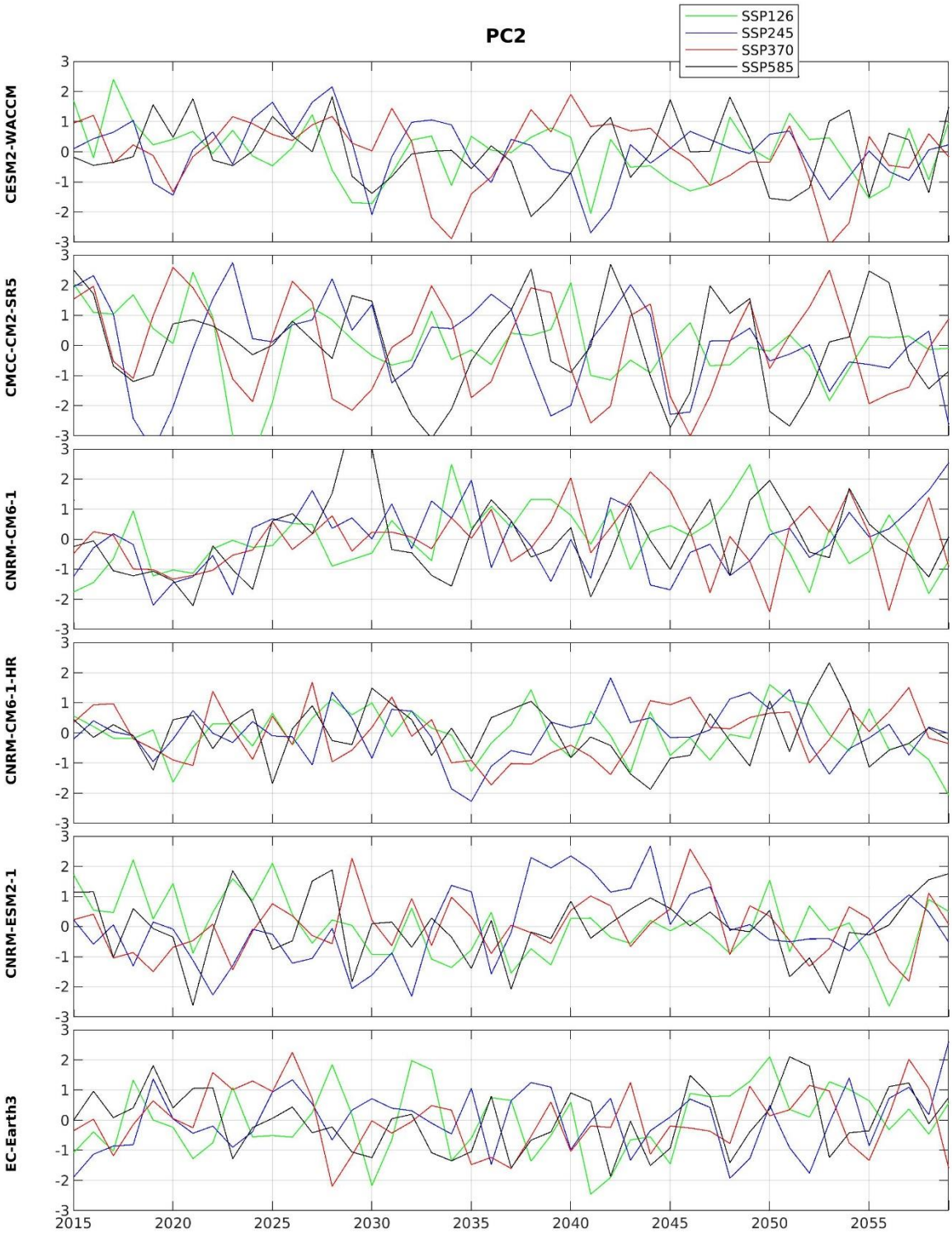

Figure A1.8b. PC2s of the AirT for the 2015-2059 period. Unit: ºC.

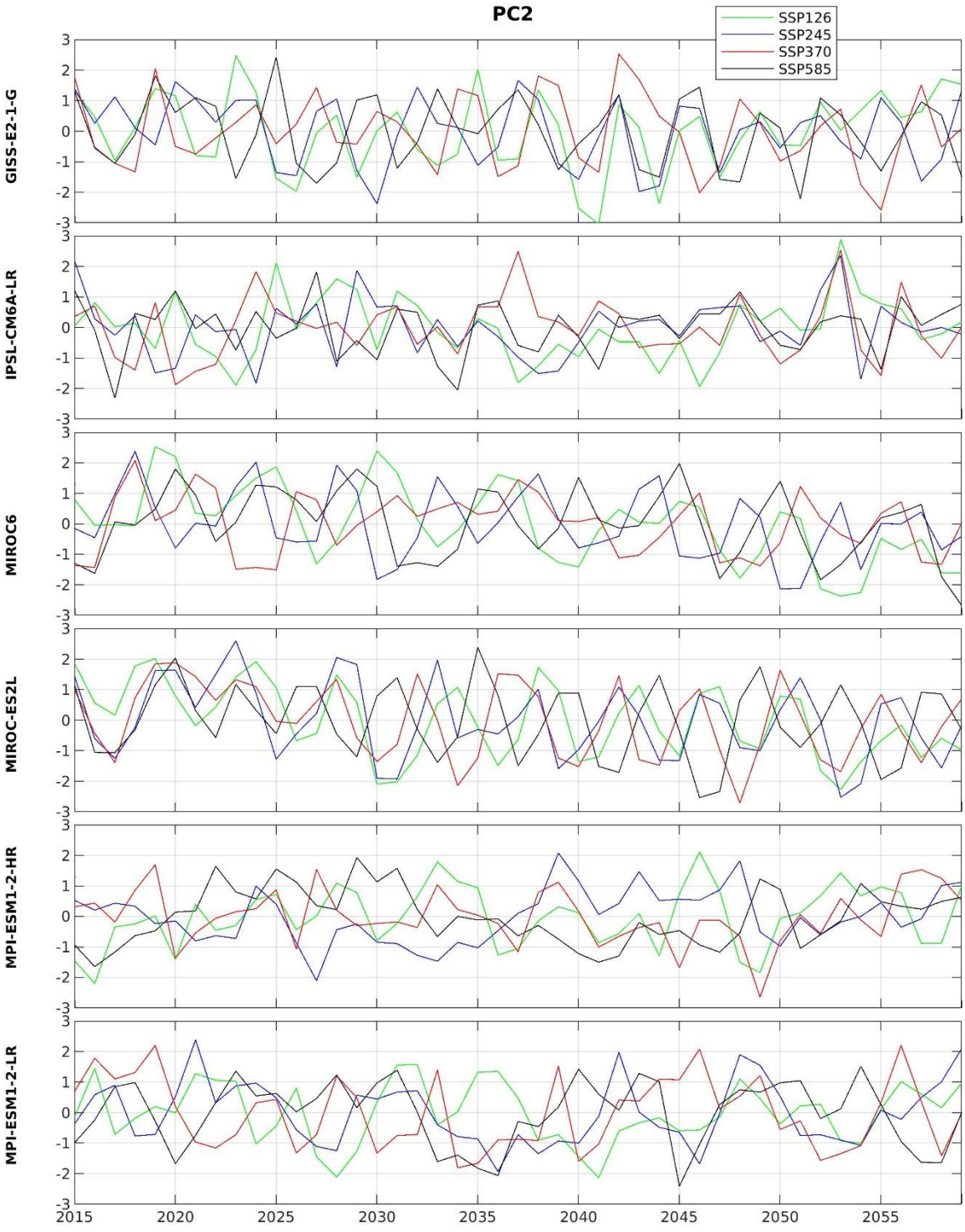

Figure A1.8c. PC2s of the AirT for the 2015-2059 period. Unit: ºC.

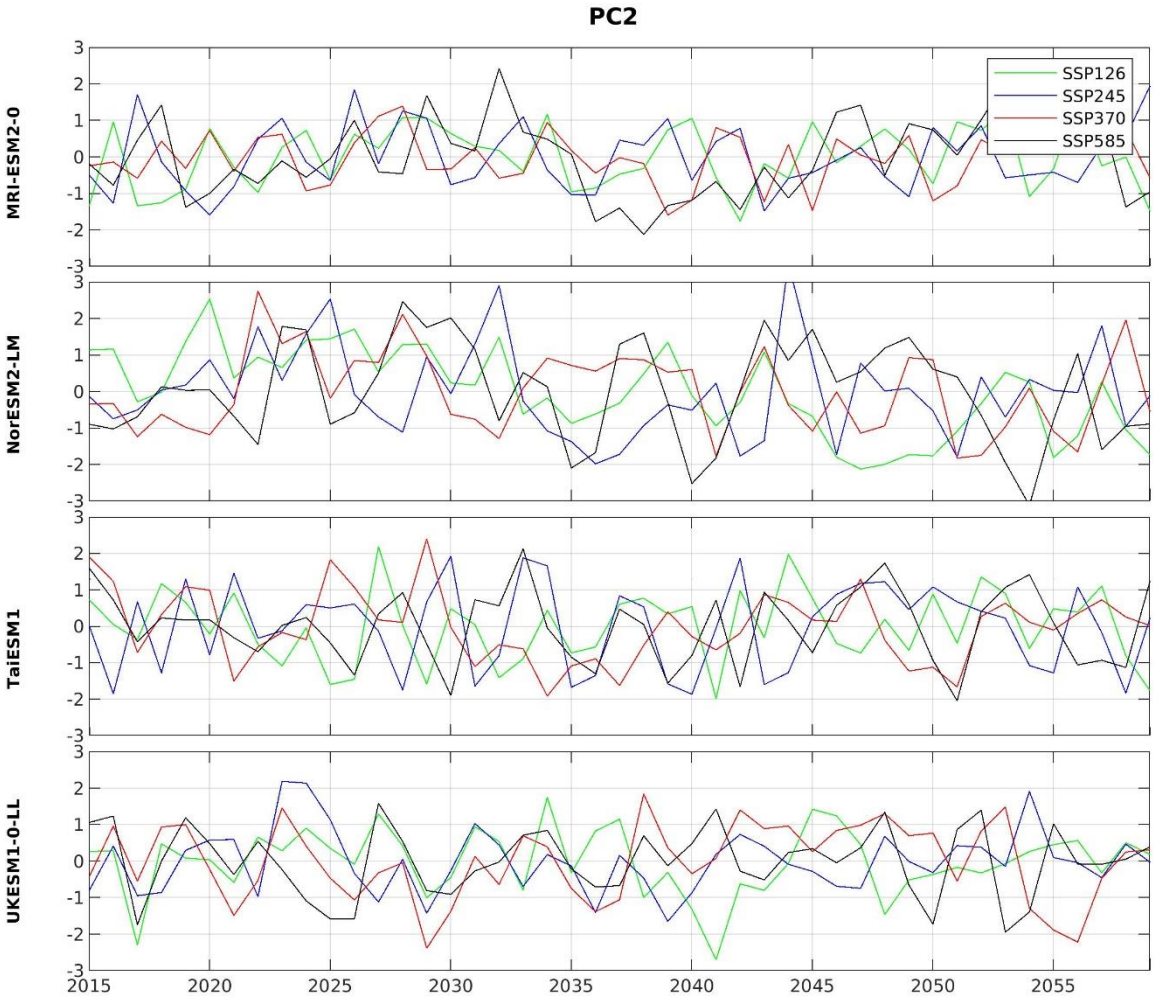

Figure A1.8d. PC2s of the AirT for the 2015-2059 period. Unit: ºC.

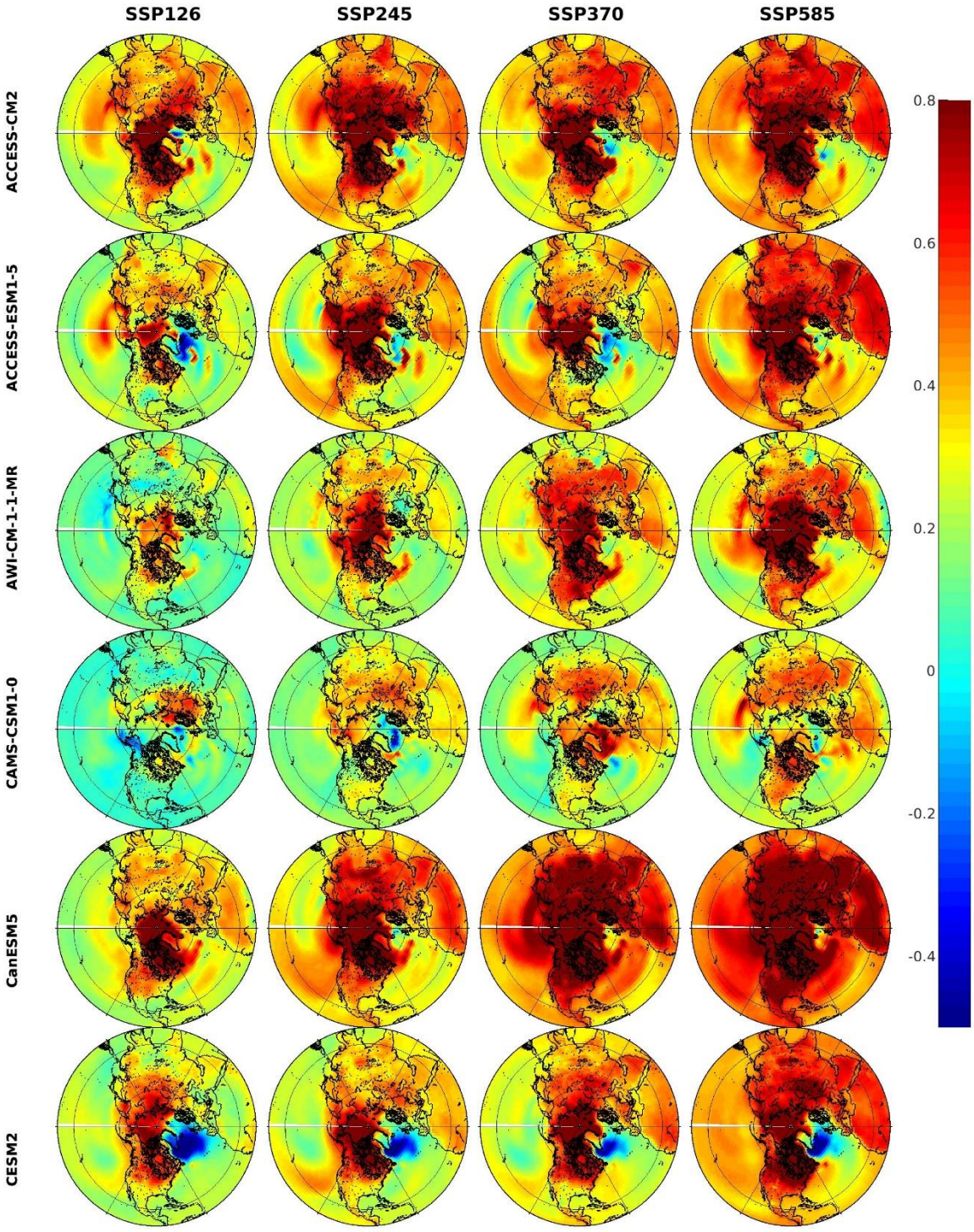

Figure A1.9a. Trends of the AirT in the 2015-2059 period. Unit: ºC/decade.

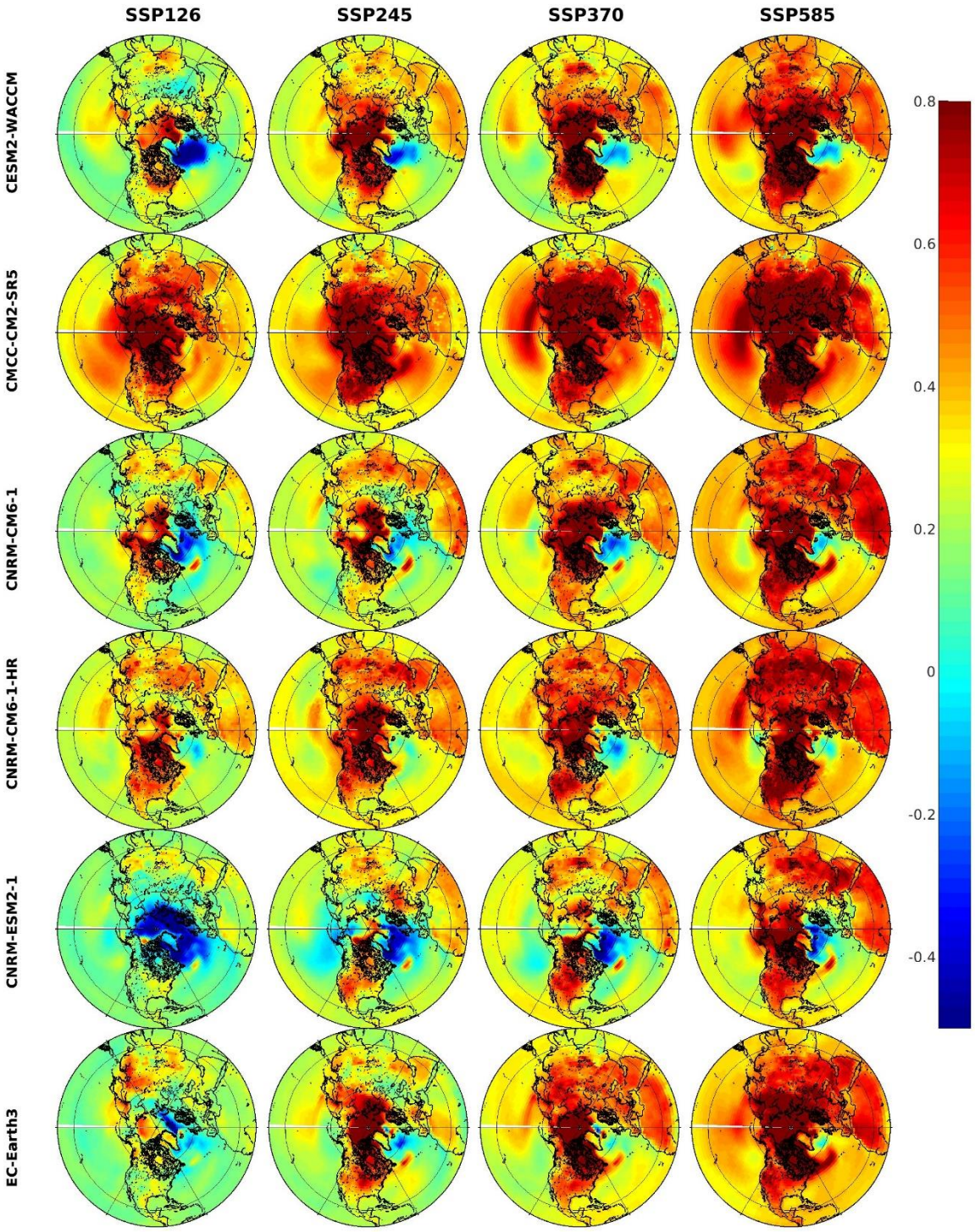

Figure A1.9b. Trends of the AirT in the 2015-2059 period. Unit: ºC/decade.

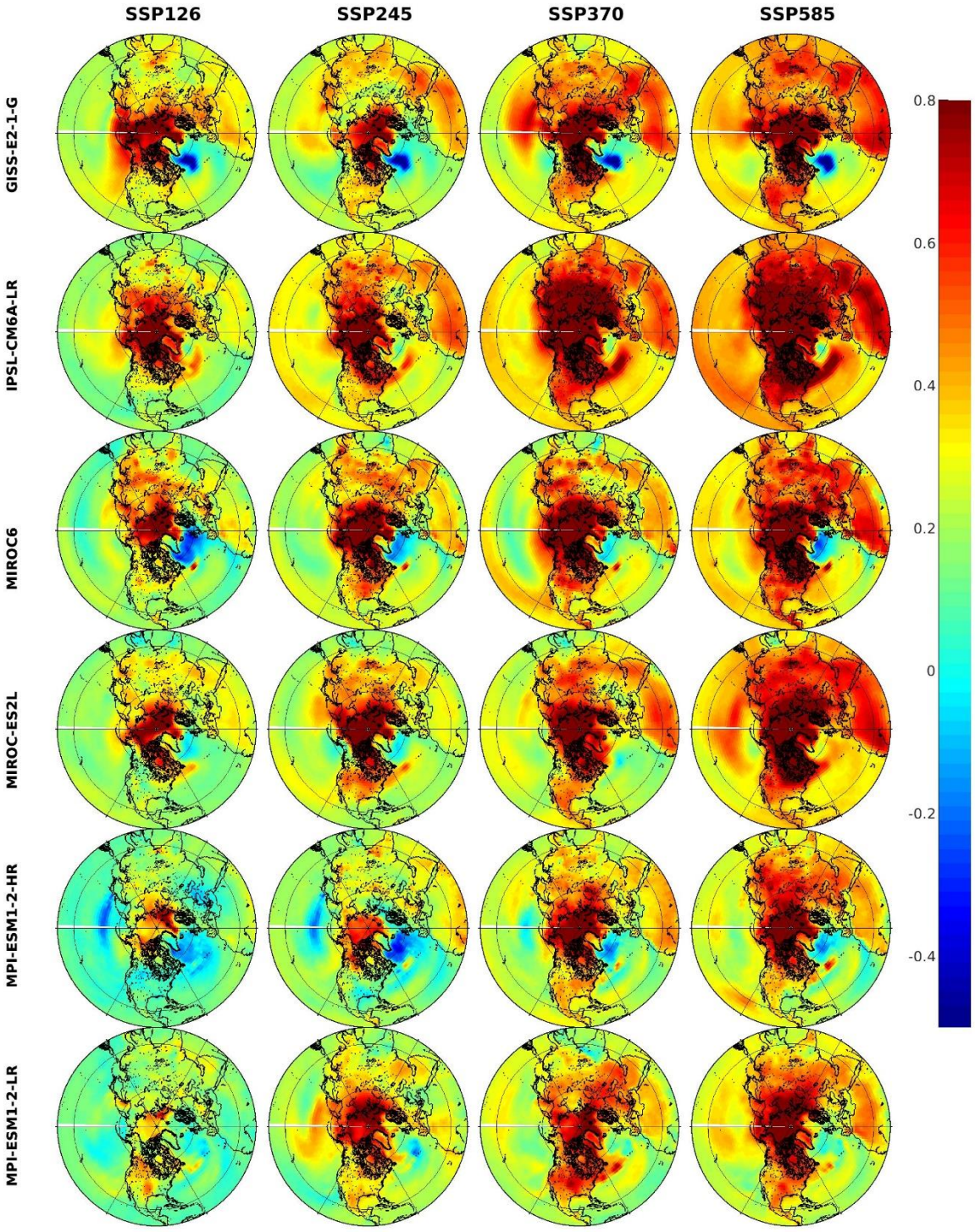

Figure A1.9c. Trends of the AirT in the 2015-2059 period. Unit: ºC/decade.

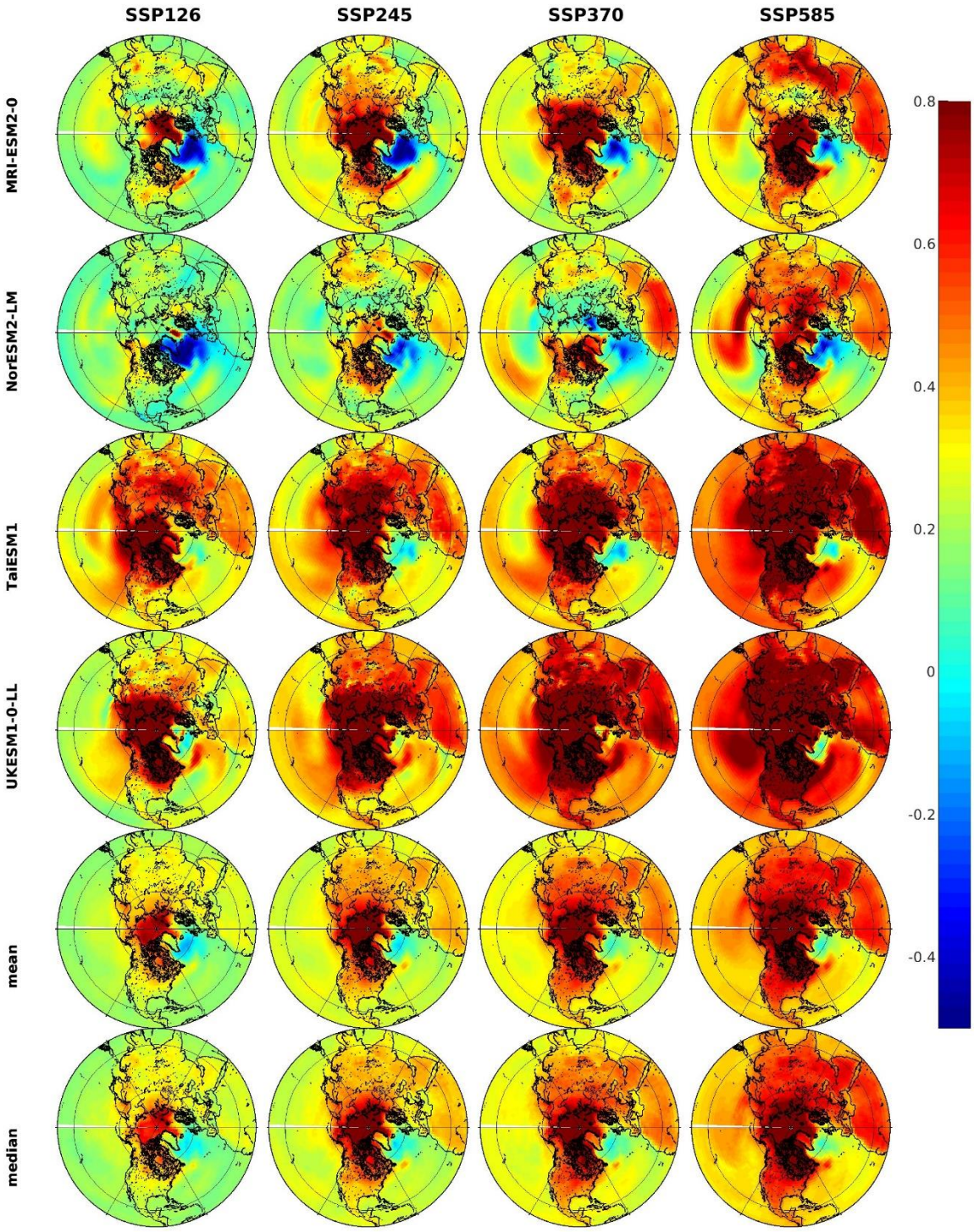

Figure A1.9d. Trends of the AirT in the 2015-2059 period. Unit: ºC/decade.

Appendix 2

Figures for the changes in the three oceans

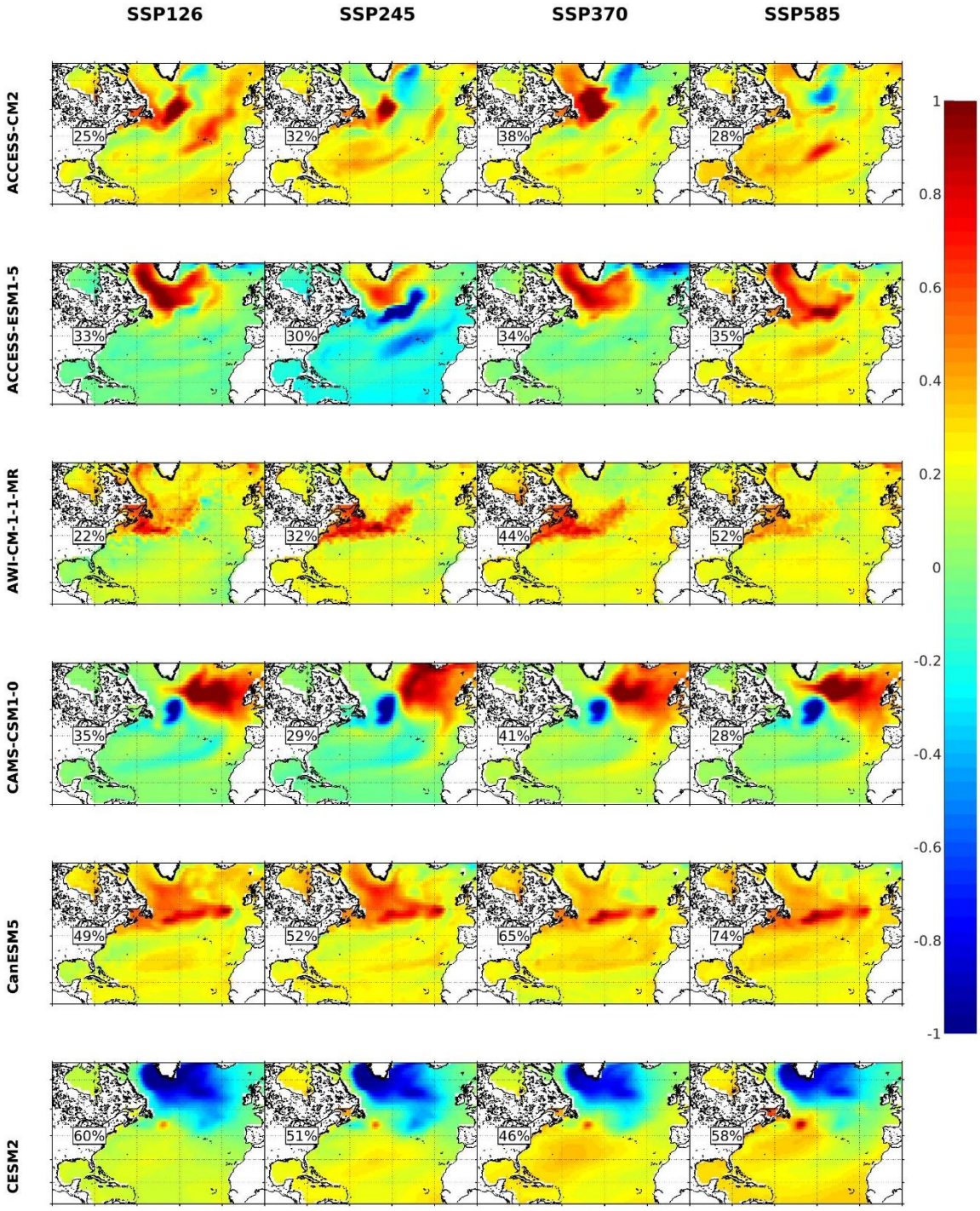

Figure A2.1a. EOF1s of the SST for the 2015-2059 period.

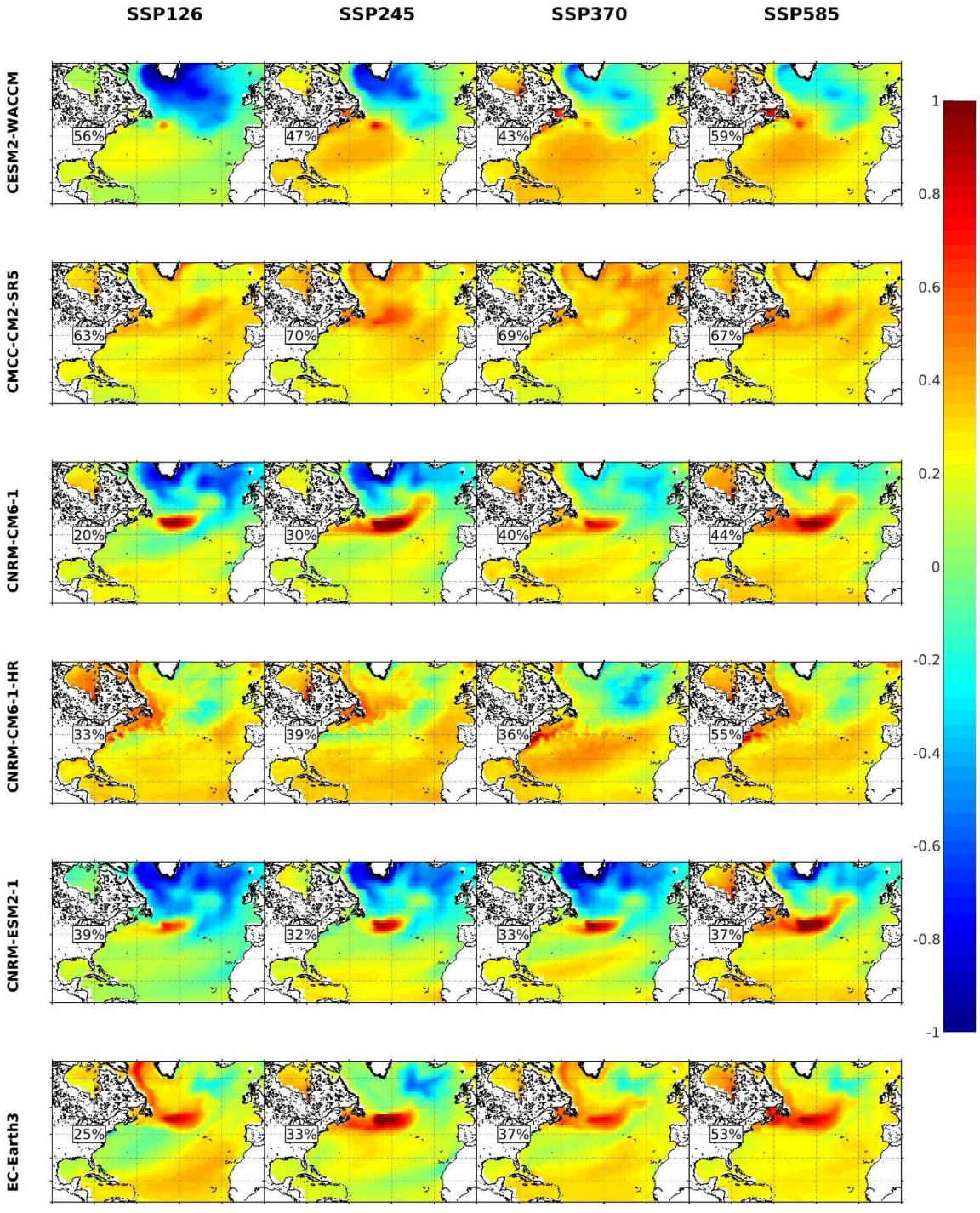

Figure A2.1b. EOF1s of the SST for the 2015-2059 period.

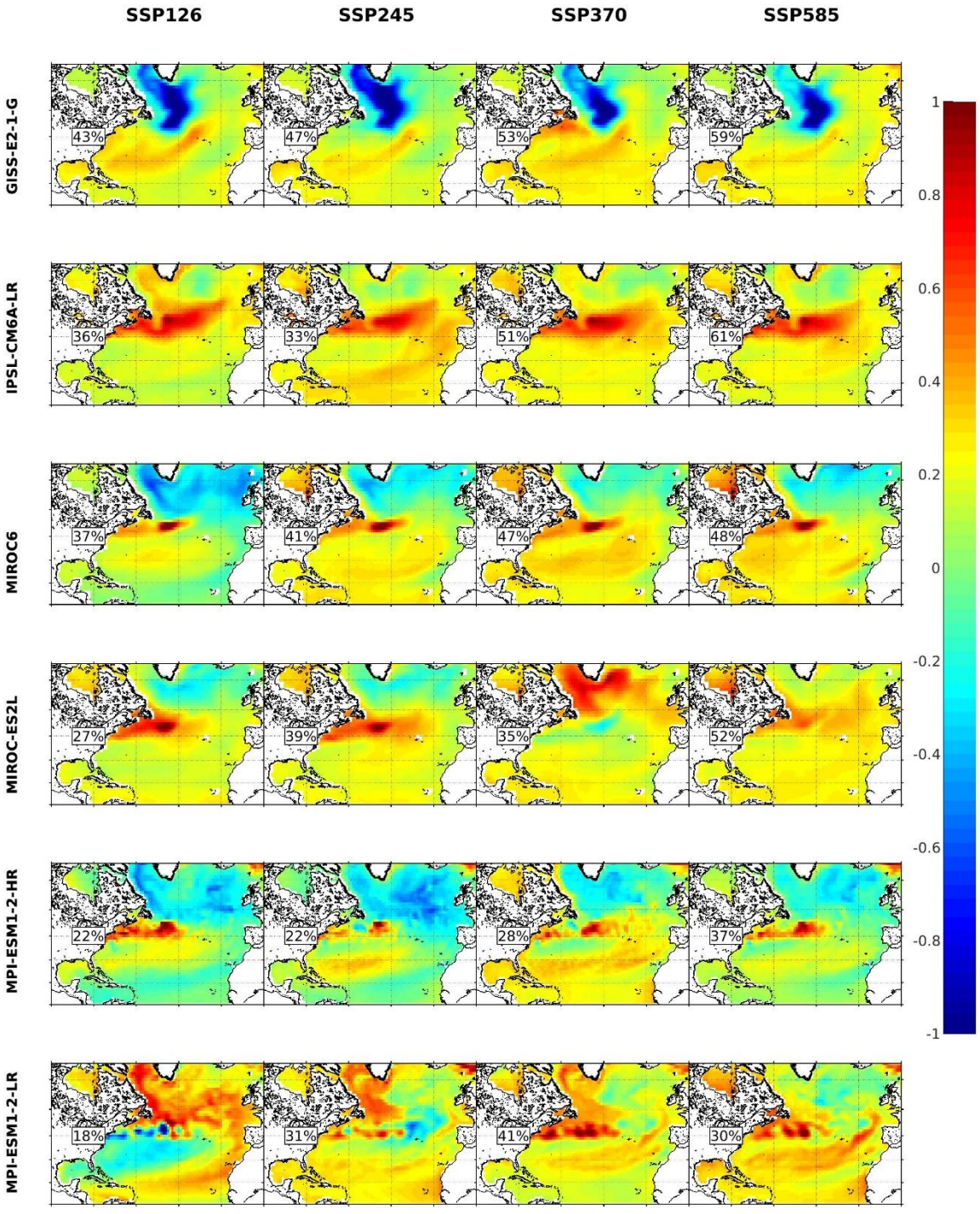

Figure A2.1c. EOF1s of the SST for the 2015-2059 period.

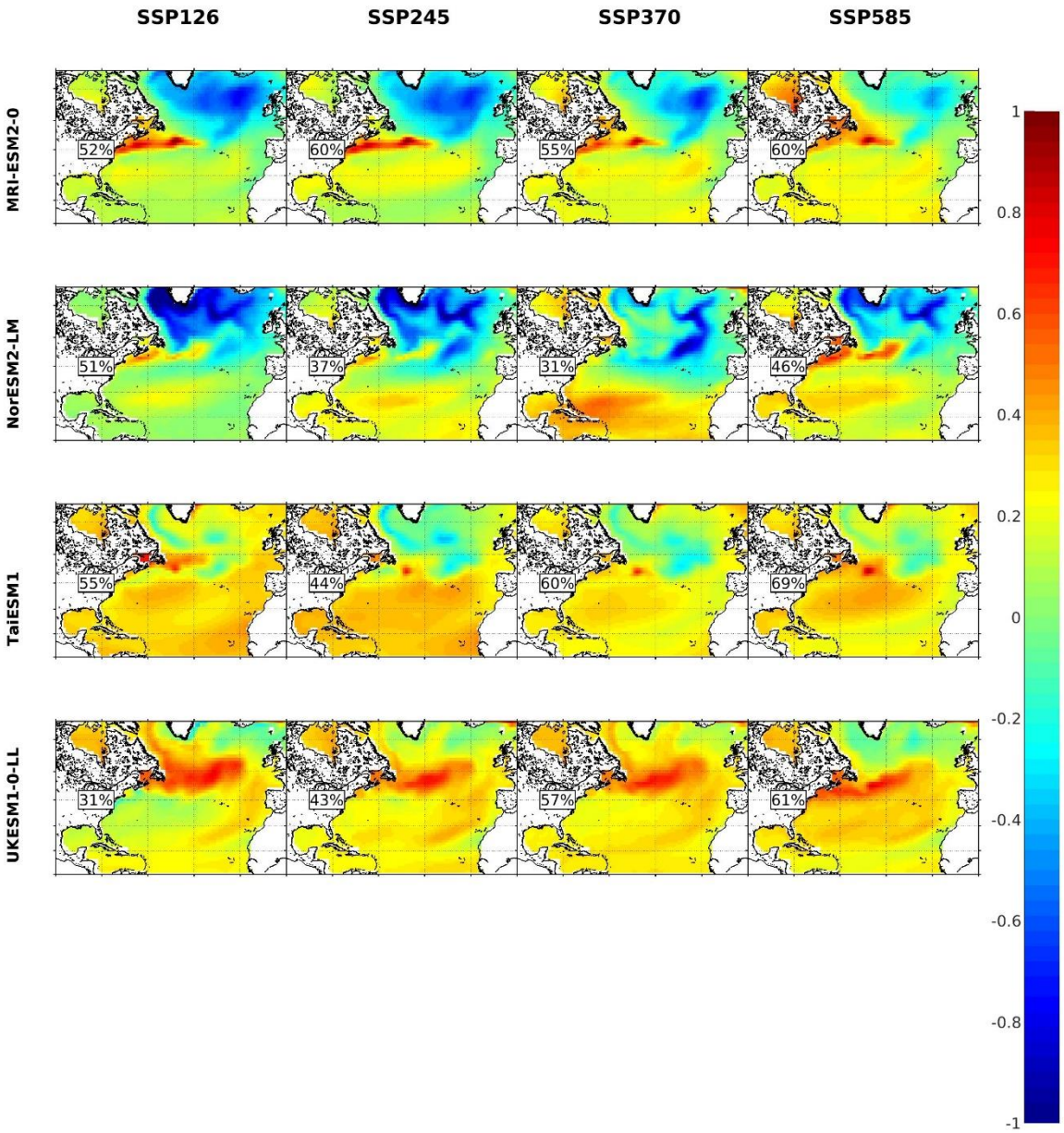

Figure A2.1d. EOF1s of the SST for the 2015-2059 period.

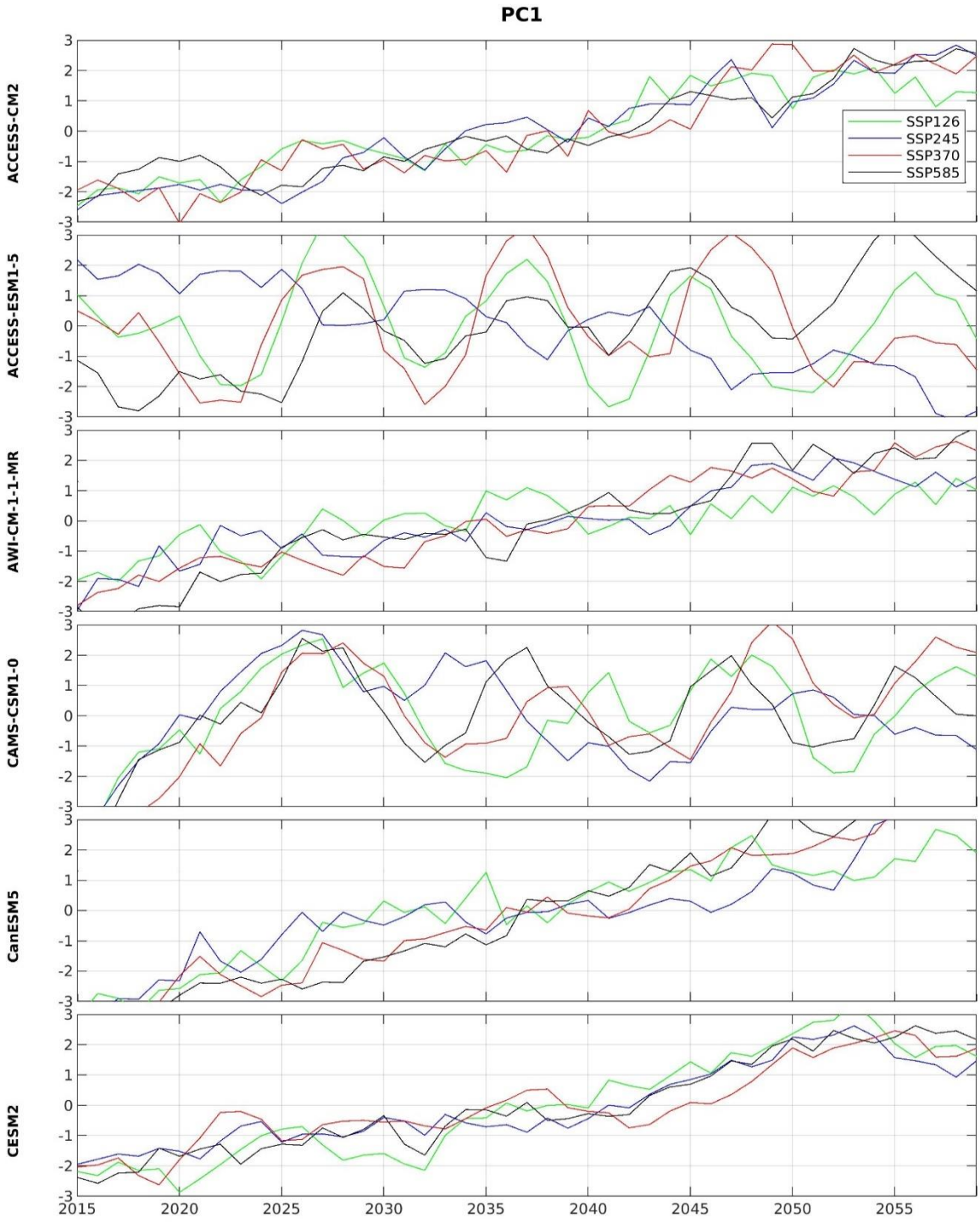

Figure A2.2a. PC1s of the SST for the 2015-2059 period. Unit: ºC.

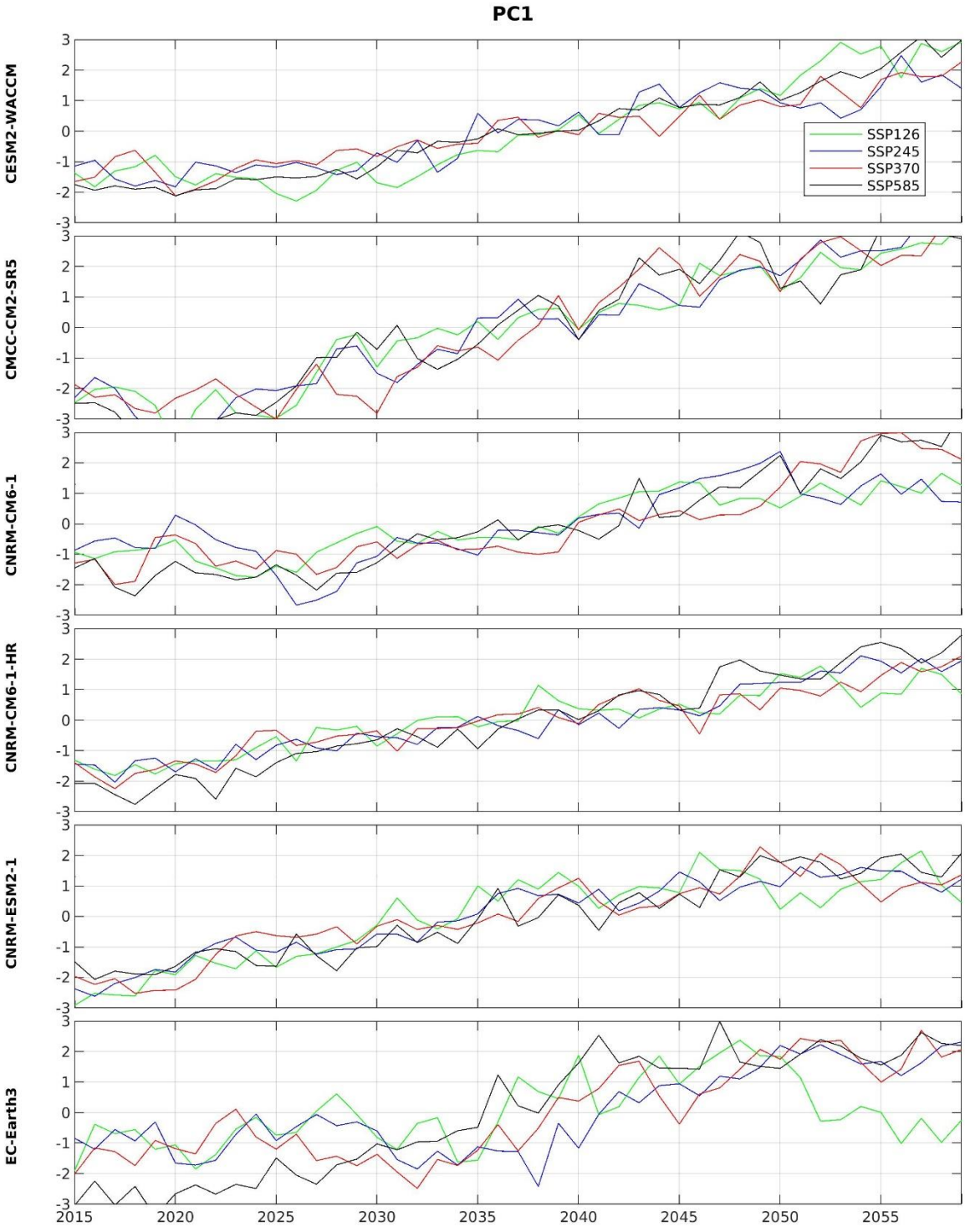

Figure A2.2b. PC1s of the SST for the 2015-2059 period. Unit: ºC.

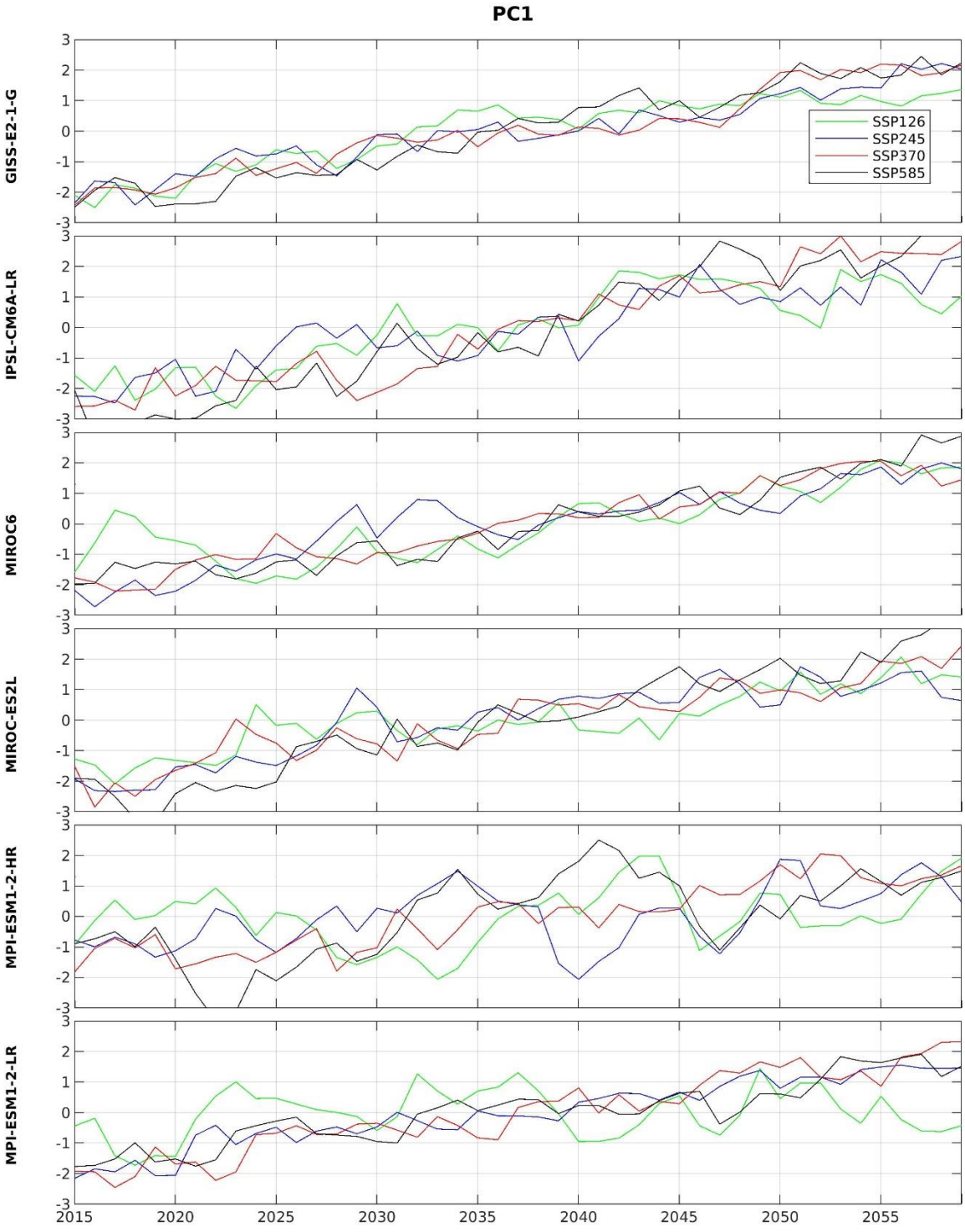

Figure A2.2c. PC1s of the SST for the 2015-2059 period. Unit: ºC.

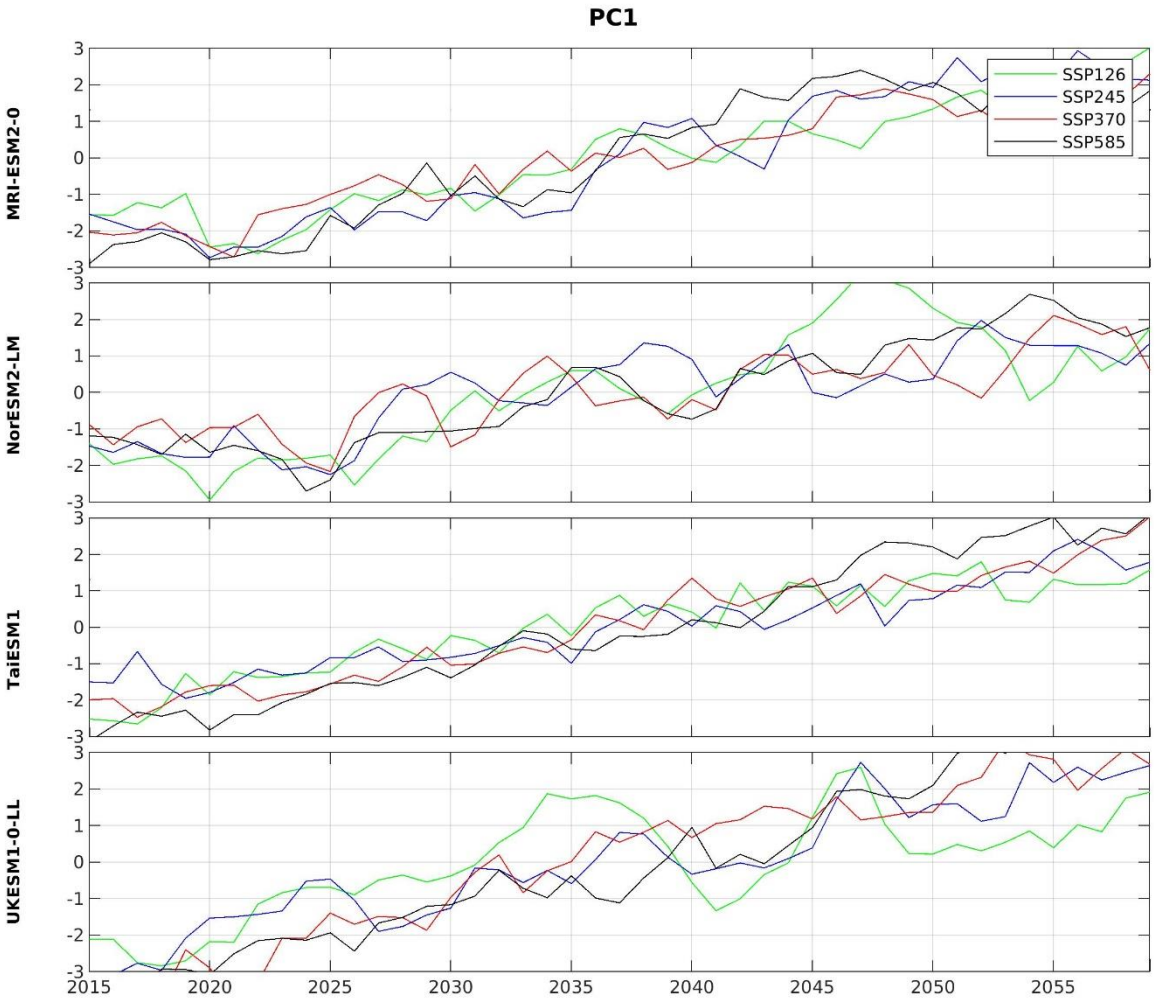

Figure A2.2d. PC1s of the SST for the 2015-2059 period. Unit: ºC.

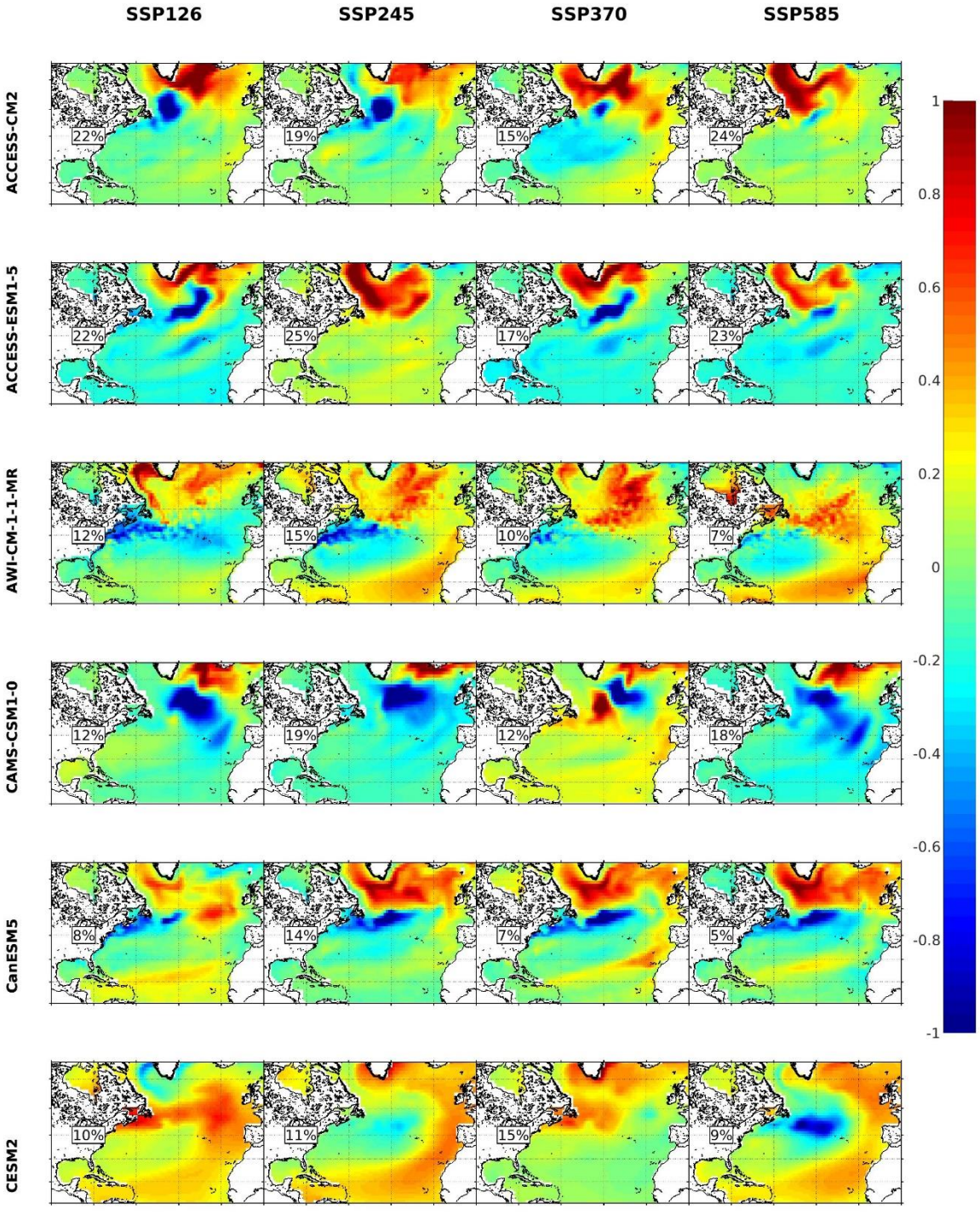

Figure A2.3a. EOF2s of the SST for the 2015-2059 period.

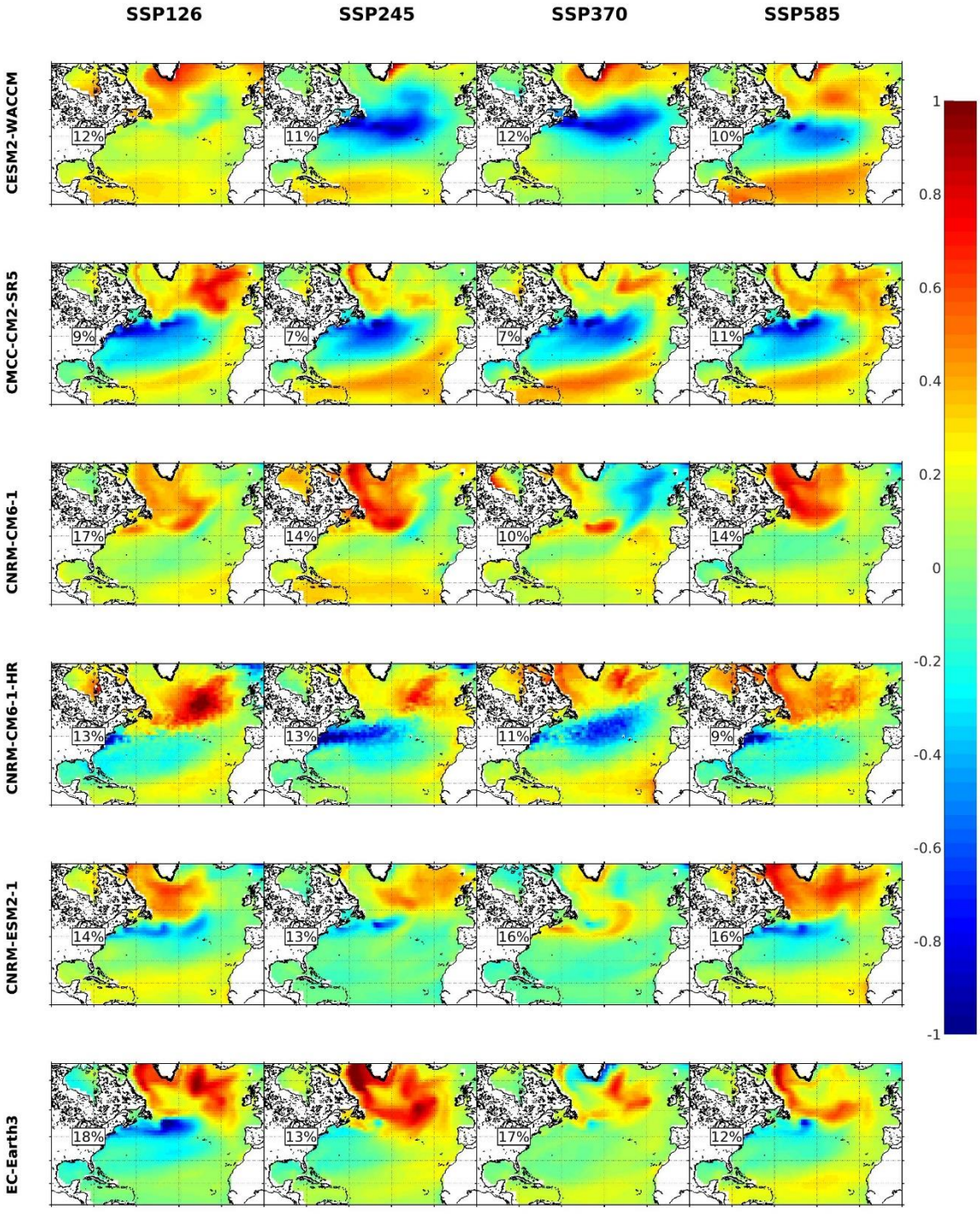

Figure A2.3b. EOF2s of the SST for the 2015-2059 period.

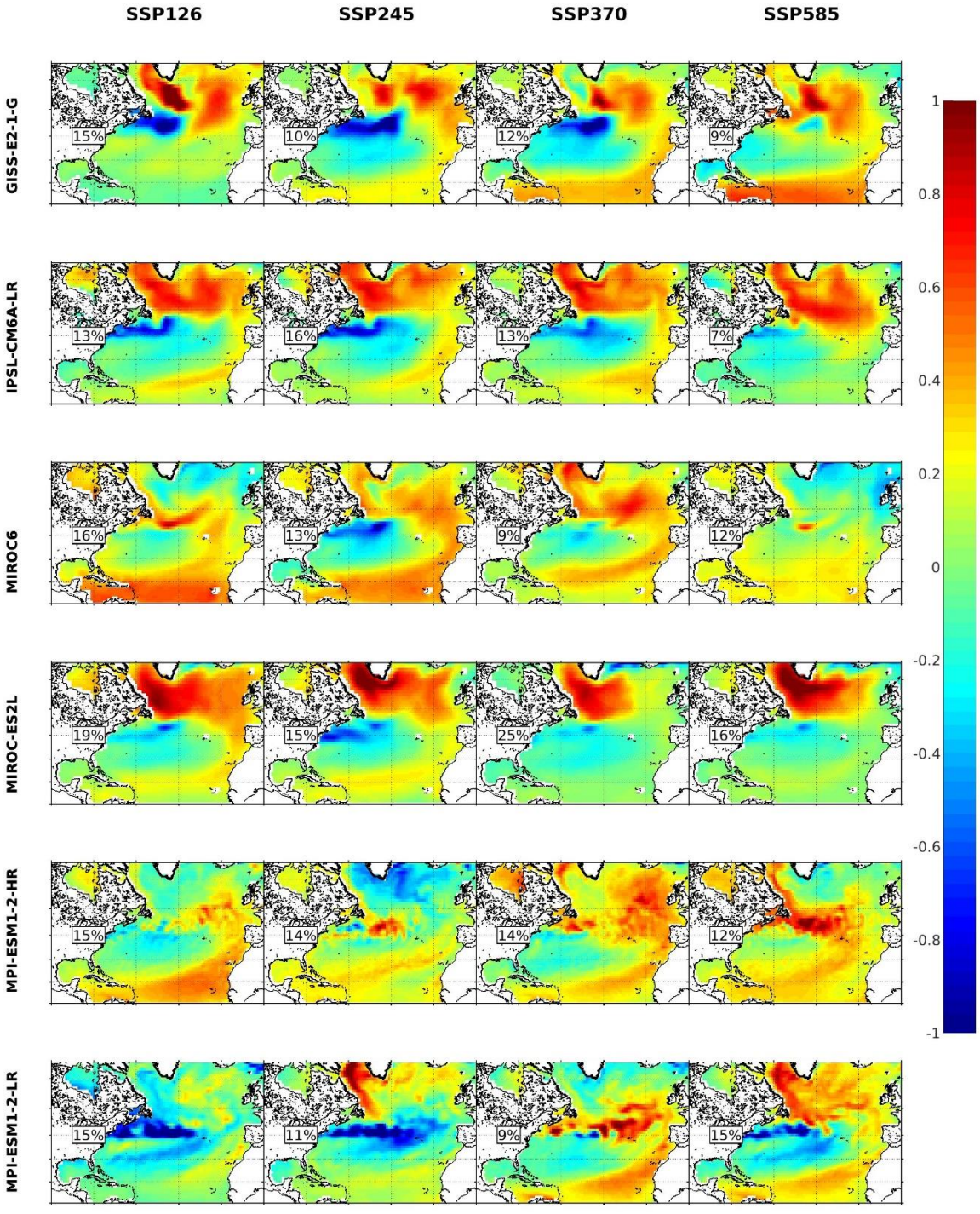

Figure A2.3c. EOF2s of the SST for the 2015-2059 period.

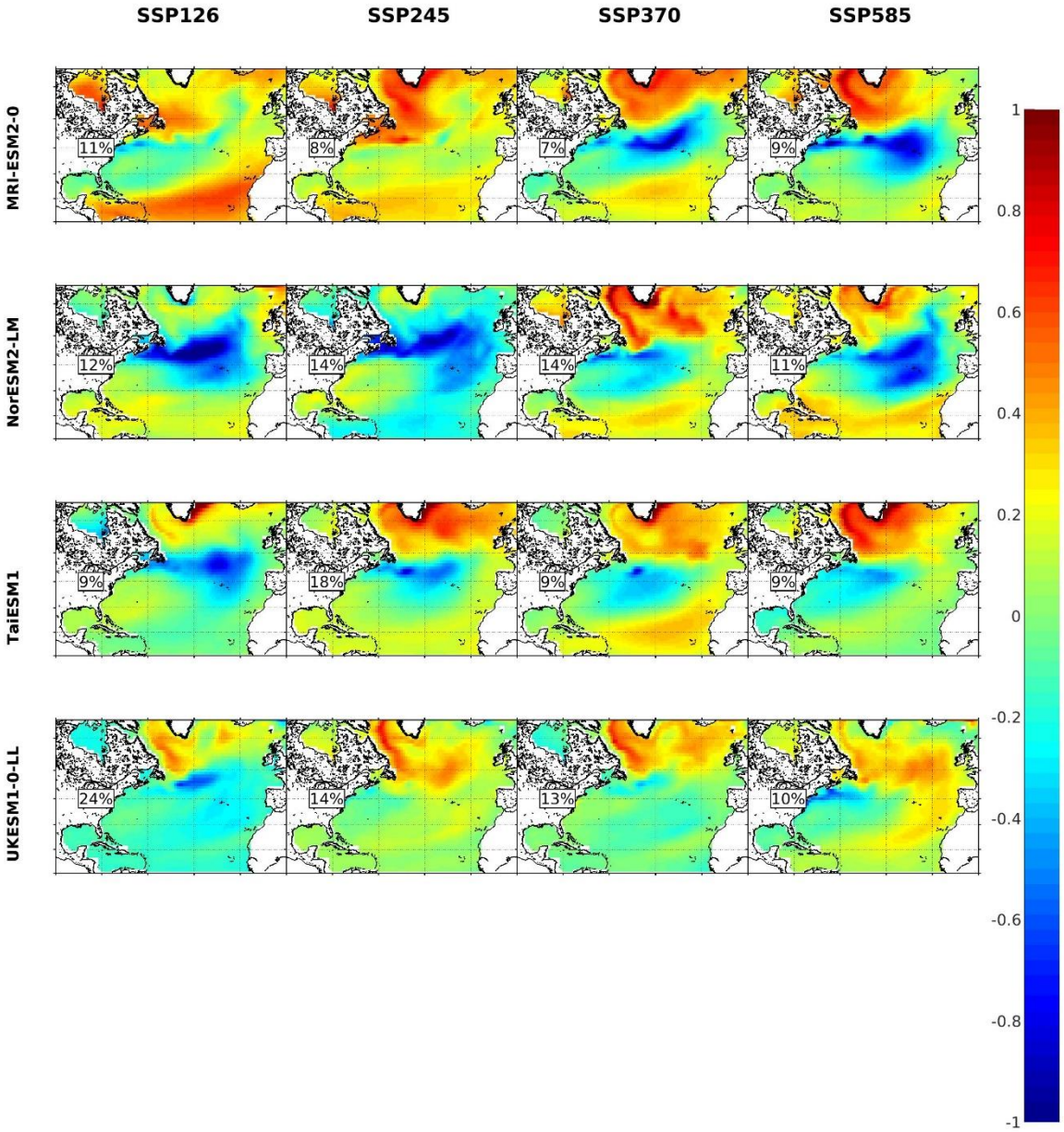

Figure A2.3d. EOF2s of the SST for the 2015-2059 period.

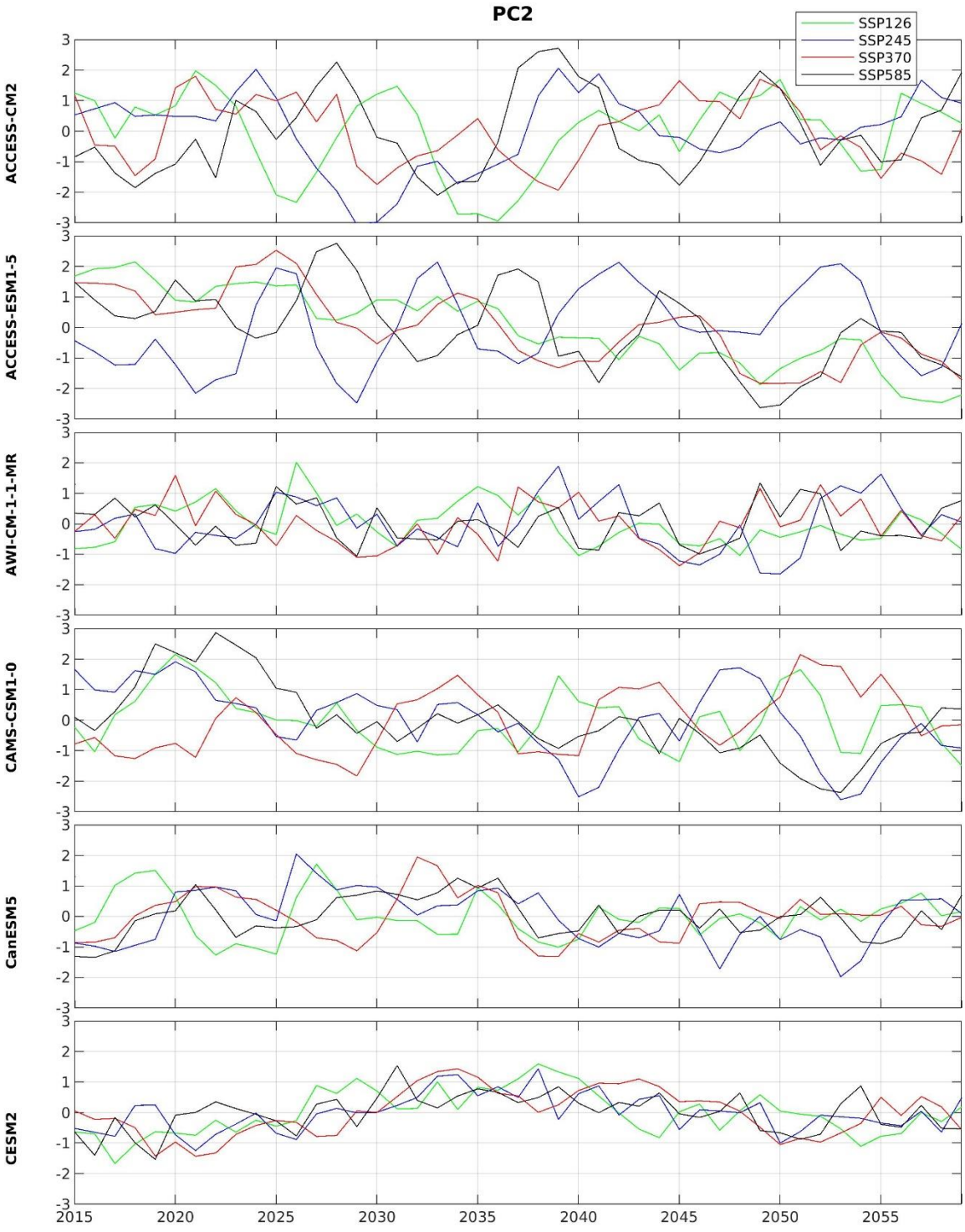

Figure A2.4a. PC2s of the SST for the 2015-2059 period. Unit: ºC.

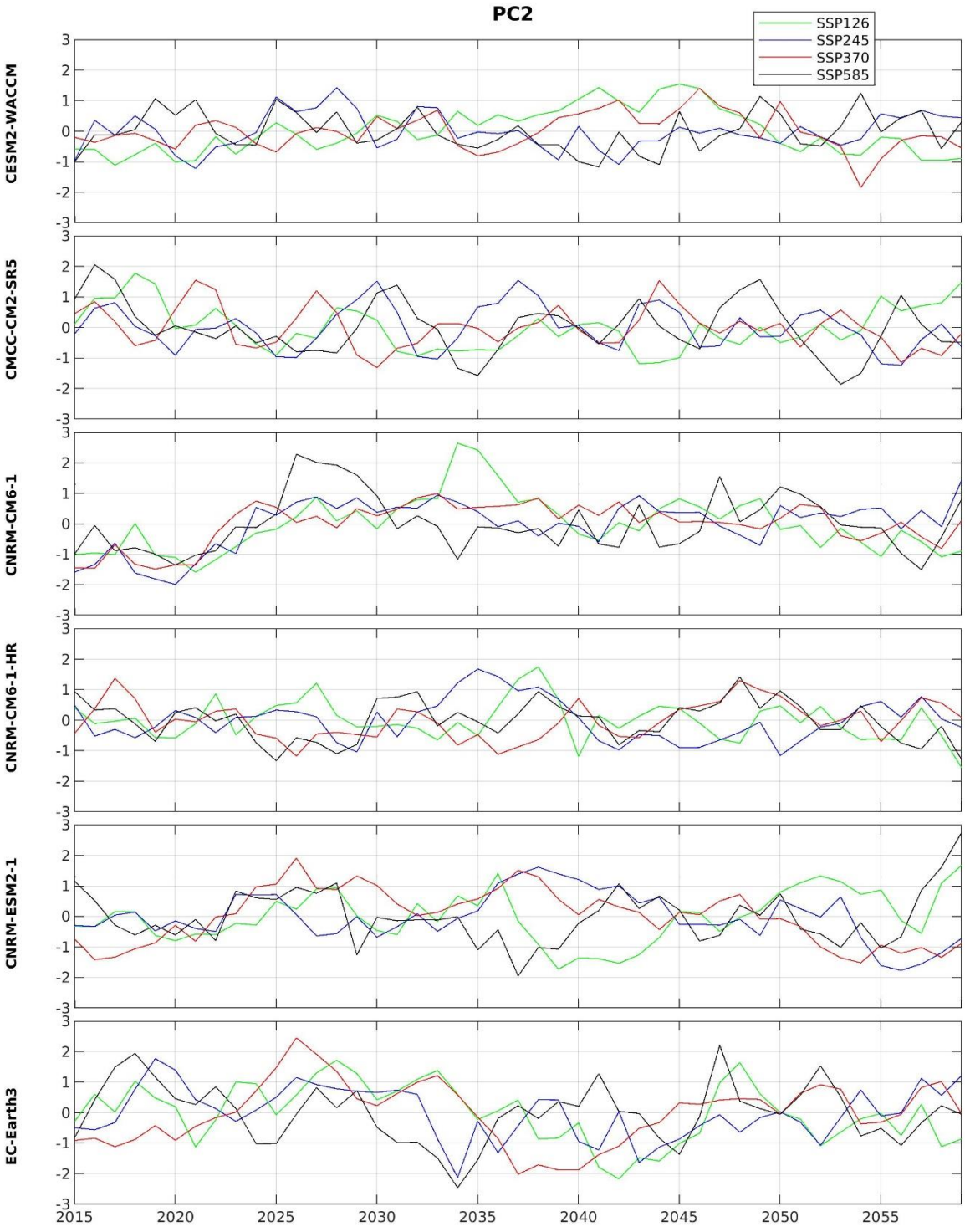

Figure A2.4b. PC2s of the SST for the 2015-2059 period. Unit: ºC.

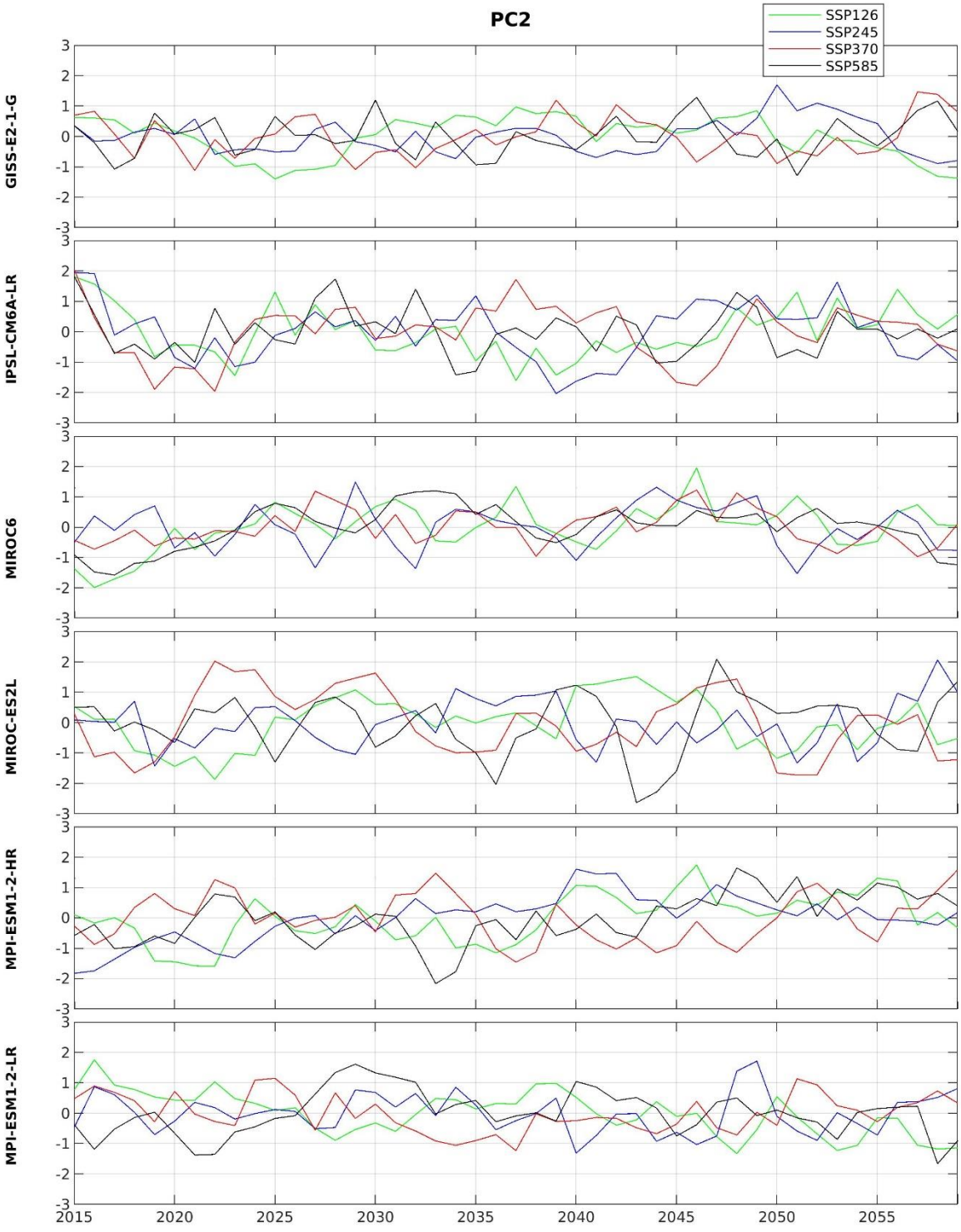

Figure A2.4c. PC2s of the SST for the 2015-2059 period. Unit: ºC.

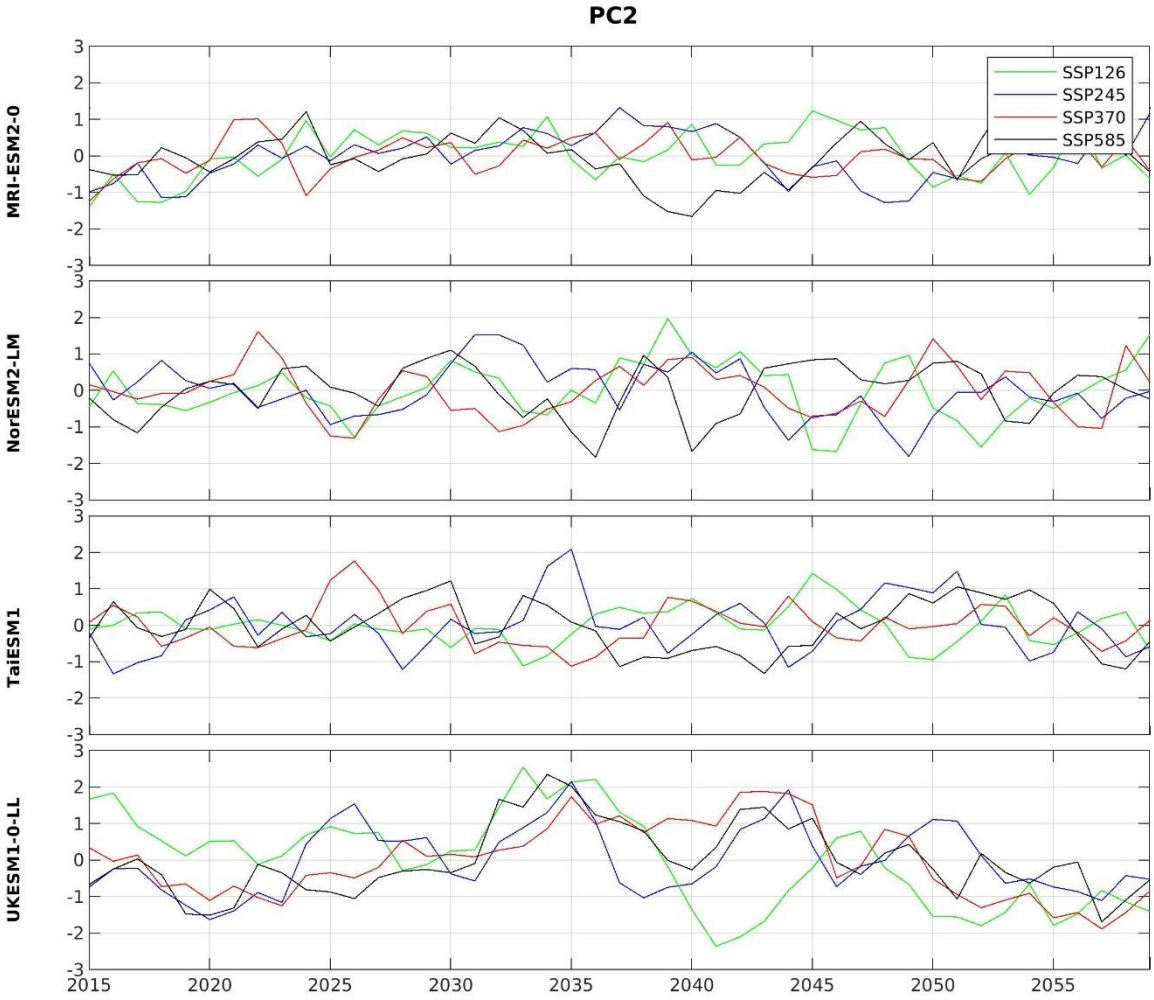

Figure A2.4d. PC2s of the SST for the 2015-2059 period. Unit: ºC.

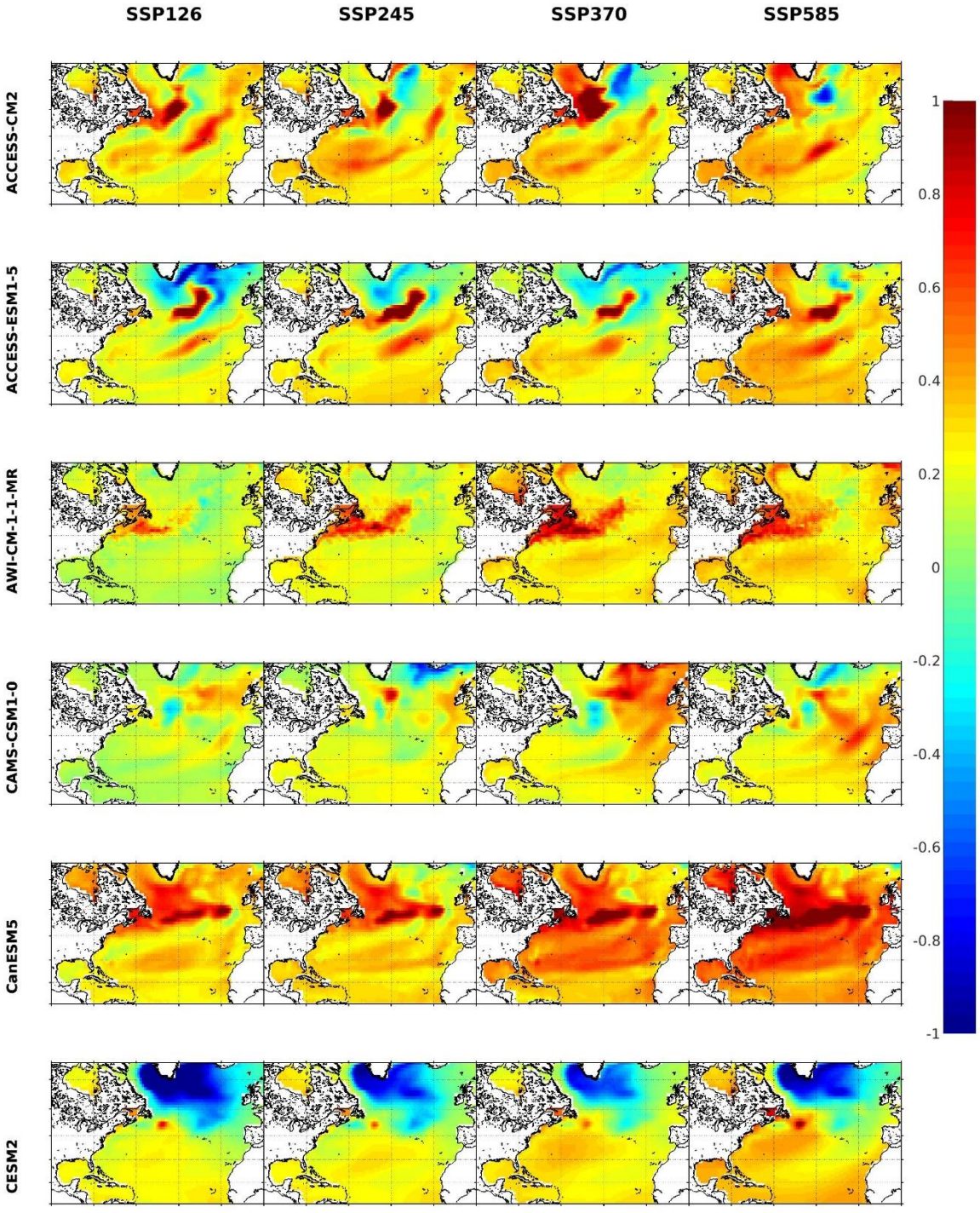

Figure A2.5a. The trends of SST for the 2015-2059 period. Unit: ºC/decade.

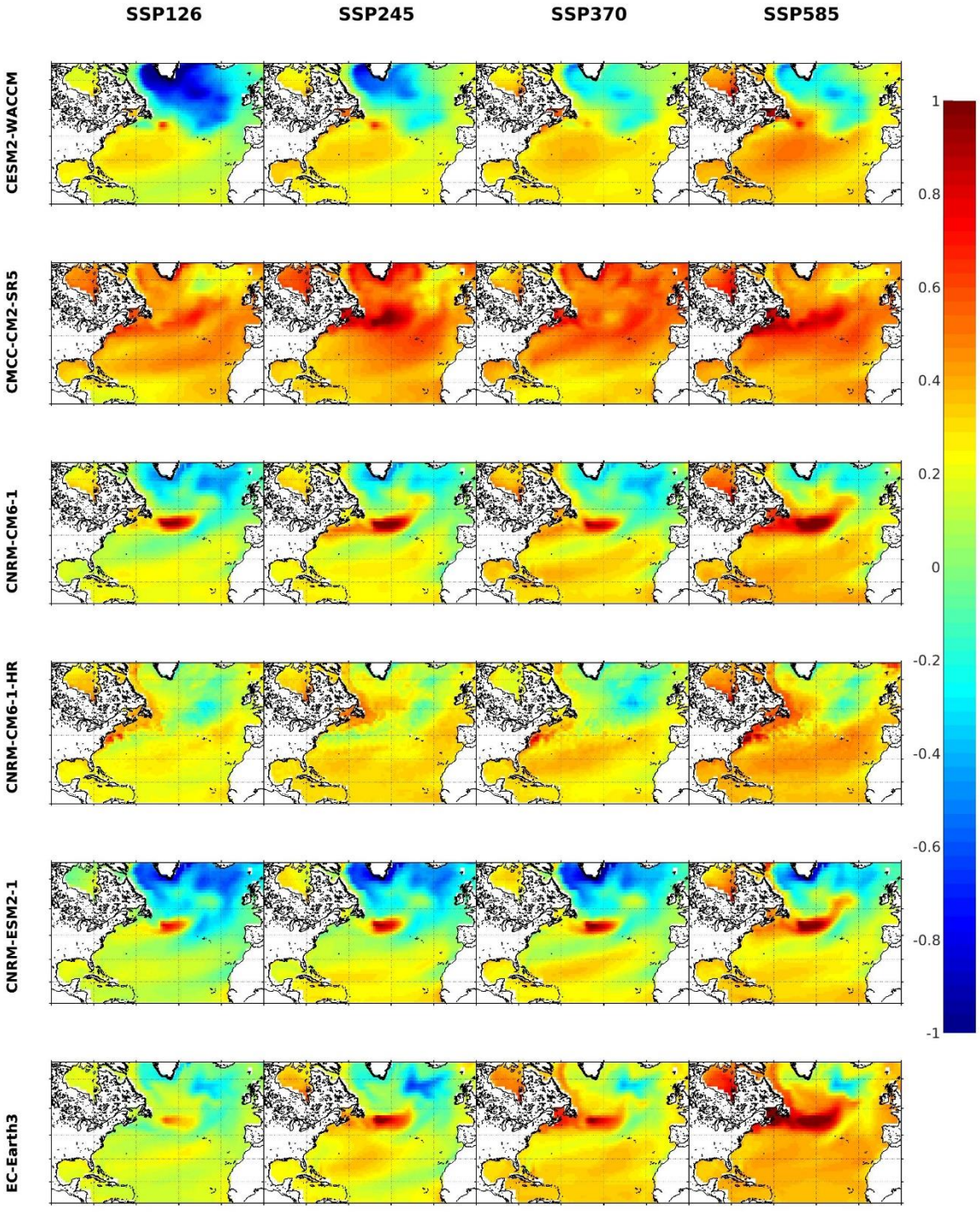

Figure A2.5b. The trends of SST for the 2015-2059 period. Unit: ºC/decade.

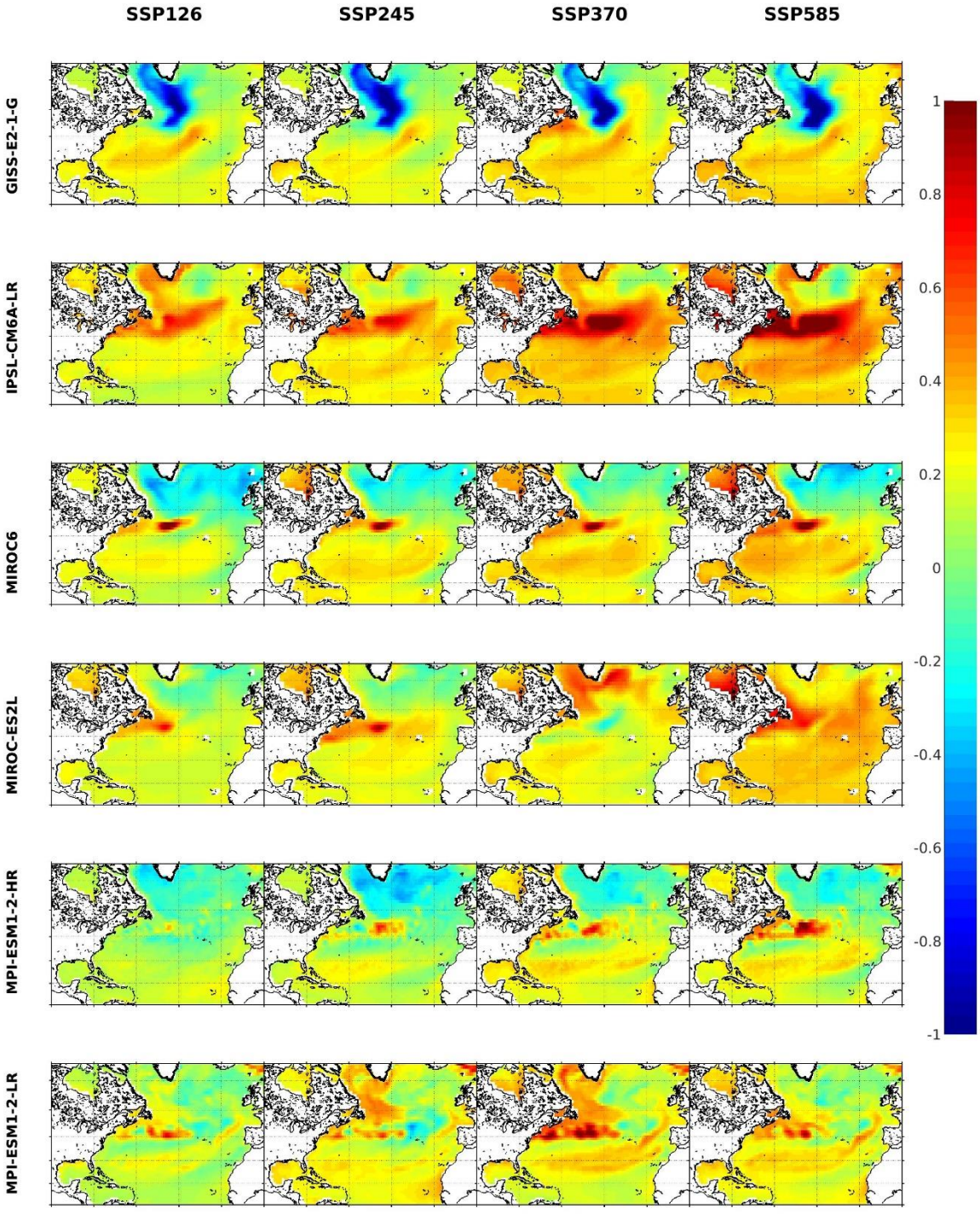

Figure A2.5c. The trends of SST for the 2015-2059 period. Unit: ºC/decade.

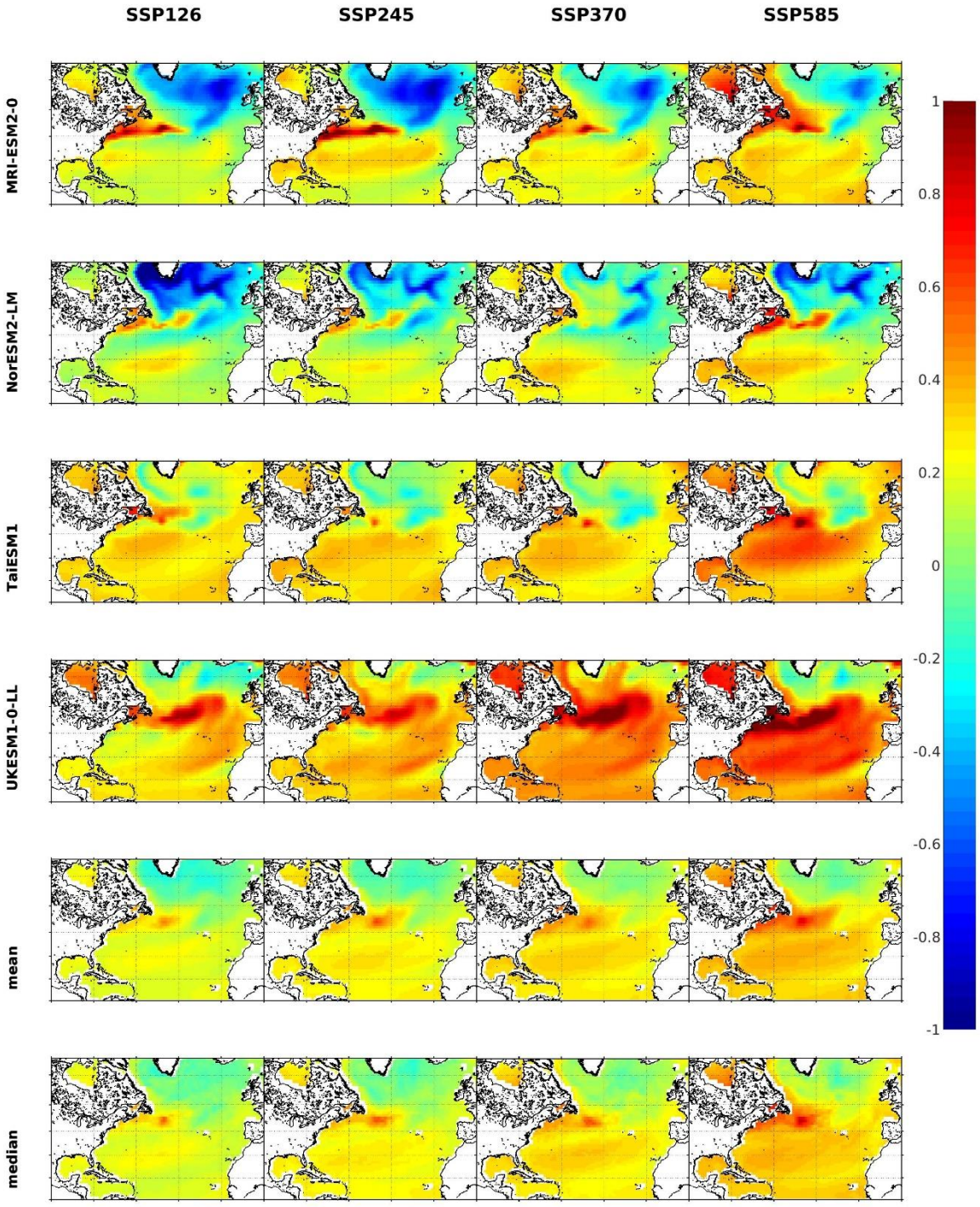

Figure A2.5d. The trends of SST for the 2015-2059 period. Unit: ºC/decade.

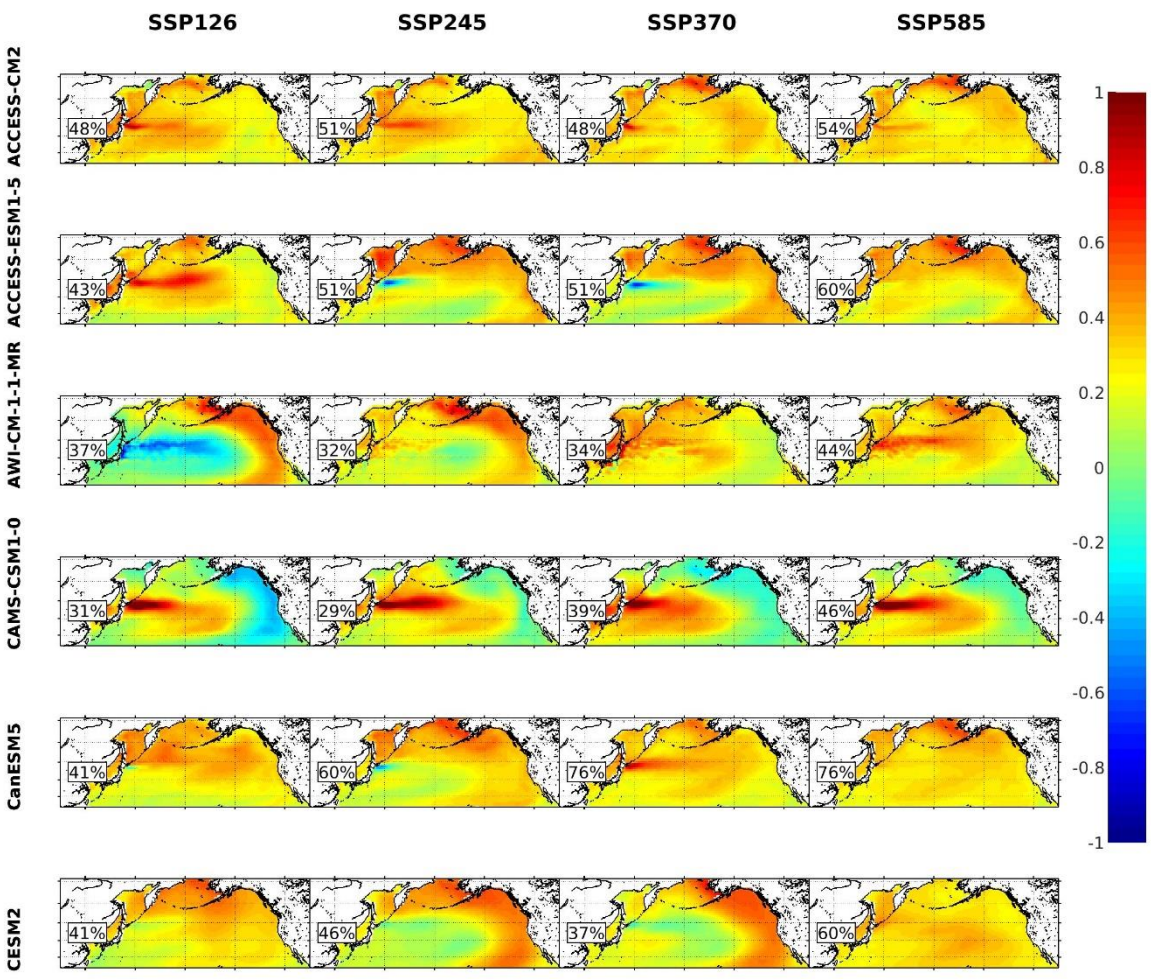

Figure A2.6a. EOF1s of the SST for the 2015-2059 period.

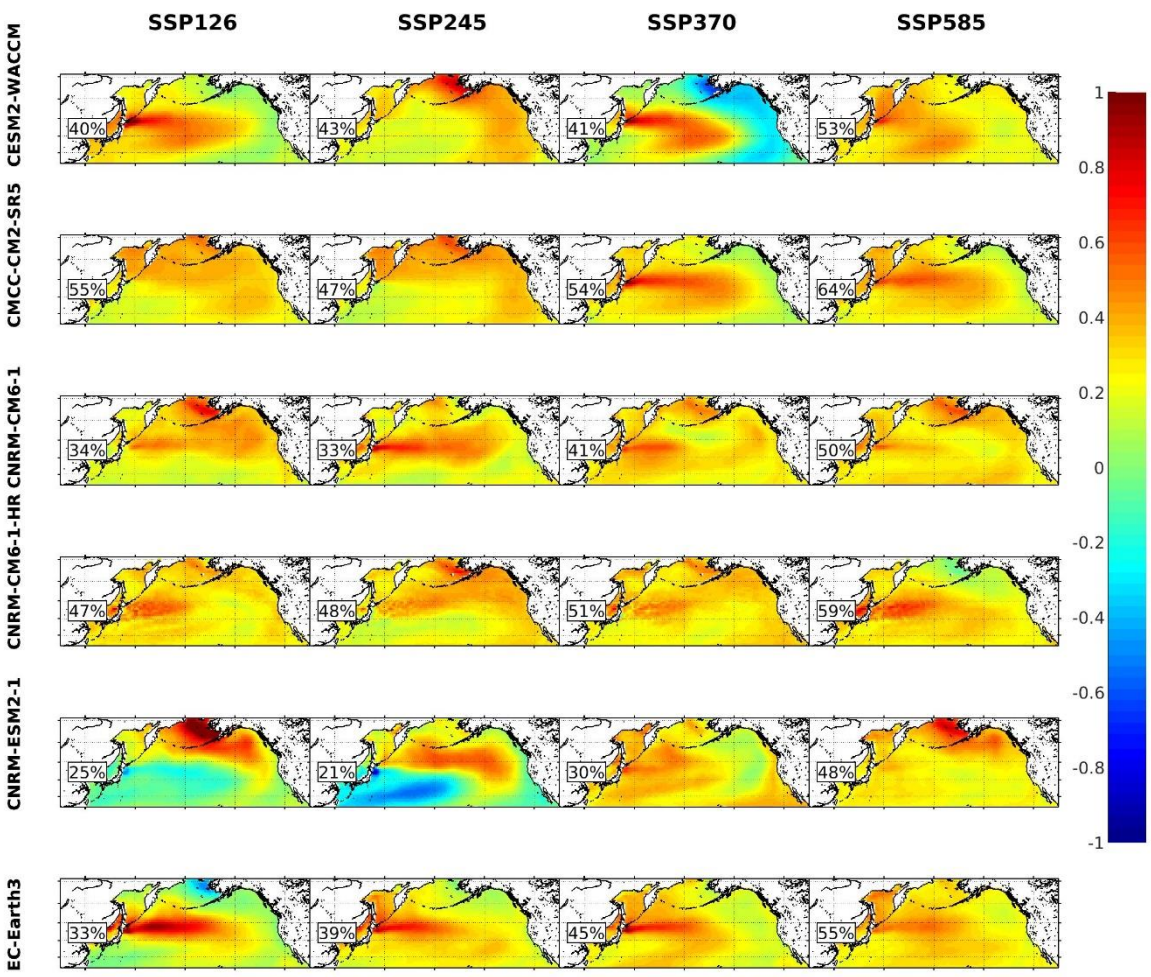

Figure A2.6b. EOF1s of the SST for the 2015-2059 period.

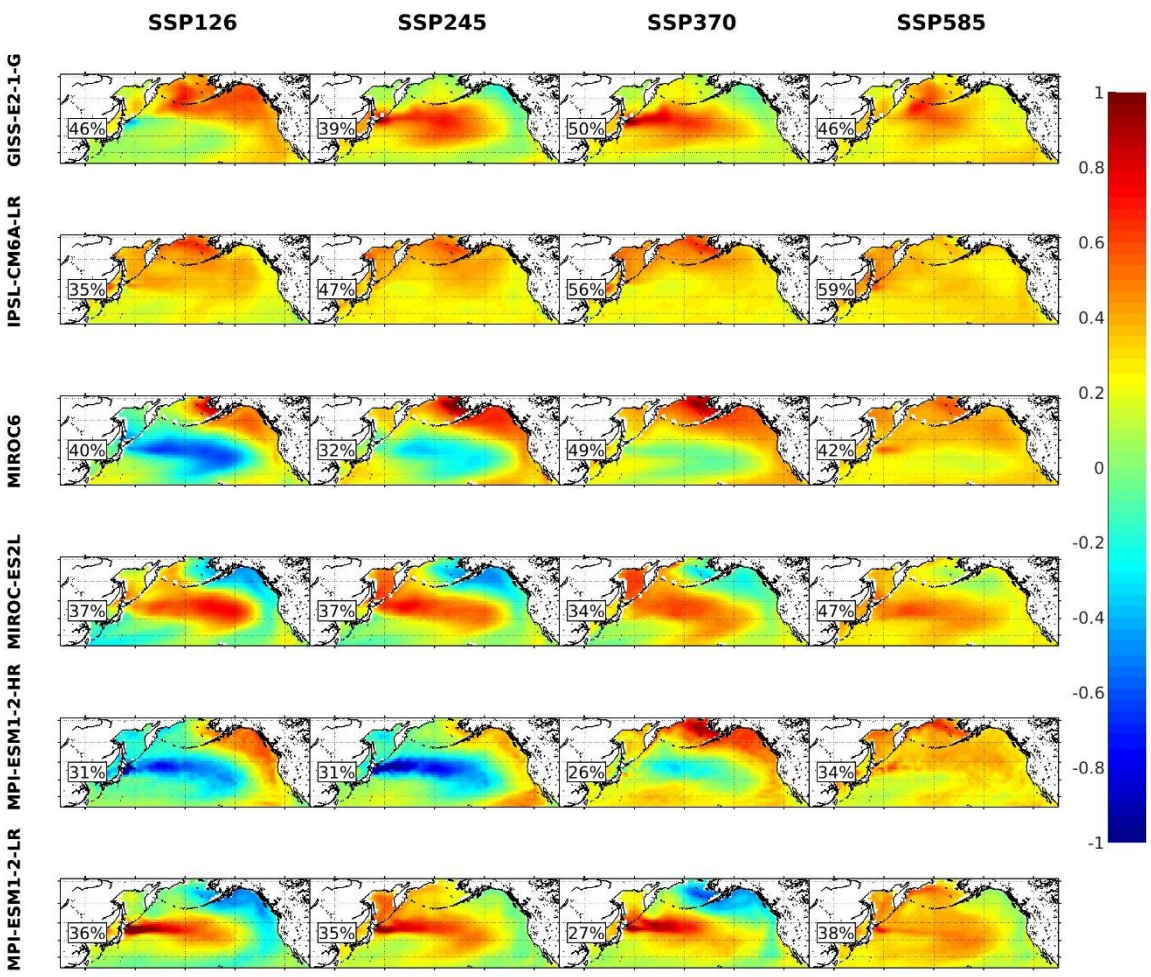

Figure A2.6c. EOF1s of the SST for the 2015-2059 period.

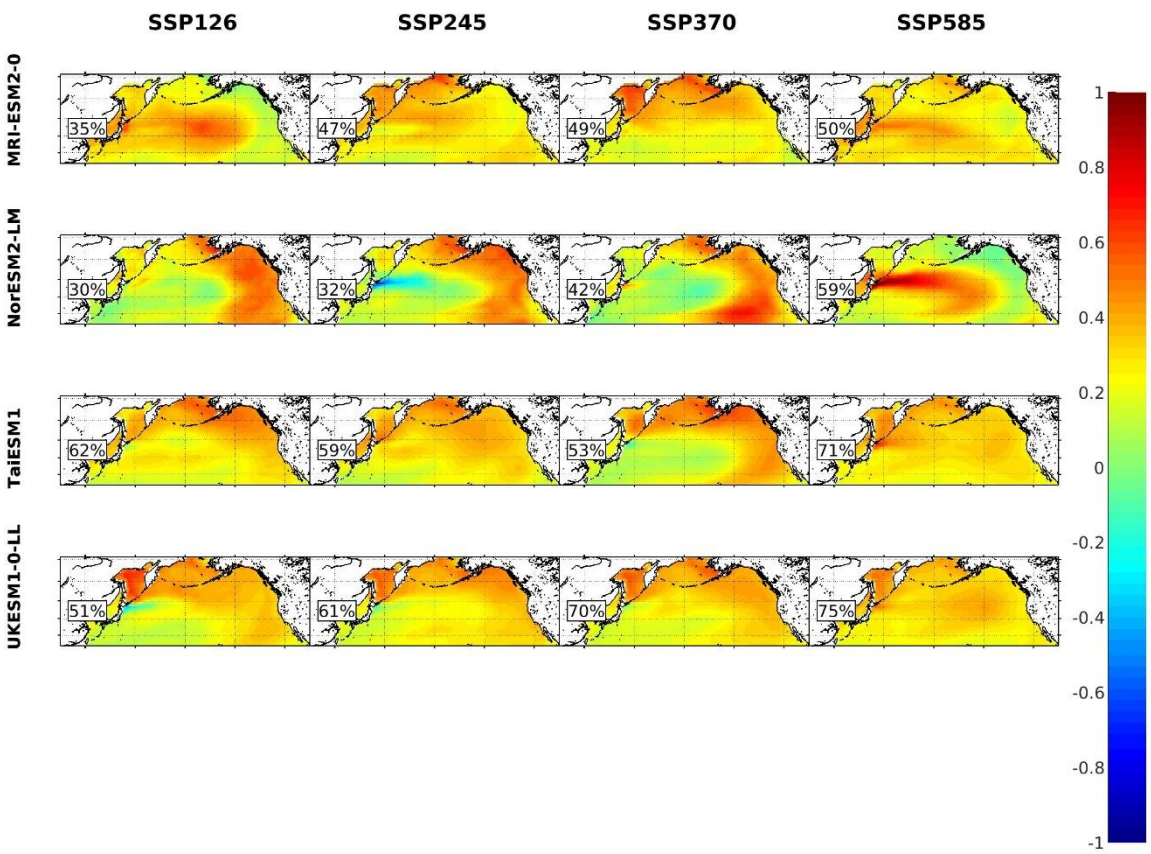

Figure A2.6d. EOF1s of the SST for the 2015-2059 period.

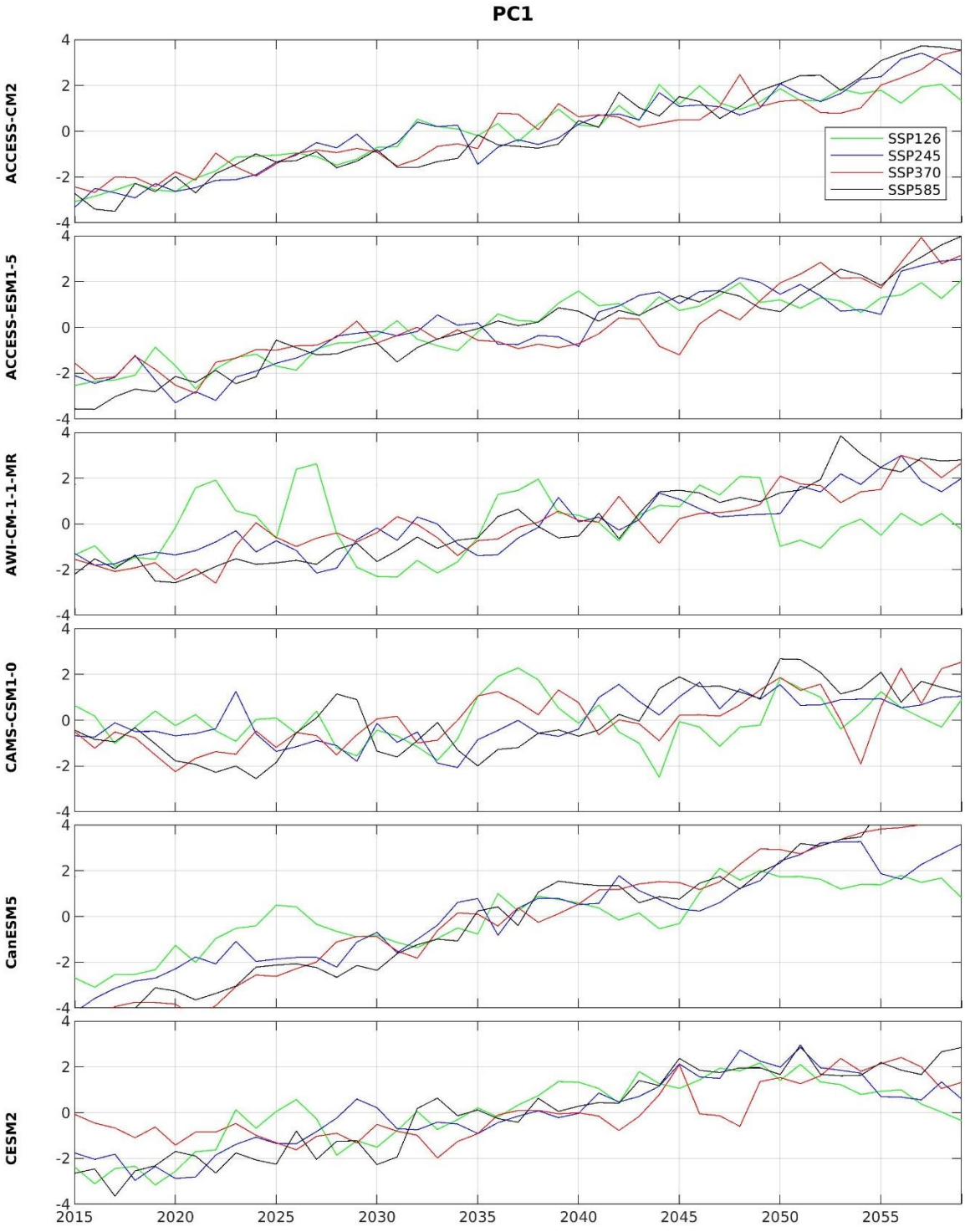

Figure A2.7a. PC1s of the SST for the 2015-2059 period. Unit: ºC.

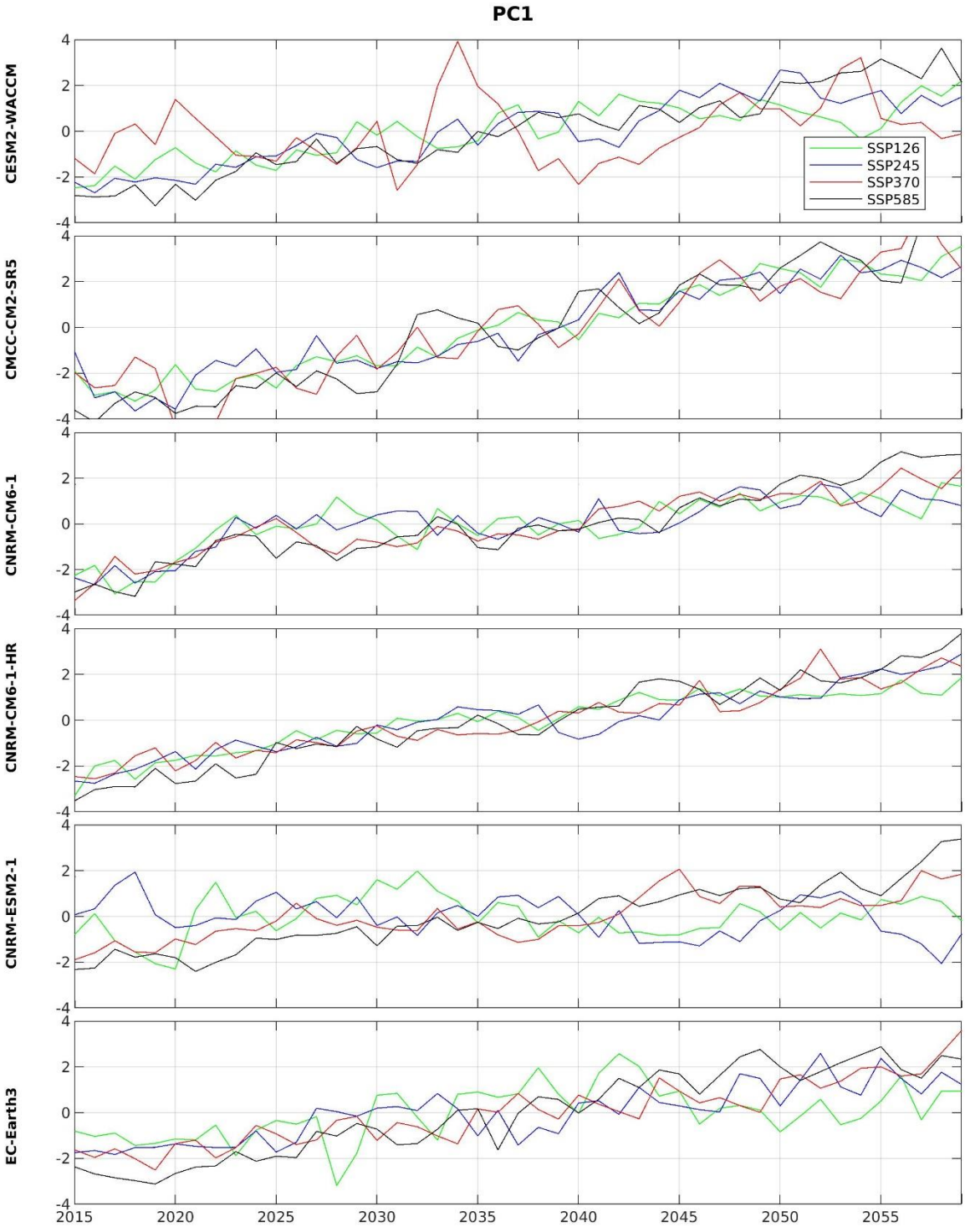

Figure A2.7b. PC1s of the SST for the 2015-2059 period. Unit: ºC.

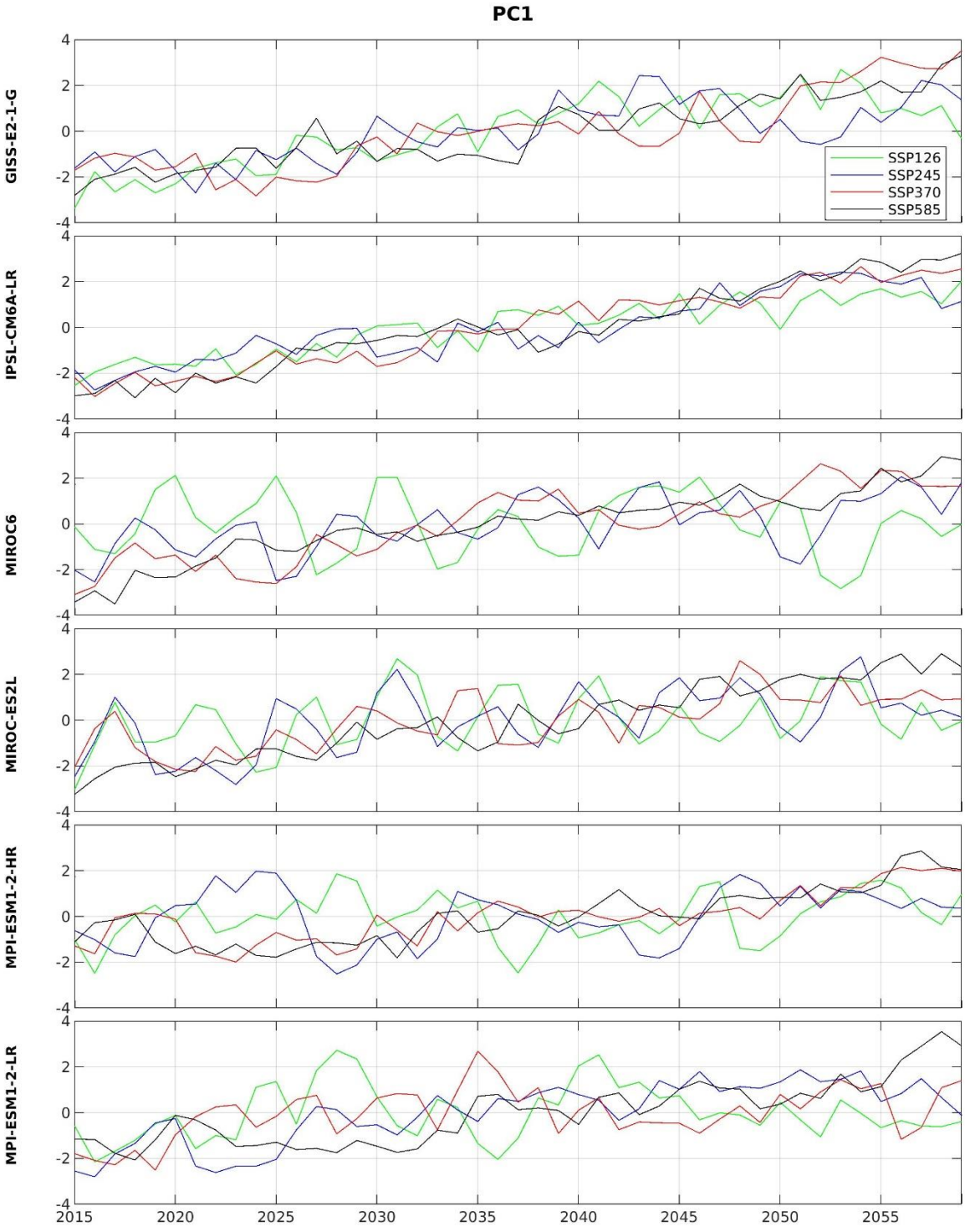

Figure A2.7c. PC1s of the SST for the 2015-2059 period. Unit: ºC.

Figure A2.7d. PC1s of the SST for the 2015-2059 period. Unit: ºC.

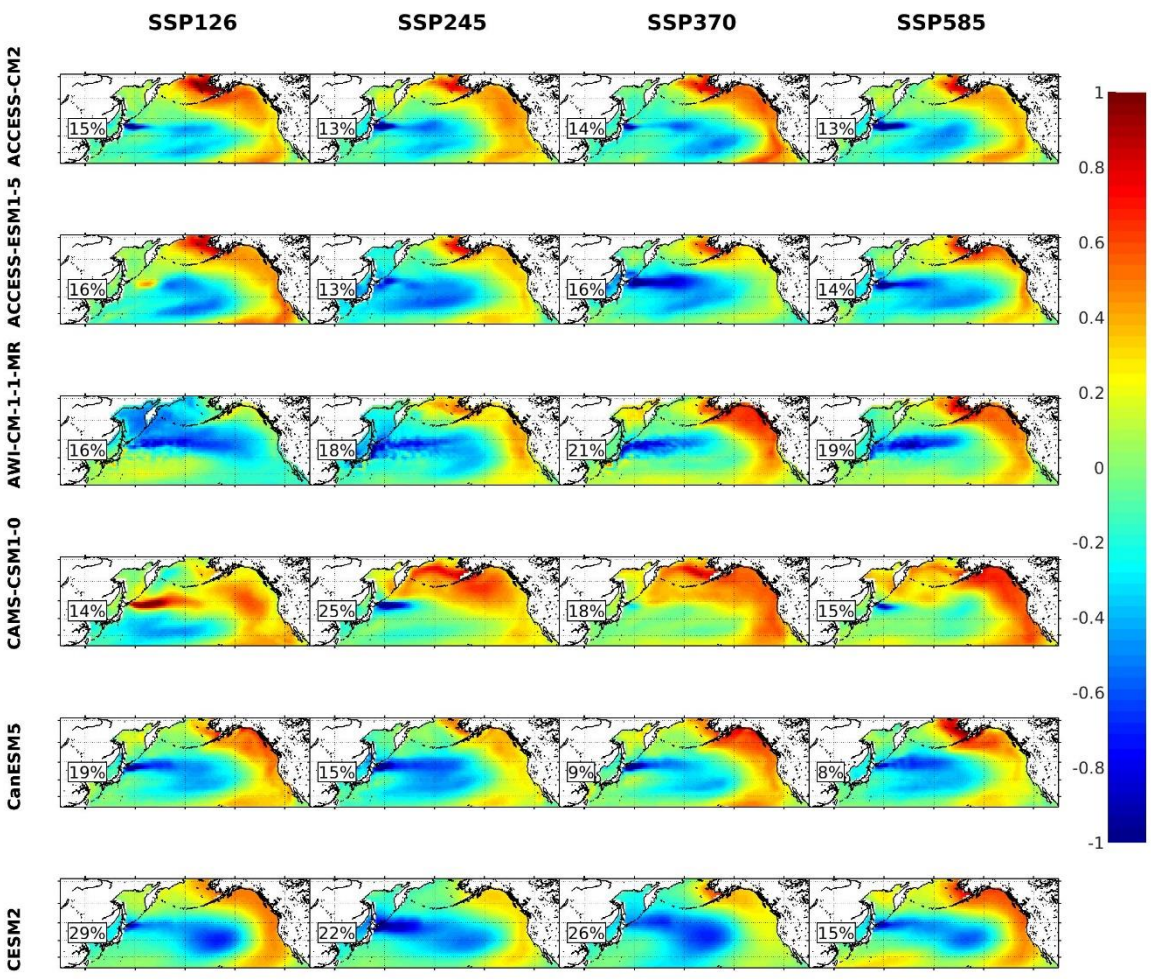

Figure A2.8a. EOF2s of the SST for the 2015-2059 period.

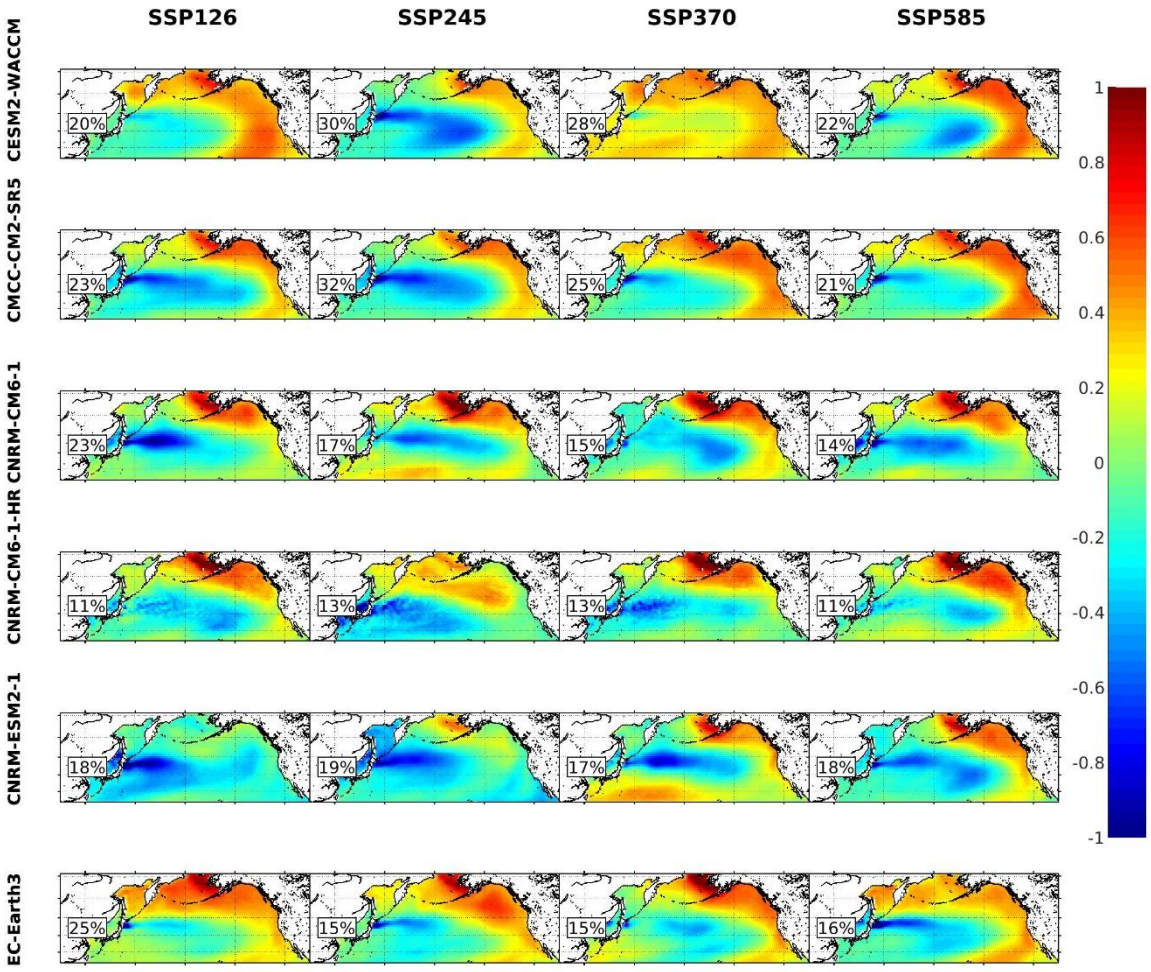

Figure A2.8b. EOF2s of the SST for the 2015-2059 period.

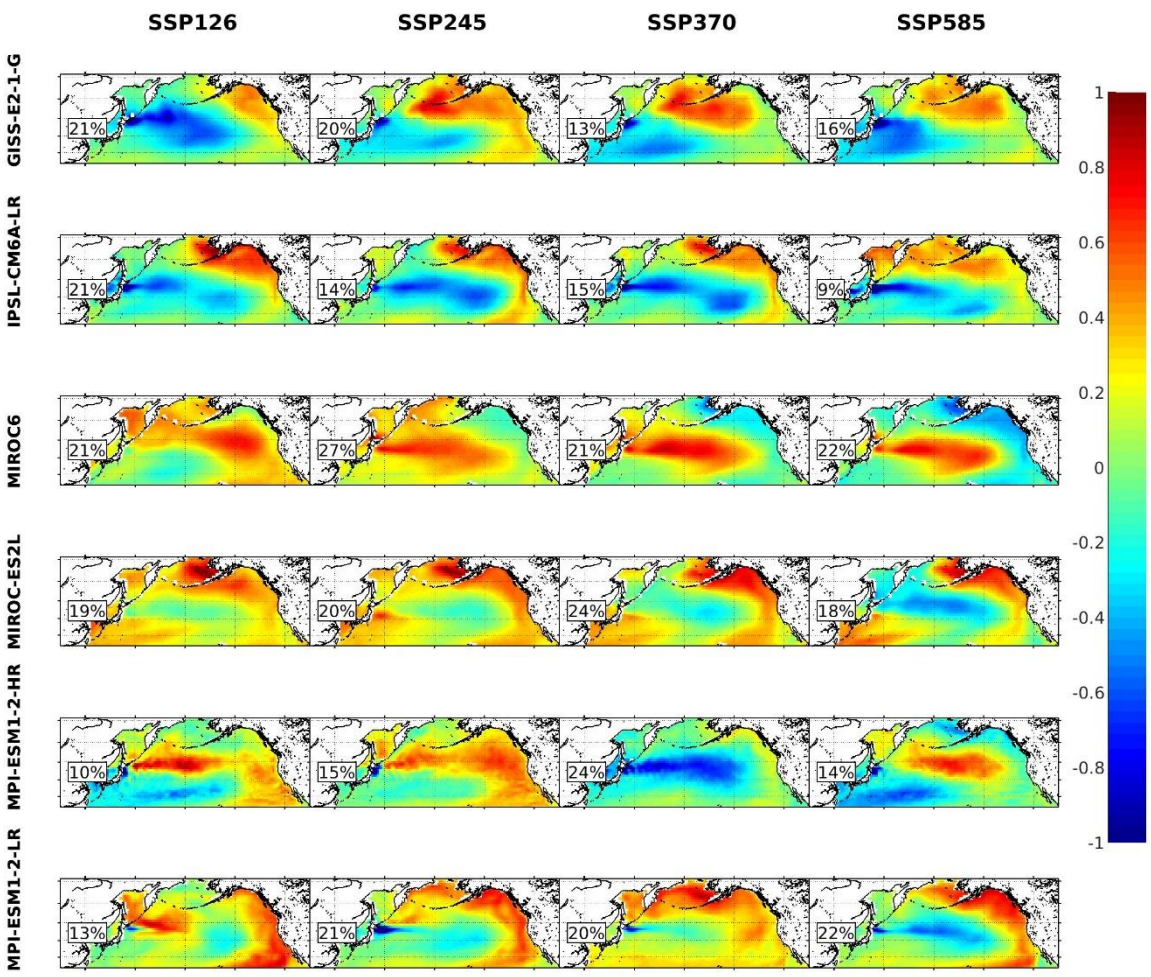

Figure A2.8c. EOF2s of the SST for the 2015-2059 period.

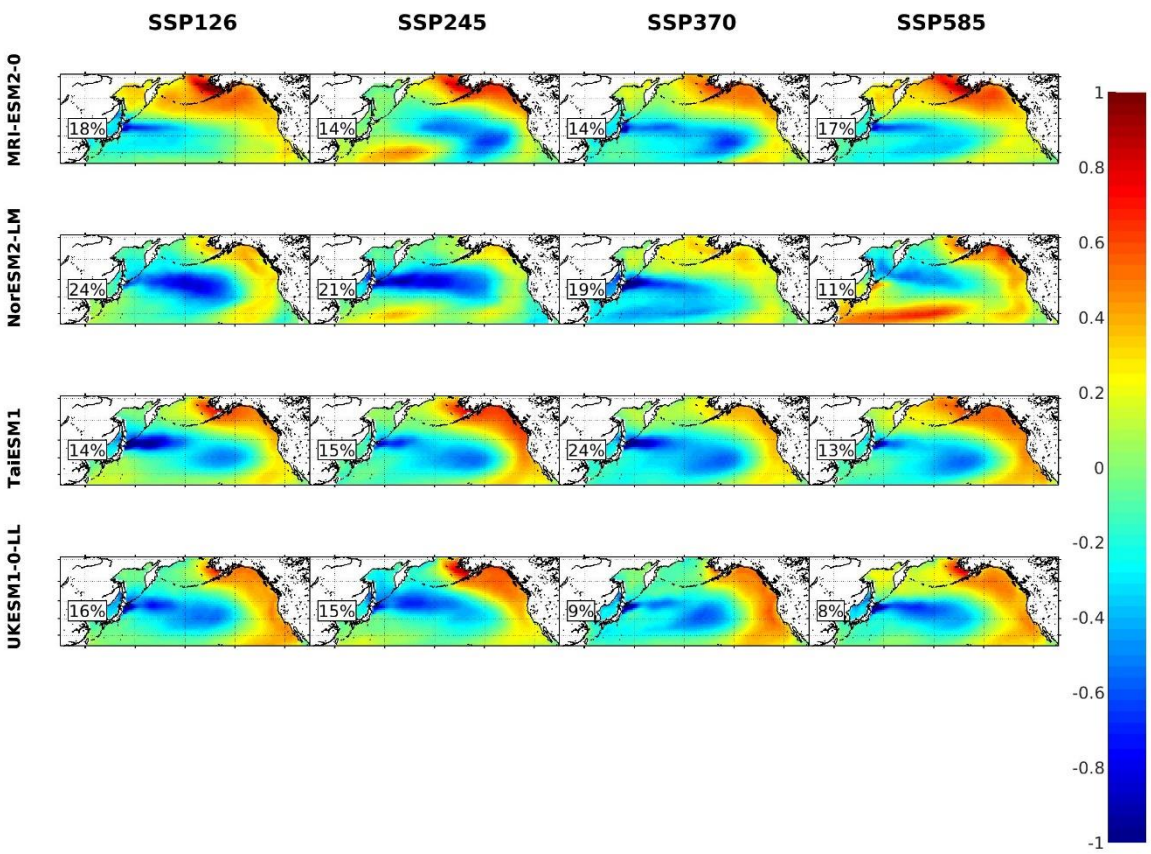

Figure A2.8d. EOF2s of the SST for the 2015-2059 period.

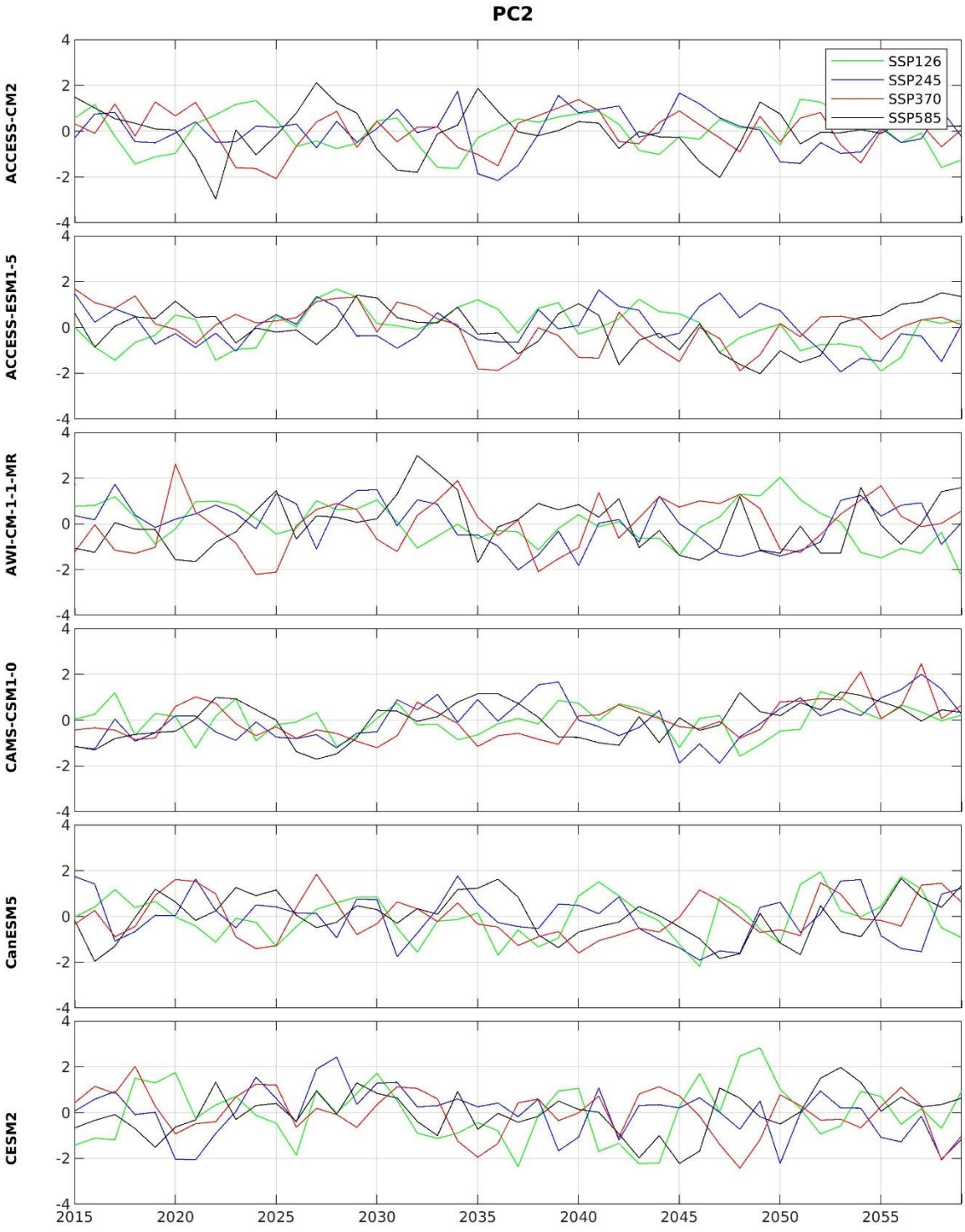

Figure A2.9a. PC2s of the SST for the 2015-2059 period. Unit: ºC.

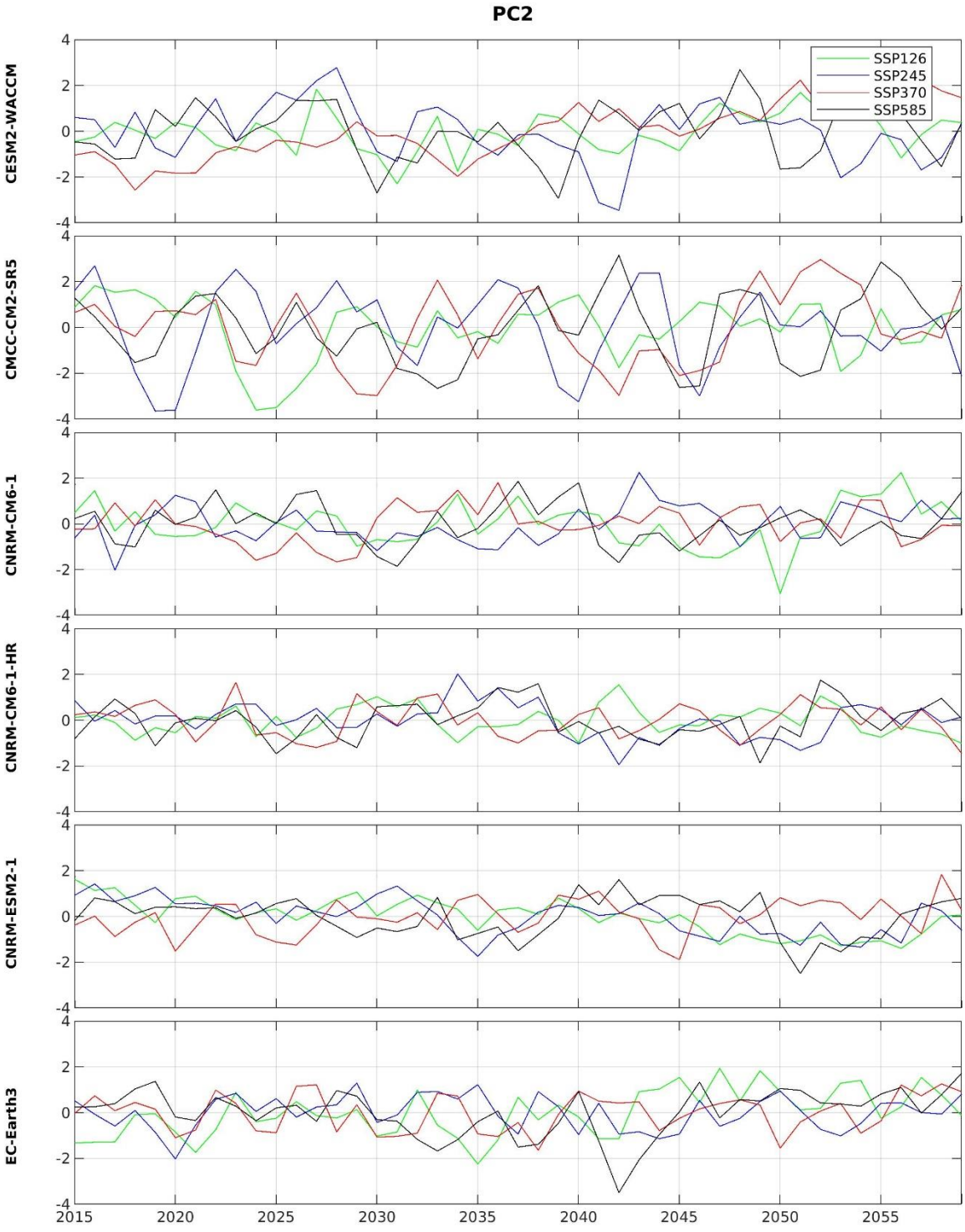

Figure A2.9b. PC2s of the SST for the 2015-2059 period. Unit: ºC.

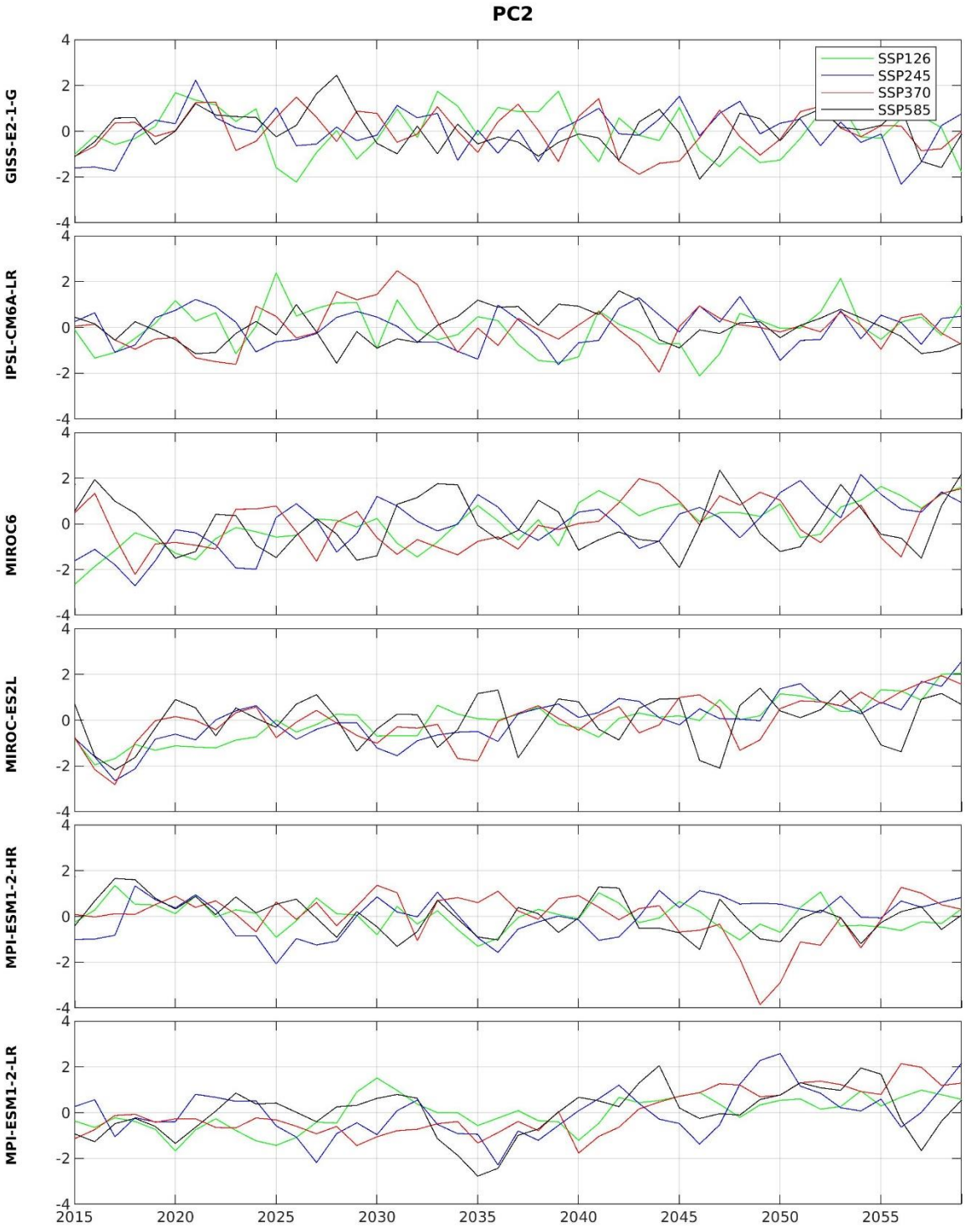

Figure A2.9c. PC2s of the SST for the 2015-2059 period. Unit: ºC.

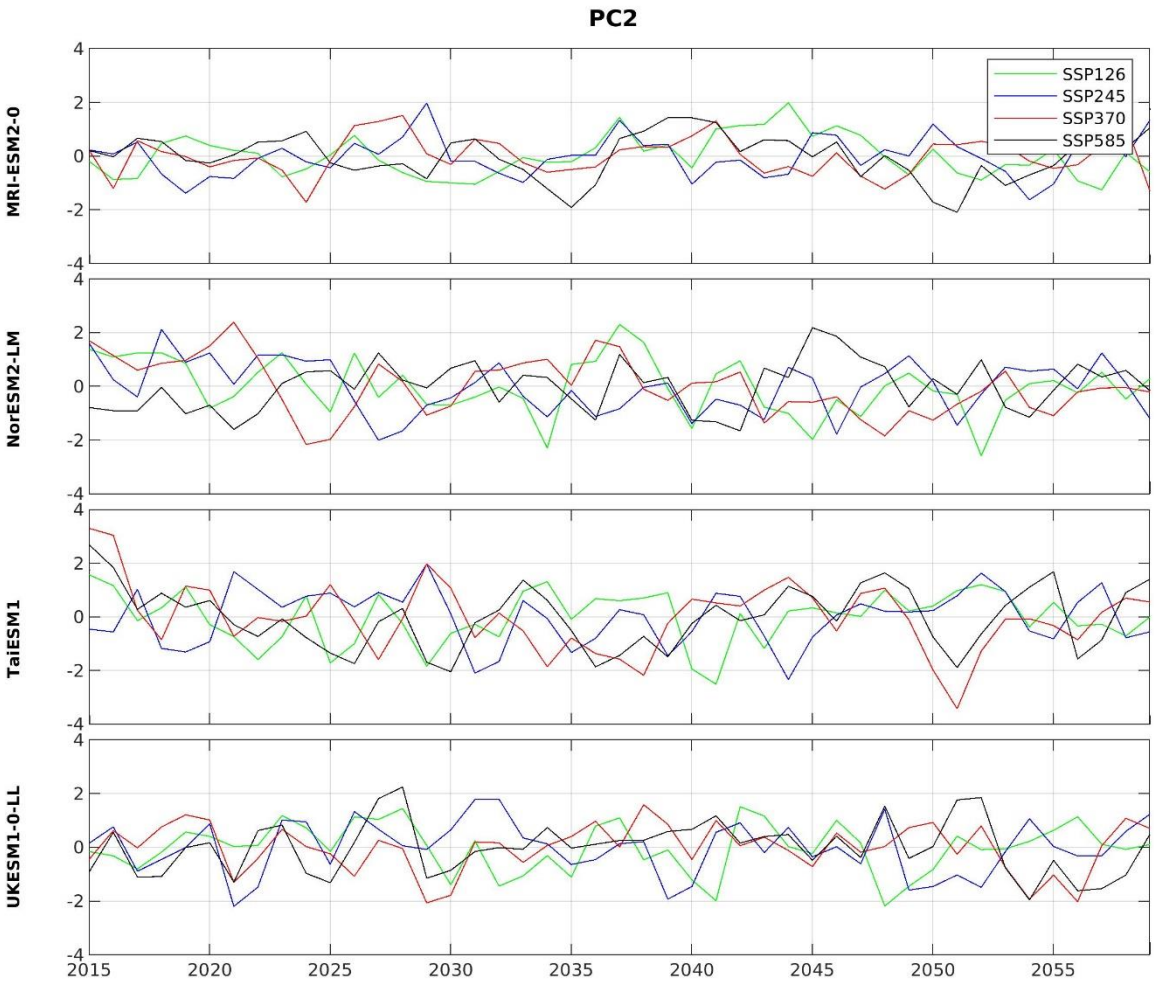

Figure A2.9d. PC2s of the SST for the 2015-2059 period. Unit: ºC.

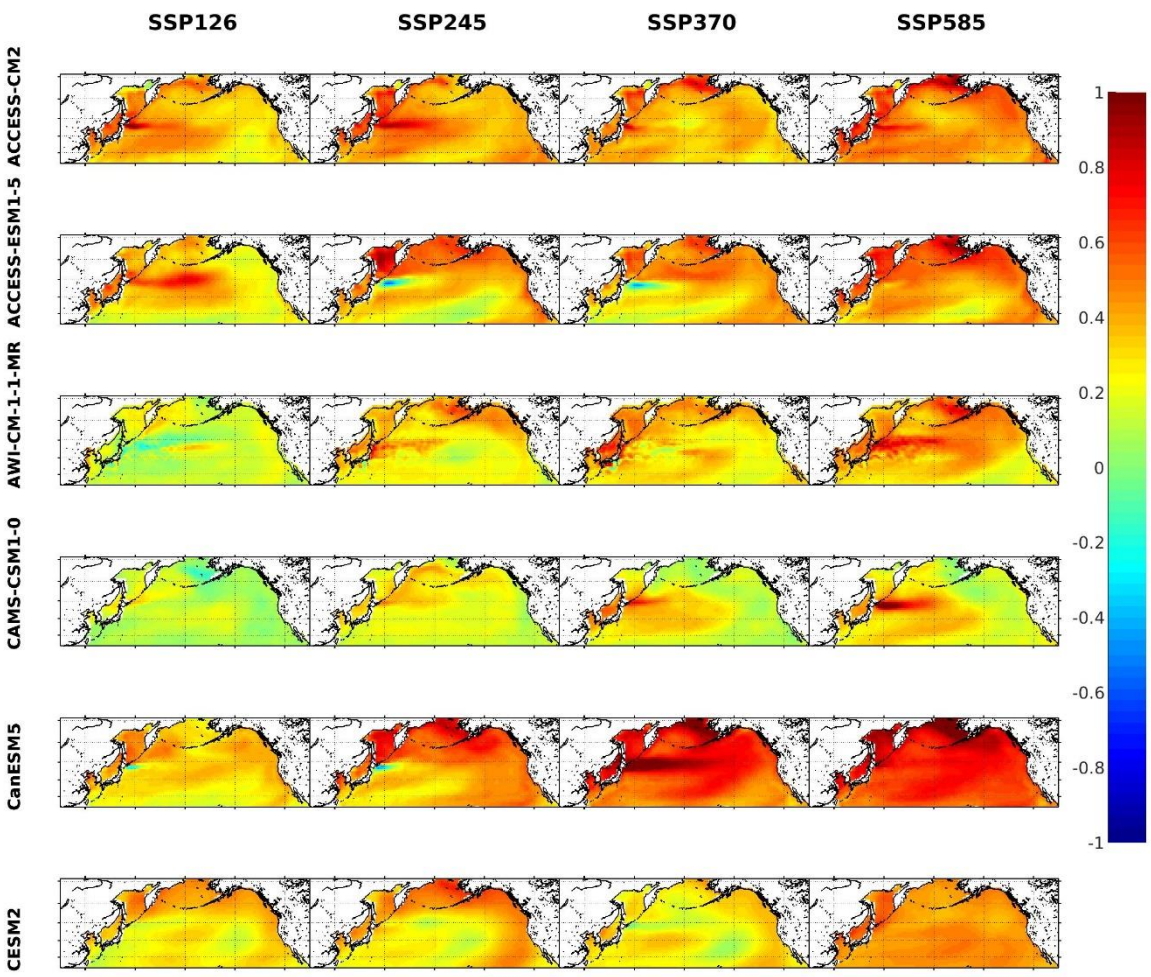

Figure A2.10a. The trends of SST for the 2015-2059 period. Unit: ºC/decade.

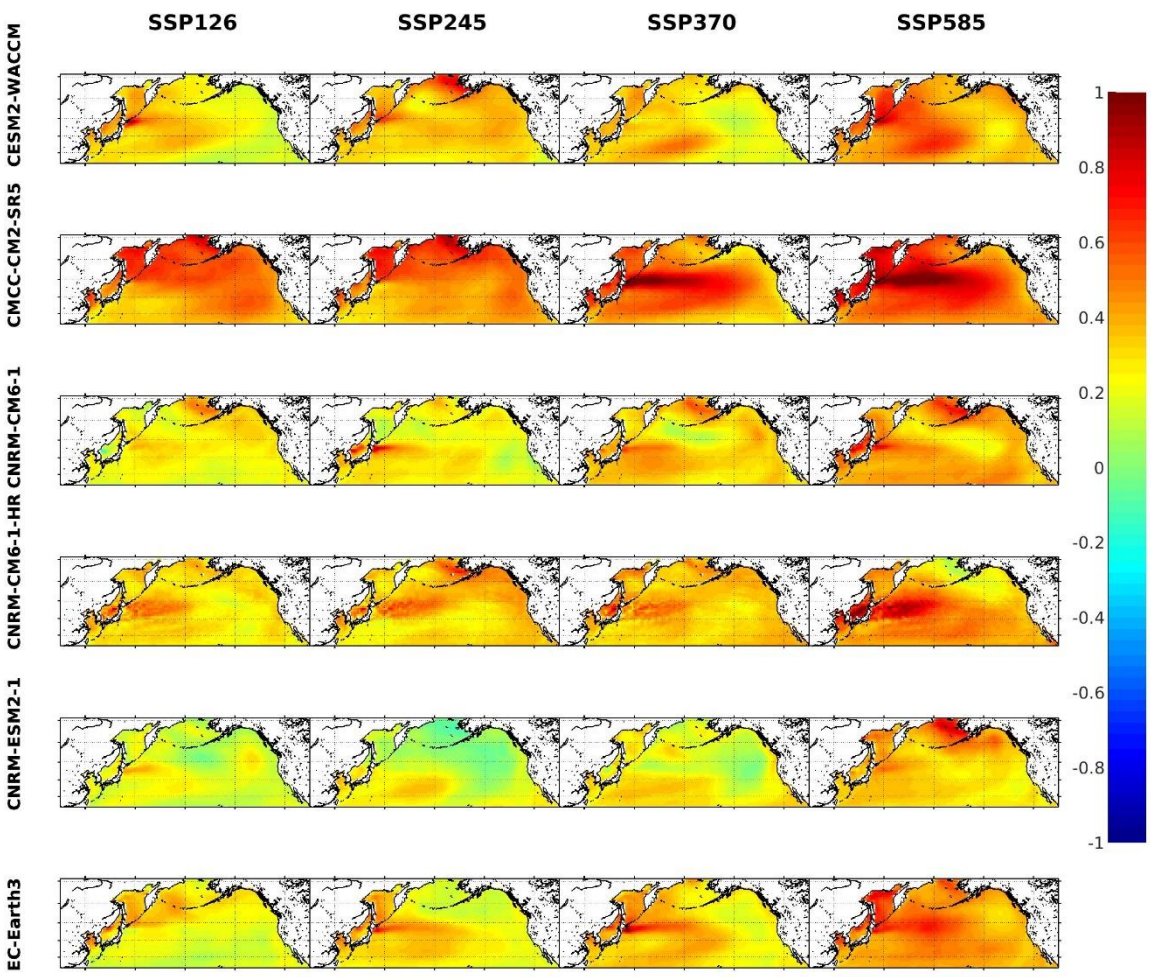

Figure A2.2.10b. The trends of SST for the 2015-2059 period. Unit: ºC/decade.

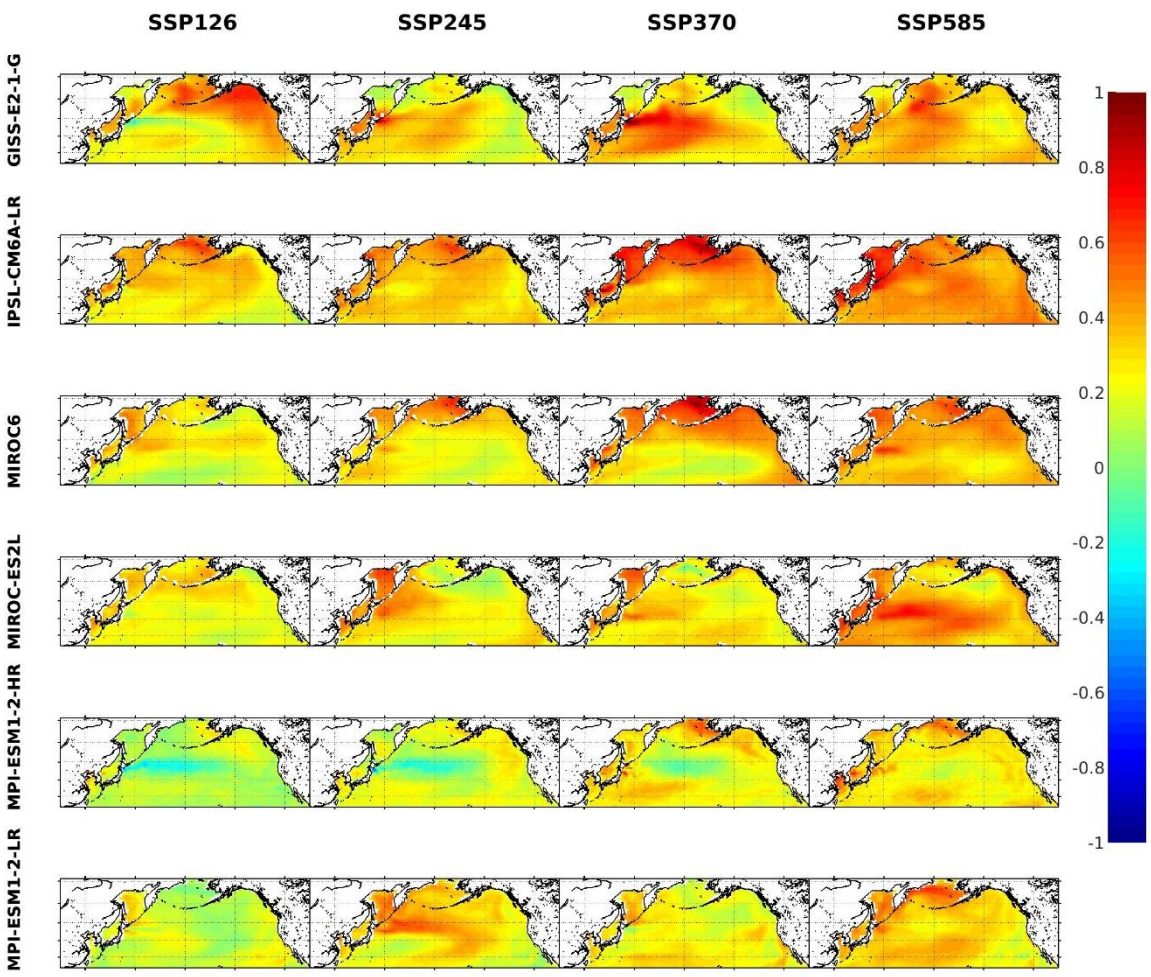

Figure A2.10c. The trends of SST for the 2015-2059 period. Unit: ºC/decade.

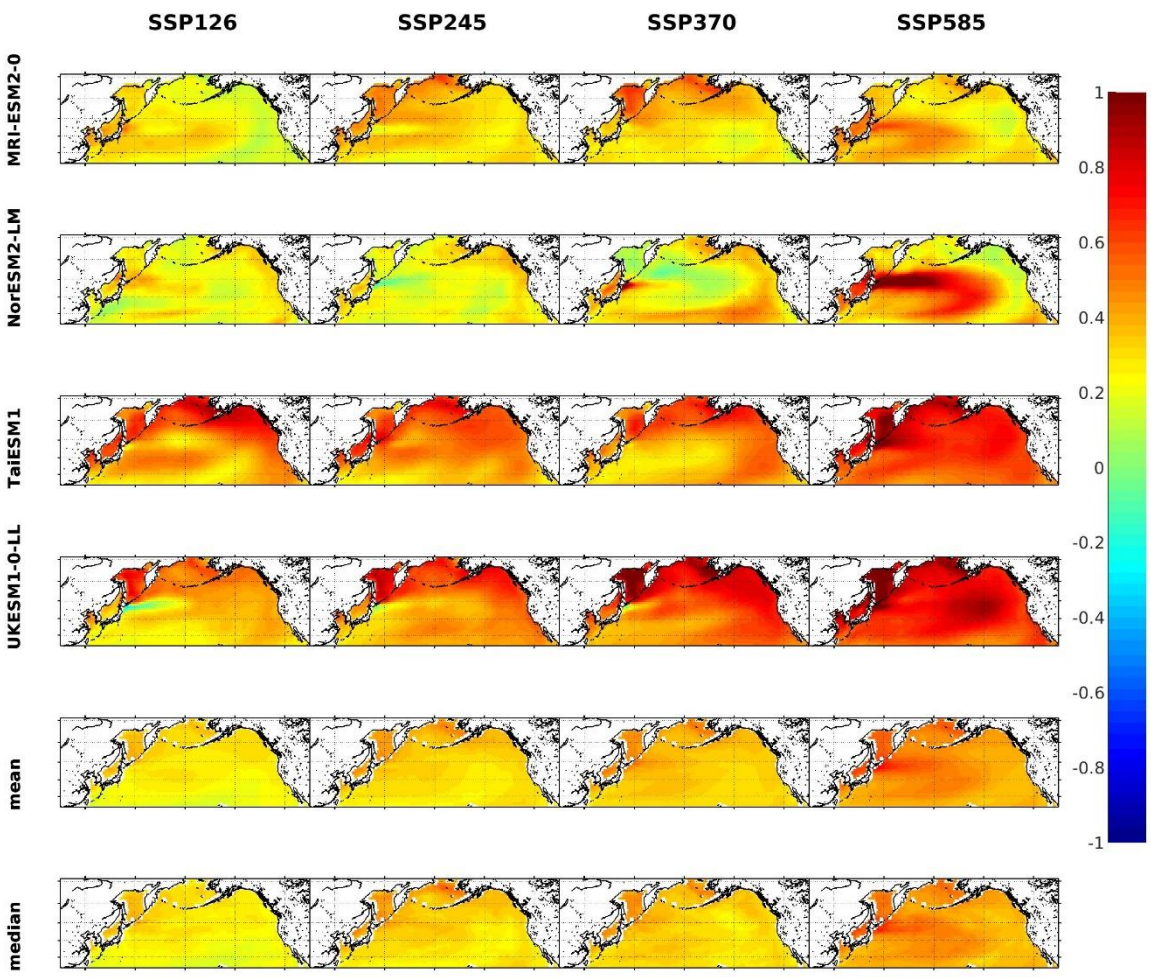

Figure A2.2.10d. The trends of SST for the 2015-2059 period. Unit: ºC/decade.